MINISTRY OF EDUCATION AND SCIENCE OF UKRAINE
Central Ukrainian National Technical University

Mykhailo Chernovol, Andrey Solovykh, Stanislav Katerinich,
Vitalii Kalinichenko, Ilya Rybak, Oleksandr Lopata

TECHNOLOGICAL AND CONSTRUCTIVE METHODS FOR INCREASING THE DURABILITY OF TRANSPORT PARTS USING ELECTRIC SPARK COATINGS

Monograph

Kropyvnytskyi 2026

UDK 620.193:620.197.5

Рекомендовано до друку Вченою Радою
Центральноукраїнського національного
технічного університету
(Протокол 9 від 27.04.2026 року.)

Technological and constructive methods for increasing the durability of transport parts using electric spark coatings / Mykhailo Chernovol, Andrey Solovykh, Stanislav Katerinich, Ilya Rybak, Vitalii Kalinichenko, Oleksandr Lopata. Ministry of education and science of Ukraine, Central Ukrainian National Technical University – Кропивницький: ЦНТУ, 2026. — 173 s.

Рецензенти:

O.F. Salenko, National Technical University of Ukraine "Igor Sikorsky Kyiv Polytechnic Institute", Doctor of Technical Sciences, Professor

V.S. Antonyuk, National Technical University of Ukraine "Igor Sikorsky Kyiv Polytechnic Institute", Doctor of Technical Sciences, Professor

Iu.V. Kulieshkov Central Ukrainian National Technical University,. Doctor of Technical V., Professor

The monograph summarizes the results of research in the field of surface hardening technologies for vehicle parts using the electrospark alloying method. The research is based on the basic principles of materials science, tribology, physical chemistry, physicochemical foundations of electrospark alloying, and the rheological-kinetic concept of wear resistance.

The monograph is devoted to the development of composite multifunctional coatings to improve the tribotechnical and strength characteristics of vehicle parts and extend their serviceability by controlling structure formation and mechanical characteristics while strengthening surface layers with wear-resistant electrospark coatings.

The application of electrospark coatings has been studied in relation to parts of internal combustion engines - pistons, liners, sliding bearings. The production of parts of vehicles with strengthening protective electrospark coatings will allow to provide them to domestic enterprises, will relieve Ukraine of export dependence on critical industries, will provide a significant economic effect.

The monograph is proposed for developers of coatings and technologies for their application, designers, technologists in the field of engine building and motor transport. The monograph may be useful for teachers, postgraduate students and applicants for higher education in the field of mechanical engineering.

CONTENT

ABBREVIATIONS

AE - acoustic emission
CVD - chemical vapor deposition
ICEs - internal combustion engine
EAS - electric arc spraying
EIL - electric spark alloying
EIP - electric spark coating
EG - exhaust gases
GIS - current pulse generator
GTP - gas thermal spraying
HTO - chemical-thermal treatment
HVOF - high-speed fuel-oxygen spraying
(high-velocity oxygen-vapor spraying)
IA - ion nitriding
K - mass transfer coefficient
KCD efficiency coefficient
KM - composite material
KP - composite coating
CTE - coefficient of thermal expansion
KVM - material utilization coefficient
KZ - combustion chamber
LO - laser processing
MAO - microarc oxidation
MEP - interelectrode gap
MO - mechanical processing
MHF - high frequency current
MRSA - micro-X-ray spectral analysis
PM - powder metallurgy
PVD - physical vapor deposition
PS - antifriction alloy metals on an aluminum base
PZ - surface hardening
REM - rare earth metals
SPD - surface plastic deformation
SSS - stress-strain state
TSP - cylinder-piston group
XRF X-ray - diffraction analysis
ZZP - strengthening protective coatings

INTRODUCTION

Increasing the durability, reliability and wear resistance of vehicle parts, reducing their specific material consumption and energy consumption is achieved, first of all, by using strengthening technologies.

The use of strengthening technologies aimed at changing the surface layer allows you to prevent the process of nucleation of deformation defects, which ensures increased wear resistance of contact surfaces. The level of strength of contact surfaces is the dominant factor determining the wear resistance of vehicle parts. There is extensive data showing that wear takes a leading place in the list of dangerous damage to vehicle parts.

The process of external friction is influenced by a large number of factors: the stress-strain state, mechanical and physicochemical properties of the contacting bodies, the environment, and others.

One of the most rational ways that allows you to purposefully change the stress-strain state in the surface layer of vehicle parts, the deformation-force parameters, and the nature of the interaction of contact surfaces is the method of electric spark alloying.

The method of electric spark alloying has a unique set of advantages: low energy consumption, environmental safety, simplicity of technology (absence of a special working environment and preliminary surface preparation), adhesion strength to the base.

Electrospark treatment ensures the formation of a layer on the surface of a part that has a structure and properties different from the initial state, depending on the parameters of the spark discharge, the composition of the electrode material, the material of the part being treated, and other factors.

A significant contribution to the establishment and development of the scientific direction of modification of surface layers of metals by the method of electrospark alloying was made by Ukrainian and foreign scientists B.R. Lazarenko, N.I. Lazarenko, A.D. Verkhoturov, B.N. Zolotikh, A.E. Hytlevych,

I.O. Podchernyaeva, B.A. Lyashenko, C. Barile, C. Casavola, Zhao, H., Feldshteina E.E., Mao Y., Xie Y.J., Wang M.C., Johnson R.N., Reynold J.L and others.

A feature of electrospark coatings is their inherent discontinuity, which provides increased wear resistance due to the discreteness of the coating structure, which is responsible for reducing residual stresses. The presence in the surface layer of areas of increased hardness, optimal continuity, geometry and depth of penetration into the surface eliminates the concentration of stresses from contact loads and interrupts the process of crack formation, plastic deformation, and also reduces the tendency to seize parts, which is significant.

The main advantage of electrospark coatings is the ability to control and minimize the stress-strain state of the surface, ensuring increased wear resistance, by changing the continuity and size of areas on the surface of the base and selecting materials based on their physical and mechanical characteristics.

Studying the features of the formation of a modified layer on the surfaces of parts during electrospark alloying, establishing the relationship between the parameters of the substructure and the stress-strain state of the modified layer with its tribotechnical characteristics is a relevant task in terms of developing technological recommendations for strengthening parts of vehicles in order to increase the service life of components and assemblies.

Establishing the patterns of influence of microgeometric and physical and mechanical properties of electrospark coatings on the tribotechnical characteristics of vehicle parts requires the development of new methods for assessing their quality.

An important direction in studying the quality of electrospark coatings is the establishment of criteria that determine the range of their serviceable state. Due to the nature of changes in such tribotechnical indicators as the friction coefficient, temperature in the frictional contact zone, thickness of the lubricating layer, and specific work of friction, it is not always possible to predict and predict them at the stage of catastrophic wear.

The information-analytical methods for determining the range of workability of a tribotechnical pair include the acoustic emission method, which is characterized by high sensitivity to elastic-plastic deformations in frictional contact.

Thus, controlling the structure formation and mechanical characteristics of the surface layers of vehicle parts by forming wear-resistant electrospark coatings will allow solving the scientific and technical problem of increasing their tribotechnical and strength characteristics and expanding the load-speed range of their serviceable state.

In each specific case, it is necessary to optimize the processing mode (selection of discharge energy, processing time), as well as select a wear-resistant electrode material. Therefore, the study of the strength and elasticity characteristics of coatings formed by the electrospark alloying method is of important theoretical and practical importance.

Since structural adaptability and changes in the tribological system during operation can significantly change the initial parameters used in predicting the resource of a friction unit, it is necessary to accumulate a large amount of experimental material on the relationship between the initial hardness of materials and their wear resistance. Coatings obtained by the method of electrospark alloying differ in structure and properties from the starting materials. The reason for this is the micrometallurgical processes that occur on the surface to be strengthened in the spark discharge zone due to the physicochemical interaction of the transferred material with the cathode material and environmental elements in the presence of pulsed thermodynamic stresses.

Increasingly greater loads, more stringent operating conditions, and the use of new materials, the properties of which have not always been studied in detail, make friction units increasingly dangerous objects that require continuous monitoring.

Many experimental studies have been conducted to study the relationship between acoustic emission parameters and wear resistance of friction pairs. The

main sources of generation of acoustic emission signals during friction include the intensification of deformation processes, the nucleation and propagation of cracks in the coating or at the coating-base interface, and structural and phase transformations in the most loaded zones of the actual contact area of friction pairs. These processes are accompanied by the accumulation of deformation energy. When this indicator reaches a critical level, irreversible changes occur in the frictional contact, leading to catastrophic wear of the tribocoupling elements.

Establishing the patterns of transition of electrospark coatings from normal to catastrophic wear based on the analysis of acoustic emission signals is a relevant direction in the prediction of their ultimate performance, which allows developing recommendations for the use of modified surfaces in a certain load-speed regime.

The monograph summarizes the results of research in the field of surface strengthening technologies for vehicle parts by the method of electrospark alloying.

The application of electrospark coatings was performed on parts of internal combustion engines - pistons, liners, sliding bearings. The production of parts of vehicles with strengthening protective electrospark coatings will allow to provide them to domestic enterprises, will relieve Ukraine of export dependence on critical industries, and will provide a significant economic effect.

CHAPTER 1

STRENGTHENING TECHNOLOGIES AND PROSPECTS OF THEIR USE IN VEHICLE PARTS

1.1. Increasing the operational parameters of vehicle parts and requirements for them

The operating conditions of vehicles are characterized by increased speeds and specific loads, temperatures and deterioration of lubrication conditions [1].

Today, the main tasks of modern vehicles, and primarily engine engineering, include reducing fuel consumption and reducing exhaust gas toxicity without worsening other engine performance. Mechanical and thermodynamic costs, wear and exhaust gas toxicity (EG) depend mainly on the tribological characteristics of the cylinder-piston group. Existing trends in the development of compact engines with high specific power and increased thermomechanical loads lead to increased requirements for tribological systems [2]. These circumstances require new solutions.

When testing gasoline automobile engines according to the new European NEDC cycle (New European Driving Cycle), about 20% of the fuel is spent on overcoming friction. The most realistic direction of reducing friction by thermal methods of improving the tribological characteristics of the cylinder-piston group and crankshaft bearings has been outlined [3].

Thermal methods involve maintaining optimal temperatures in the contact points of tribocompounds, taking into account the fact that friction decreases with increasing temperature [3]. The most effective measure to reduce friction in crankshaft bearings may be the transition from plain bearings to rolling bearings [2].

With an increase in the number of engine revolutions and dynamic loads, such a negative phenomenon in friction and wear as fretting increases significantly [4-6]. In this case, material damage is associated with sliding conditions. Thermal

stresses have a significant impact on the durability of engines. They arise as a result of uneven temperature fields in structural elements during engine operation with frequent starts and stops. The level of thermal stress can exceed operational stresses. Under the influence of thermal stress, plastic compression deformations occur on the surface of the part, which lead to a decrease in resource [7, 8].

The simultaneous action of such operational factors as mechanical loads, aggressive working environments, high temperatures and sharp thermal changes leads to non-additivity of the strengthening effect on the structural elements of vehicle parts [9]. With the simultaneous influence of these factors, the service life of parts can be reduced by an order of magnitude or more.

Vehicle parts are operated at high temperatures under conditions of joint wear, fatigue and intermittent friction [10]. The critical role of the interaction of corrosion and stress-strain state (SSS) in the initiation and development of cracks has been revealed [11].

Thus, the main operational indicators of vehicle parts are tribotechnical characteristics: wear resistance, friction coefficient, and galling resistance [12-14]. These characteristics are provided by a complex of physical and mechanical properties: hardness, elastic modulus, viscosity, heat resistance, heat resistance, low coefficient of thermal expansion (CTE), strength and yield strength, vibration decrement, and corrosion resistance [12, 15-18].

The main requirements for power units of vehicles remain high performance, increased fuel efficiency, and reduced harmful emissions into the environment. Along with these requirements, the high-technological nature of engine production is crucial, which is determined by the optimal choice of structural materials and their processing technology.

Composite materials for antifriction purposes are used as alternative ones in friction units of internal combustion engines of automobiles, in the production of pistons, cylinders, and bearings [19-21] (Fig. 1.1).

The state of the theories of friction and wear, theories of strength and durability do not guarantee a forecast in the selection of materials for difficult

operating conditions of vehicle parts. The decisive factor in the selection of materials for tribo-compounds of vehicles is a set of properties such as fatigue strength, resistance to wear and scuffing, resistance to abrasive wear and cavitation erosion, high heat resistance and resistance to thermal fatigue, resistance to oil corrosion [22, 23].

Fig. 1.1. Details of an automobile engine

It should be noted that in the scientific and practical direction of friction and wear, such a direction as automotive tribology has been formed [24].

To assess the wear resistance of the surfaces of vehicle parts, it is necessary to establish the mechanisms of mechanical, physical and chemical changes that occur in the process of structural adaptation during friction.

A promising direction in this regard should be the involvement of the basic provisions of the molecular-mechanical and structural-energy theories of friction, which will allow us to identify the main changes occurring in frictional contact and determine the dominant factors that ensure an increase in the wear resistance of tribosystems.

1.2. Analysis of methods for increasing the wear resistance of parts surfaces

Increasing the resistance of vehicle parts to fracture under various types of operational loads can be achieved by technological methods of bulk or surface hardening. Bulk hardening increases the static strength of parts in which the working stresses are distributed more or less evenly over the cross section. High-strength steels and alloys, composite materials are used for such parts. Most vehicle parts operate in conditions in which operational loads are perceived mainly by their surface layer.

Therefore, wear resistance, the initiation and development of fatigue cracks, and the occurrence of corrosion sites depend on the resistance of the surface layer to fracture. For parts of vehicles, the destruction of which begins from the surface, a large number of surface strengthening methods have been developed, based on the application of coatings or changes in the state (modification) of the surface [51-54].

When applying coatings, strengthening of parts of vehicles is achieved by depositing on their surfaces materials that differ in their properties from the material of the parts, but most fully meet the operating conditions (wear, corrosion, chemical exposure, etc.). All known strengthening methods can be conditionally divided into 6 main classes [55]:

1. Hardening with the creation of a film on the surface:

a) deposition by chemical reactions (oxidation, sulfidation, phosphating, application of a hardening lubricant, deposition from the gas phase);

b) vapor deposition (thermal evaporation of refractory compounds, cathode-ion bombardment, direct electron-beam evaporation, reactive electron-beam evaporation, electron-chemical evaporation);

c) electrolytic deposition (chromium plating, nickel plating, electrophoresis, nickel phosphating, boriding, borochroming, chromium phosphating);

d) spraying of wear-resistant compounds (plasma spraying of powder materials, detonation spraying, electric arc spraying, laser spraying, vortex spraying, induction cauterization of powder materials).

2. Hardening with a change in the chemical composition of the surface layer of the metal:

a) diffusion saturation (boriding, cyaniding, nitriding, nitrocarburization, etc.)

b) chemical and physicochemical effects (chemical treatment, ion implantation, electric spark treatment, etc.).

3. Hardening with a change in the structure of the surface layer [56, 57]:

a) physical and thermal treatment (laser hardening, plasma hardening);

b) electrophysical treatment (electrocontact, electrical discharge, magnetic treatment);

c) mechanical (vibration hardening, friction-hardening treatment, shot blasting, explosion treatment, thermomechanical, electromechanical);

d) surfacing of alloyed elements (gas flame, electric arc, plasma, laser beam, ion beam, etc.).

4. Hardening with a change in the energy reserve of the surface layer [58]:

a) treatment in a magnetic field (thermomagnetic treatment, pulsed magnetic field, magnetic field);

b) treatment in an electric field.

5. Hardening with a change in the surface microgeometry and hardening [59]:

a) cutting treatment (turning, grinding, high-speed cutting);

b) plastic deformation (rolling, rolling, rolling, smoothing, vibrorolling, vibrosmoothing, calibration, centrifugal impact hardening, etc.);

c) combined methods (anode-mechanical, surface alloying with smoothing, cutting with the influence of ultrasonic vibrations, magnetic-abrasive processing, etc.).

6. Strengthening with a change in the structure of the entire volume of the metal [60, 61]:

a) heat treatment at positive temperatures (quenching, tempering, normalizing, thermomagnetic treatment, etc.);

b) cryogenic treatment (quenching with cold treatment, thermal cycling).

These methods, aimed at strengthening the surface layers of tribocoupling parts of vehicles, also have disadvantages [1, 62, 63]. При легуванні і модифікуванні спостерігається підвищена витрата матеріалів, так як легуючий елемент розподіляється у всьому об'ємі заготовки, а зносу піддається тільки тонкий шар контактної поверхні металу. Велика кількість легуючих елементів йде в металобрухт зі стружкою при механічній обробці та відходами з ливниковою системою.

The disadvantages of the magnetic field processing method include grooving of the part during hardening. The disadvantages of strengthening parts by plastic deformation include a decrease in the thermal conductivity of the material as a result of plastic deformation and thereby an increase in the thermal stress of the unit and relatively low results in increasing wear resistance (only 8-10%).

The main disadvantages of volumetric heat treatment are: distortion of the part during hardening; residual stresses and uneven hardness across the part's cross-section; surface decarburization; formation of hardening cracks, especially with a large cross-section; high energy intensity of the process.

To improve the performance of vehicle parts, almost all traditional surface modification technologies and the application of wear-resistant and corrosion-resistant coatings are used. However, there is no universal method for strengthening parts, so the same method in some operating conditions can give a positive effect, and in others a negative one.

Therefore, in some cases, combined strengthening of parts is used, based on the use of two or three strengthening methods, each of which allows enhancing a certain performance characteristic of the resulting strengthened surface layer. In

addition, the choice of a particular method of surface strengthening is determined by economic considerations.

Thus, to increase the wear resistance of vehicle parts, it is necessary to apply surface strengthening technologies with functional coatings that would ensure both the proper economic level of the technological process of their formation and would exhibit effective operational characteristics in accordance with their purpose.

Significant research on improving the tribotechnical characteristics of vehicle parts is related to nitriding [64], the use of laser technology [65, 66], gas thermal spraying (GTP) [67], chemical (CVD) [68] and physical (PVD) deposition [69, 70] from the gas phase. Surface plastic deformation [71] and microarc oxidation [72] technologies are used for surface strengthening of vehicle parts.

1.3. Surface strengthening of parts with functional coatings

To improve the performance characteristics of vehicle parts, strengthening protective coatings are used. The use of strengthening protective coatings significantly expands the use of vehicle parts in friction conditions [73, 74].

To improve the performance characteristics of vehicle parts, technologies for applying wear-resistant and corrosion-resistant coatings are used [75, 76].

A significant amount of research is related to nitriding (Fig. 1.4) to create wear-resistant nitride on the surface of vehicle parts [77-81].

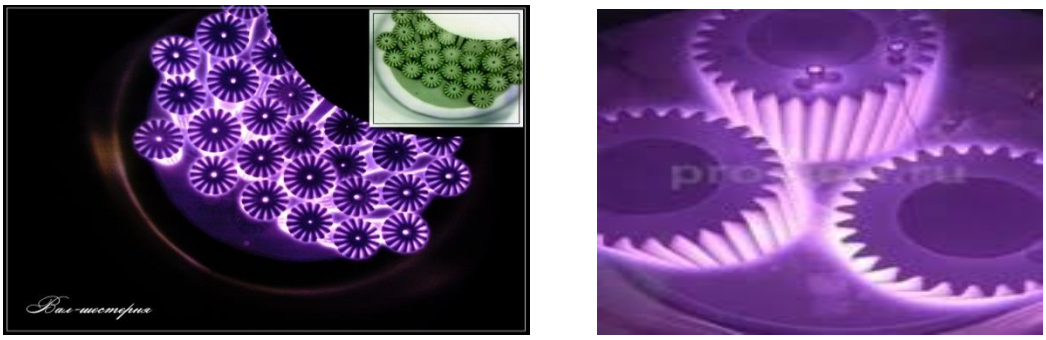

Fig. 1.4. Ion nitriding of internal combustion engine parts

Applying nitrides to the surface of vehicle parts is an effective method of protection against wear. Nitride-based composite coatings provide a high level of tribotechnical properties [82, 83].

Research involving laser technologies is spreading. Thus, in [84] it is shown the possibility of surface strengthening of vehicle parts by applying a slurry containing boron B, nickel Ni, chromium Cr and copper Cu with subsequent melting by a laser beam. Optimal hardness and homogeneity of coatings are achieved by using copper compounds Cu and chromium Cr in the composition of the charge.

Laser doping of the surface of vehicle parts is implemented from coatings, using the Charpy principle, according to which high wear resistance of tribocompounds is ensured by the inhomogeneity of the structure of the "hard inclusion in a soft matrix" type. Laser technologies (Fig. 1.5) are successfully used in industry for surface hardening of pistons and liners of internal combustion engines (ICEs) [85, 86, 87].

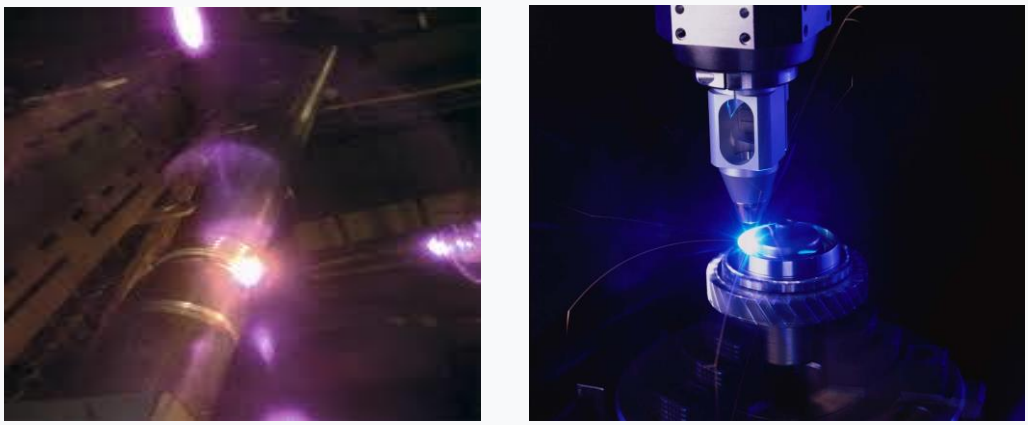

Fig. 1.5. Laser processing of vehicle parts

Gas thermal spraying (GTP) of vehicle parts (Fig. 1.6) has found wide industrial application [88]. Modern equipment for plasma spraying allows obtaining coatings from both dispersion-strengthened composite materials [89]. As

materials for applying wear-resistant coatings on the surface of vehicle parts by gas thermal spraying methods, Fe-C-Cr systems and others are used.

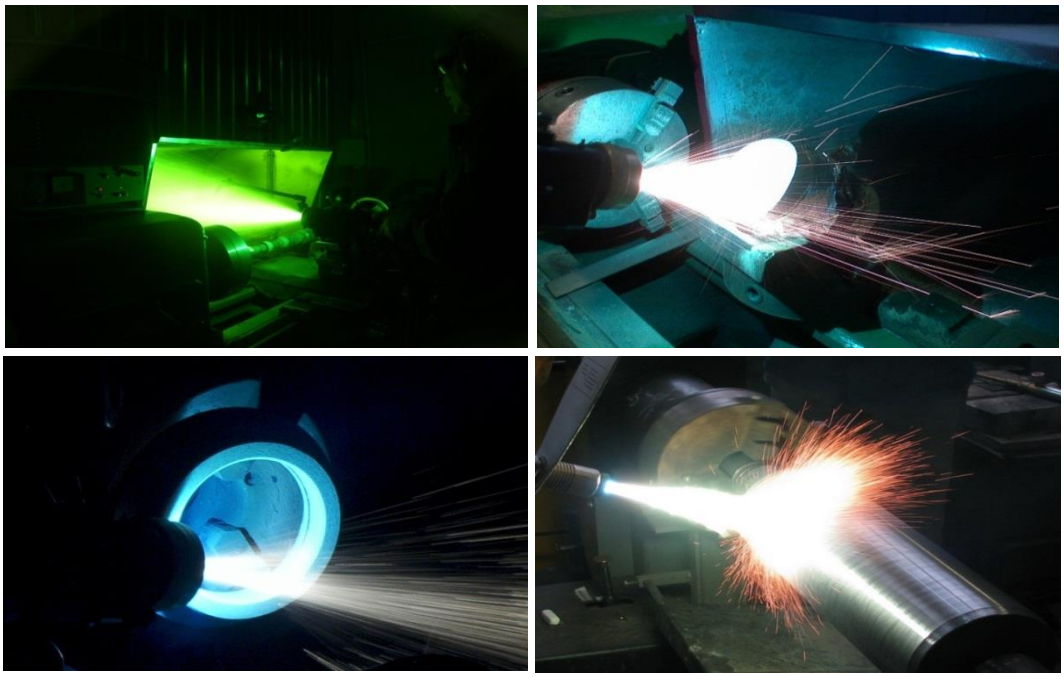

Fig. 1.6. Gas thermal spraying of vehicle parts

The tribotechnical characteristics of vehicle parts surfaces are improved by the method of high-speed fuel-oxygen spraying (HVOF) and activated electric arc spraying (EAS) [90]. The method of chemical vapor deposition (CVD) makes it possible to create a superhard coating of tungsten carbide WC with high wear resistance on the strengthening surfaces of parts [91]. For surface strengthening of parts, complex alloying of the surface with nickel Ni and titanium Ti, iron Fe and titanium Ti metals is used. Surface strengthening of parts by plasma spraying of powder materials is known [92].

To increase the wear resistance of the working surfaces of vehicle parts that are not available for coating by gas-thermal spraying methods (inner surfaces of cylinders, inner cavities of pistons, combustion chambers, etc.), technologies based on the principle of anodic spark processes in water-based electrolytes have been developed and are widely implemented [93, 94].

Anodic spark processes are also called microarc oxidation (MAO). In the process of microarc oxidation, complex oxides are created that are part of the complex anion of the electrolyte [95]. In the course of many studies [95-99], the peculiarities of oxide formation at electric field strength, which causes micro-breakdown of the coating, have been elucidated. Based on the results of the studies, it is possible to predict the thickness of the coatings (depending on the electric field strength within 300...1000 μm) and their porosity (up to 50% on the surface near the base [96]). Positive results in increasing wear resistance were obtained by combining the technology of micro-arc oxidation with the application of an outer layer of pyrolytic chromium [99].

Surface hardening of vehicle parts by physical vapor deposition (PVD) is at the research stage. Ion-plasma coating of titanium nitride (TiN) with a thickness of 10...15 μm reduces the wear intensity of parts by 50-60 times, and the friction coefficient is reduced by 1.5 times. This allows to increase the durability of parts by 1.5-2 times. A number of promising materials for ion-plasma coatings have been developed [100-103]. The structure of such coatings contains quasi- and nanocrystalline intermetallic phases, which provide a combination of high hardness, wear resistance and fracture toughness.

For surface strengthening of vehicle parts, traditional surface plastic deformation (SPD) methods are used. Impact riveting of the surface with rollers increases wear resistance and fatigue resistance [104]. The expansion of the scope of application of parts made of light metal alloys with a high level of tribotechnical properties became the basis for the development of combined coatings. In this direction, two main tasks are solved for vehicle parts: increasing the operating temperature of the metal by applying heat-protective barrier layers; increasing the wear and corrosion resistance of alloys by applying gradient ceramic coatings.

In [105], a scheme for applying a heat-protective barrier layer to the surface of vehicle parts using high-velocity oxygen-vapor (HVOF) spraying is proposed. Another scheme for applying ceramics to the hardened surfaces of parts [106, 107] involves the sequential gas-thermal application of a layer of aluminum powder

adjacent to the hardened surface of the part, then a layer of a mixture of aluminum with ceramic powder, and finally a surface layer of ceramic powder. After each spraying stage, the surface is irradiated with a laser beam. The ceramic content in the coating layers gradually increases to the outer surface. The coating obtained in this way is characterized by high wear and corrosion resistance.

1.4. Design and technological methods for increasing the durability of vehicle parts

When developing pistons for internal combustion engines, the main tasks are: reducing the mass of the piston, the mass of parts adjacent to it, and its operating temperature; improving the thermal state of the piston; increasing the wear resistance of the piston and its reliability [108].

To increase the durability of pistons, coating technologies have been widely used. The most common are galvanic, chemical-thermal and gas-thermal methods, as well as ion plating [109-111]. To protect the piston crown from burnout and reduce the temperature in the area of the first annular groove, hard anodizing is used [112]. A heat-protective coating on the crown, applied by the gas-thermal spraying method, increases the engine efficiency by 21% [113].

Traditional coatings used to increase the power of internal combustion engines are destroyed before the established period of their operation [113]. This circumstance requires constant improvement of coating application technologies. The design features of the annular groove (height - 2...3 mm and depth - more than 5 mm) limit the possibilities of traditional coating application technologies. Positive results in strengthening the shelves of the annular groove of pistons were obtained by: electron beam and laser technologies [114-121]; chrome plating; frictional-mechanical rubbing, which is a variant of chemical-thermal treatment (CTP) in the solid phase and uses friction heat.

To strengthen the pistons of automobile and tractor internal combustion engines, technological methods of arc surfacing with additional alloying of the molten bath with a special material or electrode wire are used. To restore and strengthen diesel pistons, a technology of pulsed arc surfacing with a melting electrode has been developed. A flux-cored wire is used as a melting electrode. This allows: to change the chemical composition of the deposited metal in wide intervals: to vary the composition of the components in the charge. The deposited metal has a fine-grained structure with a uniform distribution of excess phases, which ensures its increased wear resistance [73, 121].

A technology of double-arc surfacing of pistons has been developed, which is used in automobile and tractor internal combustion engines. The work [122] presents the technological features of surfacing of pistons of automobile engines with an electrode of lanthanated tungsten of the EVL brand with a diameter of Ø 10 mm. In this case, the hardness of the metal increases from HB 85…90 to HB 160…170. Operational tests have shown that at a hardness of HB 160…170, the resistance of the metal to abrasive wear and dynamic loading increases. To increase the wear resistance of the upper piston groove, plasma-arc remelting of the groove zone with alloying of the melt with nickel Ni, chromium Cr and iron Fe metals to a depth of up to 10 mm is used [123].

Production and operation of pistons, along with advantages, have specific disadvantages. Thus, a high-strength insert in the annular groove area increases wear resistance and ensures uniform wear of parts of the cylinder-piston group. However, this method has the following disadvantage - due to the high specific gravity of the insert, the mass of the piston increases.

The increase in piston mass leads to an increase in the dynamic stress of internal combustion engines and as a consequence: a decrease in the fatigue life of the crankshaft and increased wear of bearing liners; an increase in the cost of production technology. The technology of casting a piston with a cast iron insert (the so-called Alfin process) is 2 times more expensive than casting a piston without an insert [124].

Arc surfacing of the annular groove zone also has a number of disadvantages [119, 123]: relatively low process productivity, which requires the use of wires made of composite materials; dispersed phases are unevenly distributed in the surfacing metal, which leads to its destruction during the operation of pistons; the need for preliminary processing of the edges in the piston body when surfacing with a flux-cored wire; intensive spattering of the electrode material; increased porosity of the surfacing metal, which requires an increase in its density.To eliminate the shortcomings of arc welding, the O.E. Paton Institute of Electric Welding of the National Academy of Sciences of Ukraine has developed a technology for local strengthening of pistons by arc welding [124].

The use of various methods of strengthening vehicle parts by applying coatings is not always economically feasible, and in some cases is complicated by excessive overheating of parts (with pulsed arc welding, gas flame and plasma spraying) or due to insufficient hardness and adhesion of the coating to the base.

In the conditions of market relations and Ukraine's dependence on imported supplies, the most suitable for industrial use is the technology of electric spark alloying. Analysis of literary sources indicates the prospects of using the technology of electric spark alloying to improve the performance of vehicle parts.
The use of electric spark alloying in modifying the surface layers of vehicle parts provides advantages compared to other technologies that are based on the use of energy-saving technology and increasing the scientific intensity of technological support for surface hardening.

Due to its simplicity and energy saving, electric spark alloying is the most suitable for restoring the dimensions of worn machine parts and strengthening them [125].

Depending on the type of electrode, it is possible to obtain both a high-strength, wear-resistant coating and a coating with the lowest coefficient of friction resistance. The process of electric spark alloying with copper, titanium or tungsten electrodes leads to the formation of various intermetallic phases in surface layers

with a thickness of 25-50 microns, which affects the relaxation resistance of the alloy under cyclic loads and thermal effects.

Establishing the kinetics of the formation of metastable dissipative structures, taking into account the energy characteristics of tribosystems when strengthening the surfaces of vehicle parts with electric spark coatings, will allow controlling wear control processes by creating wear-resistant secondary structures, which will provide an opportunity to expand the range of serviceable state of strengthened parts.

However, to improve the quality of the electrospark alloying process, it is necessary to take into account the degree of continuity of the coating, its microgeometric and strength characteristics. A comprehensive assessment of the quality of electrospark alloying will allow developing technological recommendations for their application using multifunctional electrodes, which will ensure the formation of a wear-resistant coating.

Conclusions on section 1

The requirements for high manufacturability of the production of vehicle parts are determined by their strengthening technologies, the optimal choice of structural materials and a favorable combination of their antifriction and mechanical properties, manufacturability and cost. Most surface strengthening technologies should be considered as alternative. Therefore, an analysis of surface strengthening technologies was carried out, primarily an analysis of their indicators such as the durability of vehicle parts, the cost of equipment and its energy consumption, and the ecological impact on the environment.

In the conditions of market relations and Ukraine's dependence on imported supplies, the most suitable technology for industrial use is the electrospark alloying technology. Analysis of literary sources indicates the prospects for using the electrospark alloying technology to improve the performance of vehicle parts, primarily internal combustion engine parts.

The use of electrospark doping in modifying the surface layers of vehicle parts provides advantages compared to other technologies that are based on the use of energy-saving technology and increasing the scientific intensity of the technological support of surface hardening. However, to improve the quality of electrospark coatings, it is necessary to take into account the degree of continuity of the coating, its microgeometric and strength characteristics. A comprehensive assessment of the quality of electrospark coatings will allow developing technological recommendations for their application using multifunctional electrodes that will ensure the formation of a wear-resistant coating.

To assess the wear resistance of the hardened surfaces of vehicle parts, it is necessary to establish the mechanisms of mechanical, physical, and chemical changes that occur in the process of structural adaptation during friction. A promising direction in this regard should be the involvement of the basic provisions of the molecular-mechanical and structural-energy theories of friction, which will allow us to identify the main changes occurring in frictional contact and determine the dominant factors that ensure an increase in the wear resistance of tribosystems.

Establishing the kinetics of the formation of metastable dissipative structures, taking into account the energy characteristics of tribosystems when strengthening the surfaces of vehicle parts with electric spark coatings, will allow controlling wear control processes by creating wear-resistant secondary structures, which will provide an opportunity to expand the range of serviceable state of strengthened parts.

CHAPTER 2
ELECTROSPARK COMPOSITE WEAR-RESISTANT COATINGS

2.1. General Characteristics of the Electrospark Alloying Process

Among the various methods for improving the physicochemical and mechanical properties of the surfaces of parts made of aluminum and its alloys, the electrospark alloying (ESA) method is promising [126 –138]. The method of applying wear-resistant coatings by electric spark alloying is based on the use of a concentrated energy flow—a plasma jet of spark discharge [133, 134, 139].

The electric spark alloying method is distinguished by [133, 134 and 139]:

- low energy consumption of the process;
- environmental friendliness;
- simplicity of the process, which does not require highly qualified personnel;
- compact equipment dimensions (Fig. 2.1);
- the ability to apply coatings locally to conductive materials;
- coating application both in a mechanized version (with process automation) and using a manual vibrator.

The comparative characteristics of plasma spraying and electric spark alloying systems presented in Table 2.1 demonstrate the advantages of EIL equipment in terms of power, dimensions (Fig. 2.1), material utilization rates, and the absence of surface pretreatment.

An analysis of economic indicators (electricity consumption and equipment set cost) when replacing chemical-thermal treatment with laser, discrete-laser, and discrete-electrospark technology [140-143] is presented in Table 2.2.

Thus, the greatest savings in the selection of alternative surface hardening technologies are achieved by transitioning from traditional chemical-thermal treatment methods to promising methods based on the use of highly concentrated

energy sources. For example, the transition from traditional high-frequency current hardening to electric spark alloying provides [130–140]:

- significant energy savings;

- 10 times lower power requirements for electric spark alloying equipment compared to high-frequency current equipment, while maintaining the same duration of the EIL and microwave hardening processes;

- a tenfold reduction in capital expenditures for a set of equipment for electric spark alloying compared to the cost of high-frequency current hardening equipment;

- a reduction in the required effective production floor space.

Table 2.1

Comparative characteristics of coating application systems

Equipment	Power, kW	Dimensions, m	KVM, %	Pretreatment
For plasma spraying (UPU, Kyiv-7, APR)	8…120	length 5.4…7.2 width 3.6…4.4 height 0.5…1.8	35…80	Sandblasting machines
For EIL (Elitron)	0,4…0,8	length 0.37…0.65 width 0.27…0.45 height 0.15…1.20	40…90	Not required

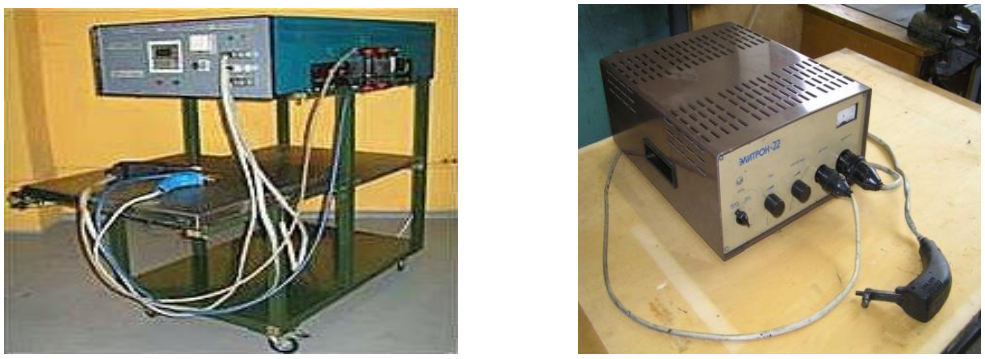

Fig. 2.1. Example of equipment for electric spark alloying

A comparison of high-frequency current hardening and electric spark alloying technologies reveals the advantages of ESA in terms of power consumption, equipment size, material utilization, equipment cost, and the need for

surface pretreatment. However, it is мimpossible to implement the technology of electric spark alloying of aluminum and its alloys using traditional electrode materials (metal alloys and composites based on metal-like refractory compounds) due to aluminum's low melting point.

Table 2.2

Economic and energy performance indicators for surface hardening technology

Hardening Method	Indicators			
	Electricity Consumption		Cost of Equipment Set	
	Thous. kWh	Savings, times	Thous. UAH	Ratio, times
Chemical-thermal treatment	5550	1	324,6	1
Laser treatment	116	48	732	in 2,25 times more expensive
Discrete laser method	23,2	239	732	in 2,25 times more expensive
Discrete electric spark method	3,9	1420	30	in 10,8 times cheaper

There are three main areas of development in the electric spark alloying method:

- in a gas atmosphere using a solid electrode [139, 144, 145];
- in a gas atmosphere using powdered material [139, 146, 147];
- in an electrolytic plasma [33, 139].

The latter option made it possible to develop the most widespread technology of micro-arc oxidation (MAO) [148–150]. Of these approaches, the method of electric spark alloying in a gas environment using a solid electrode has found the widest application and development [139, 144, 145]. The essence of the method lies in the fact that during a spark discharge in a gas environment, erosion of the anode material occurs and the erosion products are transferred to the cathode (the surface of the workpiece being strengthened), on the surface of which a layer with a modified composition and structure is formed, both due to material transfer

and as a result of the impact of pulsed and thermal loads arising during electric spark alloying [151–155].

The technology for surface hardening by the method of electric spark alloying of steels and titanium alloys is described in the literature [156–158]. Information on surface hardening by the method of electric spark alloying of aluminum alloys is limited. This is due to aluminum's low melting point (660°C), which causes its intense erosion during electric spark alloying. Therefore, it is impossible to implement the technology of electric spark alloying of aluminum alloys using traditional electrode materials due to cathode mass loss.

Detailed studies of the electric spark alloying process for AK-4 and AL-25 aluminum alloys are presented in [215]. The following materials were used as electrodes: iron (Fe), titanium (Ti), copper (Cu), hard alloys VK-2, VK-4, VK-6, VK-8, T16T, T15K6, and aluminum-based alloys AL-25 [145-147, 215]. Alloying was performed on mechanized equipment, assembled with a lathe equipped with an EFI-25M pulse generator, operating at working currents of 80–100 A [1, 131, 135, 139, 158, 215].

The results of the studies showed that alloying the AL-25 aluminum alloy with hard alloy electrodes is accompanied by a loss of cathode mass. When alloying AK-4M and AL-25 aluminum alloys with materials having a melting point similar to that of aluminum, the cathode mass increases under certain electrical conditions [215]. The cathode growth can be controlled by changing the parameters of electric spark alloying, for example, the duration of the spark discharge pulse.

Figure 2.2 shows the dependencies of the cathode weight gain for the AL-25, D16, and AK-4 alloys on the pulse duration in the range of 200–1000 μs [215]. The cathode growth was measured at an operating current I_{work} = 10–15 A. The obtained dependencies show that stable cathode growth is achieved at pulse durations ranging from 600 to 900 μs. At the same time, as the content of alloying additives in the alloys increases, the pulse duration during their processing should decrease within the specified range.

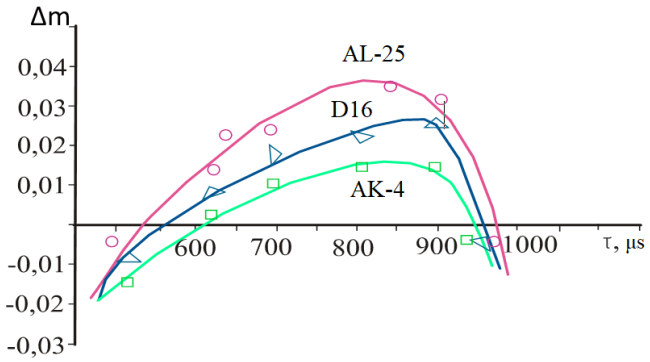

Fig. 2.2. Relationship between the weight gain of aluminum alloys and the duration of the spark pulse

A characteristic feature of electro-spark coatings on AL-25 aluminum alloy [215] when alloyed with copper electrodes is the formation of individual “islands” with a height of 0.8–1.5 mm. During copper alloying, high hardness of the alloyed layer (2.1–2.2 GPa) and high adhesion strength (0.08–0.1 GPa) are observed due to the formation of the intermetallic compound $AlCu_2$ and copper oxide in the alloyed zone [215]. The efficiency of the electric spark alloying process using copper electrodes is largely determined by the selected process parameters – current intensity (I) and the number of passes (n) of the alloying electrode.

Mass transfer during electric spark alloying of aluminum alloys using different classes of electrode materials was investigated in both manual and mechanized versions [136, 153–155]. It was established that the extent of erosion of the aluminum cathode significantly depends on the nature of the electrode material and correlates with its melting point.

Given the importance of addressing the issue of improving the wear resistance of aluminum alloys via electrospark alloying with composites based on refractory compounds, measures were taken to eliminate the electroerosion of the aluminum cathode by [151, 152]:

- spark alloying through a layer of metal powder poured onto the cathode surface;

- metered powder feeding, which was performed from a hopper equipped with a special metering device.

It was assumed that the powder would serve as a shield and ensure an increase in the cathode's mass. Experiments showed that when powder is fed during electric spark alloying, cathode erosion decreases sharply, regardless of the nature of the powder material.

The hardness of the formed coatings is close to that of the deposited materials. Thus, when feeding TN-20 powder (80% TiC, 20% Ni), the coating hardness reached 17–18 MPa [130, 216.

The authors of [151, 152] attribute the sharp reduction in cathode erosion to the redistribution of discharge energy within the anode-interelectrode gap-cathode system and the additional heating of powder particles by short-circuit current.

Electroslag alloying of the D16T aluminum alloy with nickel- and graphite-based powder mixtures significantly increases wear resistance [217-220]. The coating shows virtually no wear at a sliding speed of 0.01 m/s and a contact zone pressure of 1–2 MPa over a period of 10 –12 hours [221]. The results of studies [146, 147, 151, 152, 205–208] indicate that by feeding powder materials into the interelectrode gap (IEG), it is possible to obtain electric-spark coatings of refractory materials on aluminum alloys without loss of cathode mass and to create wear-resistant friction pairs.

It should be noted that feeding powder into the interelectrode gap significantly complicates the technology, increases its cost, and complicates the automation of the electric spark alloying process. The explosive nature of the spark discharges leads to significant powder losses due to its dispersion. Powder electro-spark alloying imposes restrictions on the geometric shapes of the workpiece. For these reasons, the powder variant of electro-spark alloying has not found widespread practical application [139, 146 and 147].

The conducted research has demonstrated the feasibility of the electric spark alloying process for aluminum and its alloys with cathode mass gain through the redistribution of energy in the interelectrode gap by varying the electrode composition. This approach was developed and implemented at the I.M. Frantsevich Institute for Problems of Materials Science of the National Academy

of Sciences of Ukraine [135]. This fundamentally new approach made it possible to create composite electrode materials using powder metallurgy. This ensured a stable increase in cathode mass, which led to the creation of a series of wear-resistant electrospark coatings on aluminum alloys.

The authors [135] utilized the principle of new-generation multifunctional electrodes. One of the main functions of such an electrode is the creation of a shielding cloud in the interelectrode gap. The decisive factor ensuring positive cathode growth is the presence of non-conductive phases in the electrode's electroerosion products, which form in the interelectrode gap in sufficient quantities to suppress cathode erosion [135].

The increased wear resistance of new-generation electric spark coatings is achieved by the formation of polyoxide tribofilms on the coating surface, which are formed under non-equilibrium conditions of the tribo-oxidation process. The composition of the tribofilm, which determines the wear resistance of the coating, is predicted by the selection of the electrode composite material's composition [135]. In the electrospark alloying of aluminum alloys, the function of selectivity in the wetting of electrode electroerosion products by the aluminum melt of the cathode was realized for the first time. The leading role of substrate material wetting of electrode electroerosion products in the formation of electrospark coatings was established.

Electrospark alloying technology is a structure-forming technology controlled by the selection of structural components of the composite multifunctional alloying electrode material [135]. Electrode materials science has become a progressive field in electrospark alloying technology [1, 128, 158, 214, 222, 223].

2.2. Generalized model of the electrospark alloying process

Addressing the materials science aspect of the problem of electric spark alloying is impossible without understanding the process model, which

includes the physical nature of the phenomena occurring on the working surfaces of the electrodes and in the interelectrode gap under spark discharge conditions [135, 136].

Let us consider a model of the electric spark alloying process for the non-mechanized vibrational type of alloying, which differs from the non-vibrational mechanized ESA by the presence of electrode contact and their vibration [135, 136]. This results in increased mechanical loads on the electrode material and a higher level of their physicochemical interaction. The main provisions of the model also apply to the non-vibrating mechanized process of electric spark alloying.

According to the generalized model of the non-mechanized vibrational alloying process (Fig. 2.3) [134], the spark discharge exerts a pulsed thermal and mechanical effect on the electrodes.

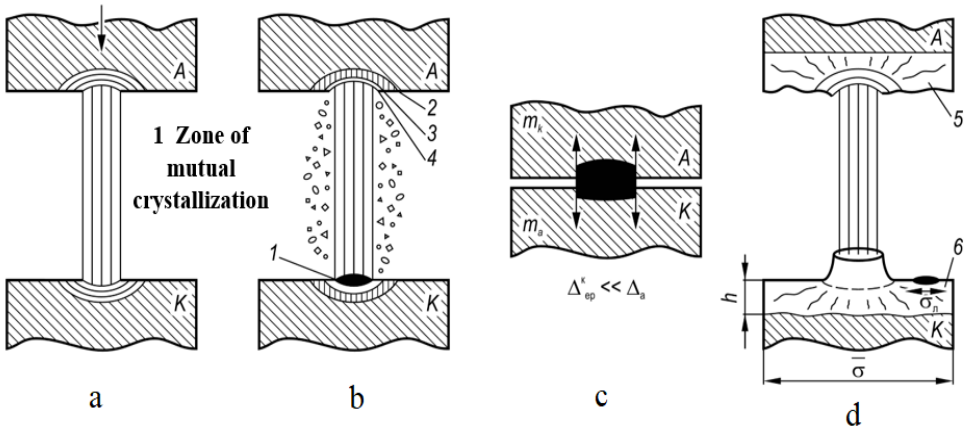

Fig. 2.3. Generalized model of the electric spark alloying process:

a) breakdown of the interelectrode gap;

b) formation of erosion pits – 1 on the anode and cathode, comprising three zones: evaporation – 4, melting – 3 and stress –2;

c) the moment of electrode contact, accompanied by welding and reverse transfer; d) formation of a secondary structure on the anode – 5 and a doped layer on the cathode – 6.

The electron flow leads to local heating of the electrode (anode), and in the transverse magnetic field, high pressure is created in the plasma discharge cord, in

which the average electron temperature $T_e \approx (5…7) \times 1000$ K is realized with an average electron density $n_e \approx (4–13) \times 10^{-16})$ cm^{-3} (Fig. 2.3, a).

As a result of this effect, volumetric heat sources appear on the electrode surfaces, leading to the formation of erosion pits on the anode and cathode. Within the pit itself, three zones can be distinguished: evaporation, melting, and stress (Fig. 2.3, b). The size of the melting and evaporation zones increases as the melting temperature T_{melt}, boiling temperature T_{boil}, and thermal conductivity coefficient of the electrode material λ decrease.

The stress zone arises due to thermal and thermomechanical stress waves resulting from pulsed heating, the reactive action of the plasma jet, and its expansion at the moment of current decay in the pulse [136].

In [135], it is shown that the variation of thermal stresses arising in the surface layer under the action of a pulsed heat source is wave-like in nature, with stresses varying from compressive to tensile stresses, decaying with increasing distance from the heat source.

High tensile stresses on the working surface of the electrode are the main cause of crack formation and solid-phase erosion, whose contribution to the overall erosion effect depends on the processing conditions and the covalence of interatomic bonds in the anode material [135, 152].

The plasma jet contains elements of the anode material and impurities of the cathode material. In the microzone on the cathode, intense mixing and chemical interaction of the cathode material with the transferred anode material occur not only in the liquid and vapor phases but also in the solid phase, with solid-phase anode material particles measuring 1–2 μm not adhering but lying on the cathode surface. The subsequent moment of mechanical contact between the electrodes is also accompanied by intense chemical interaction of the materials, which may lead to electrode welding and the transfer of material from the cathode to the anode due to the Thomson, Köller, and Peltier effects.

The main conclusion from the consideration of the generalized model of the electric spark alloying process is the need to account for the physicochemical

interaction of the products of electrode material electroerosion with each other and with the cathode material in the interelectrode gap and on the electrode surfaces, taking into account high-temperature oxidation and reverse mass transfer.

2.3. Kinetics of mass transfer and phase formation during electric spark alloying

Mass transfer of electroerosion products from the anode to the cathode is characterized by the mass transfer coefficient K, which is equal to the ratio of the total mass gain of the cathode $\sum \Delta_k$ to the total erosion of the anode $\sum \Delta_a$ over the processing time t:

$$K_t = \sum \Delta_k / \sum \Delta_a \qquad (2.1)$$

The maximum value of the mass transfer coefficient, which ranges from 60% to 90% for steels and titanium alloys, is one of the conditions for the effectiveness of the electric spark alloying process. In cases where the electrical erosion of the cathode material exceeds the mass gain resulting from the transfer of anode material, a decrease in cathode mass occurs ($\sum \Delta_k < 0$) and the mass transfer coefficient loses its physical meaning, taking on negative values. This is precisely the situation that occurs during the electro-spark alloying of low-melting-point metals, including aluminum, using traditional electrode materials—metal alloys and composites of the “metal-like refractory compound–metallic binder” system [153].

Fig. 2.4 shows the mass transfer kinetics in conjunction with changes in the composition of the anode and cathode materials during the electrospark alloying of steel with nickel [153]. In all cases, the total increase in cathode mass according to the gravimetric method (curve 2) is less than the nickel content in the steel (curve 1). This is despite minimal degradation of the cathode material (iron) during the

electric spark alloying process. As a rule, the increase in cathode mass tends toward saturation (curves 1, 2) with prolonged processing time.

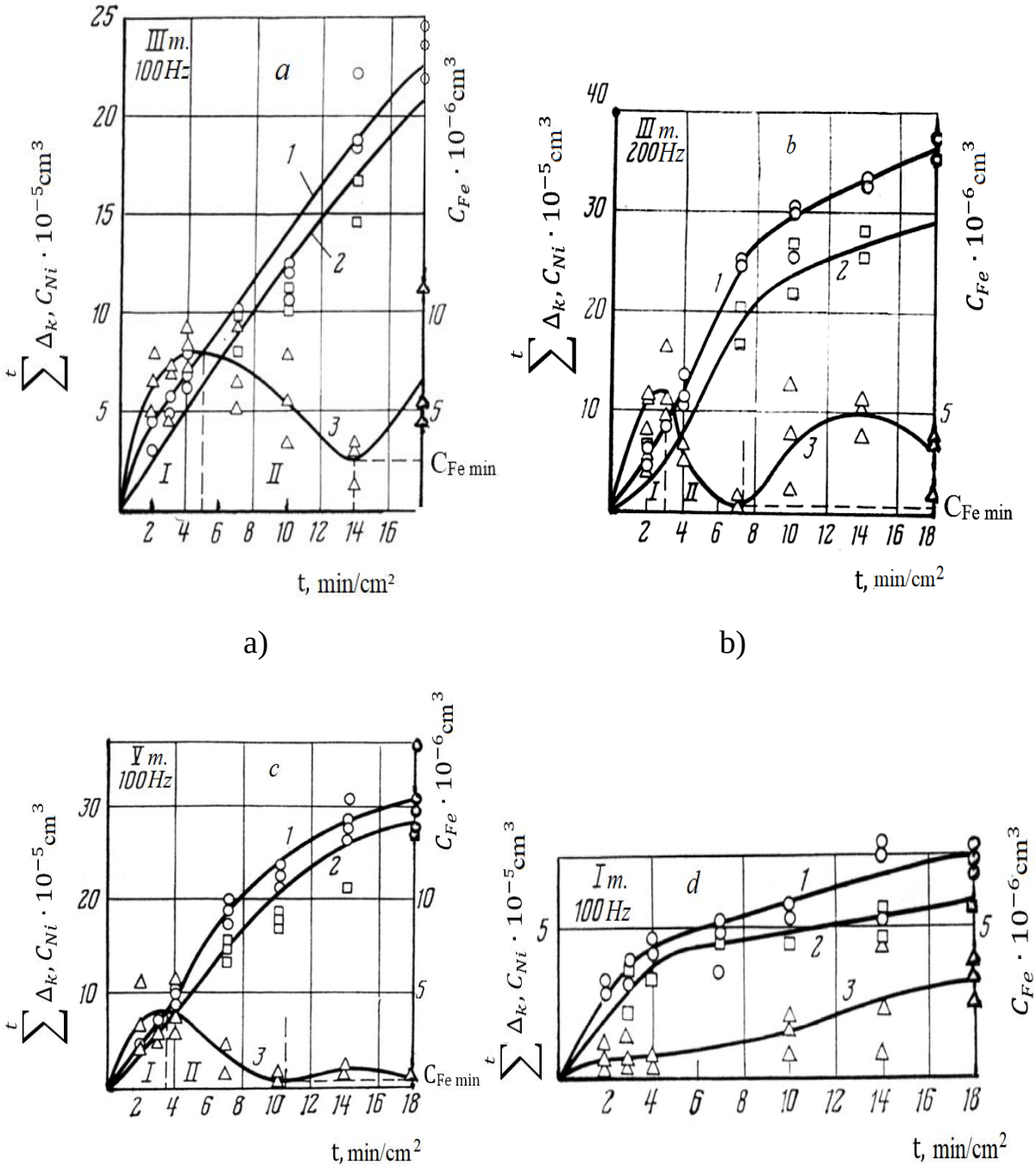

Fig. 2.4. Mass transfer kinetics for different modes of electric spark alloying of steel 55 with nickel:

1 – nickel content in steel 55 (C_{Ni}), determined by atomic absorption spectroscopy;

2 – total cathode growth ($\sum \Delta_k$);

3 – iron content in the Ni anode (C_{Fe});

a) Mode III – 100 Hz; b) Mode III – 200 Hz;

c) Mode V – 100 Hz; d) Mode I – 100 Hz.

The formation of the surface layer during electric spark alloying is a dynamic process in which, within a single cycle, erosion and transfer of anode material to the cathode occur, as well as constant mutual movement of the electrodes [133, 134, 139, 151–155]. The transfer of electrode material to the workpiece, which is a specific feature of electric spark alloying and occurs under normal conditions, has a limit (varying for different modes and materials) that corresponds to the maximum on the cathode mass gain curve (Fig. 2.5).

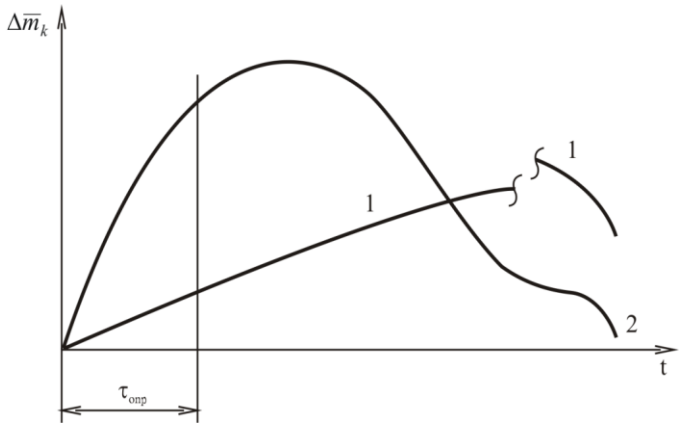

Fig. 2.5. Dependence of mass gain on processing time for mild (1) and coarse (2) modes of electric spark alloying

The limitation on coating thickness is evident in the kinetic curves of the specific weight gain of the cathode (Fig. 2.6, a) [153]. The cathode growth per minute of treatment decreases at a specific duration $t \geq 4$ min/cm², which characterizes the brittle fracture threshold of the alloyed layer t_x. This limitation on the thickness of the alloyed layer is due to several factors [158], the main ones being:

– brittle fracture of the coating due to internal stresses arising from the pulsed thermomechanical effect of the spark discharge and differences in the thermal expansion coefficients of the phase components in the layer;

– the formation of a dispersed structure;

– the formation of a secondary structure on the anode's working surface via reverse mass transfer from the cathode to the anode [153].

The secondary structure arises due to the pulsed thermomechanical effect of the spark discharge, which leads to the densification of the anode's surface layer and grain refinement, as well as due to the interaction of the anode material with elements of the interelectrode medium and with the cathode material (as a result of reverse transport), which leads to surface modification.

Taken together, this generally results in an increase in the erosion resistance of the anode material or its fluctuation as the duration of the electrospark alloying process (t) increases (Fig. 2.6, b). Reverse mass transfer of material (from the cathode to the anode) is one of the most important factors in the formation of the secondary structure on the anode. Atomic absorption spectroscopy data indicate the non-stationary nature of this process (curves 3, Fig. 2.4).

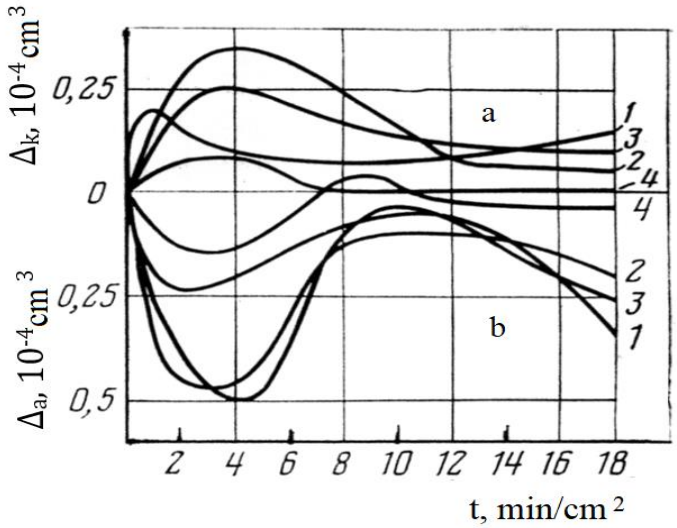

Fig. 2.6. Kinetic dependencies of the specific cathode weight gain Δ_k (a) and anode erosion Δ_a (b) during electric spark alloying of 55 steel with nickel for different processing modes: I) Mode III – 100 Hz; 2) Mode III – 200 Hz; 3) Mode V – 100 Hz; 4) Mode I – 100 Hz

During the initial stage of electric spark alloying ($t \leq 2$ min/cm²), the concentration of anode and cathode materials in the opposite electrode increases,

with the reverse transport (C_{Fe}) being consistently lower than the forward transport (by an order of magnitude).

During the time t = 2 min/cm², a secondary structure forms on the anode due to reverse mass transfer and the interaction of the anode material with elements of the interelectrode medium—oxygen O_2 and nitrogen N_2 (Stage I).

However, with a further increase in the duration of the electric spark alloying process (t), the amount of iron in the anode (C_{Fe}) decreases (Stage II), which is associated with the destruction of the anode's working surface under the action of cyclic loads from spark discharges, initiated by the formation of brittle oxide and nitride phases in the near-surface layer of the anode.

Thus, the kinetics of reverse mass transfer is divided into two stages associated with the formation of the secondary structure (Stage I) and its destruction (Stage II) [153–155]. The frequency of cycles of destruction and restoration of secondary structures increases with the growth of pulse energy and with an increase in pulse frequency (Fig. 2.6, curves 3).

External thermomechanical and physicochemical effects inevitably lead to the destruction (erosion) of secondary structures, but these same effects and the associated transport processes from the cathode and the interelectrode medium ensure the regeneration of the secondary structure on the anode during prolonged treatment. During the process of electric spark alloying, electrical erosion of the electrode material occurs.

The products of electrical erosion interact in the liquid-vapor and solid phases with the workpiece material and atmospheric oxygen in the molten pool on the working surface, where active mechanical mixing takes place [141, 157]. At the same time, despite the short duration of the electrical pulse (t = 10^{-3} s), conditions are created in the interelectrode gap for thermally activated plasma-chemical reactions to occur. This is ensured by the high plasma temperature ($5 \times 10^3 \ldots 10^4$ °C) and the presence of an ion-plasma phase in the flow of eroded anode material [151].

The high temperature and ionization of the eroded particles activate plasma-chemical reactions and diffusion processes in the interelectrode medium, creating conditions for high-temperature oxidation of the components and their interaction leading to the formation of new phases. As a result, electrospark coatings are formed, the phase composition of which differs from that of the alloying electrodes [141].

2.4. Features of electrospark alloying

Given the absence of high-hardness intermetallic compounds in aluminum, there is potential for developing surface hardening methods—including electric spark alloying—that would ensure the formation of structures on the surfaces of aluminum and aluminum alloy components, structures not determined by the phase diagrams of aluminum alloys [224], but rather by the formation of composite materials involving refractory compounds to effectively improve the physical and mechanical properties of aluminum alloys. In this regard, it is advisable to apply protective coatings using refractory compounds as the deposited material, which allow for a significant increase in the wear, heat, and corrosion resistance of the material on the surfaces being hardened.

2.4.1. Electrospark Alloying with Compact Electrodes

Detailed studies of the electrospark alloying process for AK-4 and AL-25 aluminum alloys were conducted in [215]. The greatest cathode growth is achieved when hard facing with D16T and aluminum alloys, while the highest mass transfer coefficient is observed during electric spark alloying with copper and the AL-25 alloy.

The efficiency of the electric spark alloying process of AL-25 and AK-4M alloys with copper is largely determined by the selected process parameters:

a) the number of passes of the alloying electrode (n). The number of passes of the alloying electrode affects the mass transfer coefficient. A decrease or increase of two to three passes relative to the optimal value (n = 4) reduces the mass transfer coefficient by a factor of 3 to 4;

b) the short-circuit current ($I_{welding}$). As the short-circuit current increases to a value of ≤ 100 A, the amount of material transferred from the anode surface to the cathode surface increases. At the same time, the hardness of the surface layer remains virtually unchanged. At a short-circuit current greater than 100 A (I welding > 100), the hardness of the alloyed layer decreases.

However, alloying at operating currents higher than 20 A is not justified, as it is known from the practice of electric spark alloying [133, 134] that when processing steels, titanium alloys, and other materials, the best results are obtained when alloying at operating currents up to 5 A. Exceeding this value leads to the formation of a large number of defects (pores, cracks) in the surface layers, unevenness of the coating itself, as well as high residual stresses within it, which in some cases exceed the tensile strength of the cathode material. These defects manifest during the spark alloying of aluminum. Thus, even if surface hardening of aluminum under the specified conditions increases surface hardness, such a surface ultimately becomes unsuitable for use due to defects.

Mass transfer during electric spark alloying of aluminum grades A95, A5, and aluminum alloys AD-31, AK-4, D16T, D20, AL-3, AL-25 and SAP-1 was investigated in the work [136, 154, 155] for various classes of electrode materials. The process was carried out in both manual and mechanized versions. The following materials were used as electrode materials [144-147, 215:

- metals: lead (Pb), zinc (Zn), aluminum (Al), magnesium (Mg), nickel (Ni), titanium (Ti), chromium (Cr), molybdenum (Mo), tungsten (W), and carbon (C);

- carbides: tungsten (WC), titanium (TiC), and a composition (TiC + Ni).

It was noted that the extent of aluminum cathode erosion significantly depends on the nature of the electrode material and correlates with its melting point. When using electrodes made of low-melting materials such as lead (Pb),

zinc (Zn), and tin (Sn), the amount of electrode electroerosion products transferred to the cathode—primarily in the liquid phase as a result of spark discharges—exceeds the erosion of the cathode material. Consequently, over time, the mass of material arriving at the cathode will gradually increase, and thus the total mass of the cathode will also increase.

As the melting point of the alloying electrode material increases, the amount of electroerosion products ejected from the surface per electrical pulse decreases. In this case, cathode erosion outweighs the transferred anode material, and its mass gradually decreases. A histogram of the change in the mass of an aluminum cathode during electric spark alloying with various materials is shown in Figure 2.7 [151-155].

As can be seen from Figure 2.7, an increase in cathode mass occurs only during its electrospark alloying with metals having a melting point lower than that of aluminum. Alloying with metals having a melting point higher than that of aluminum results in cathode erosion exceeding the mass gain due to the transfer of electrode electroerosion products (i.e., the cathode mass decreases).

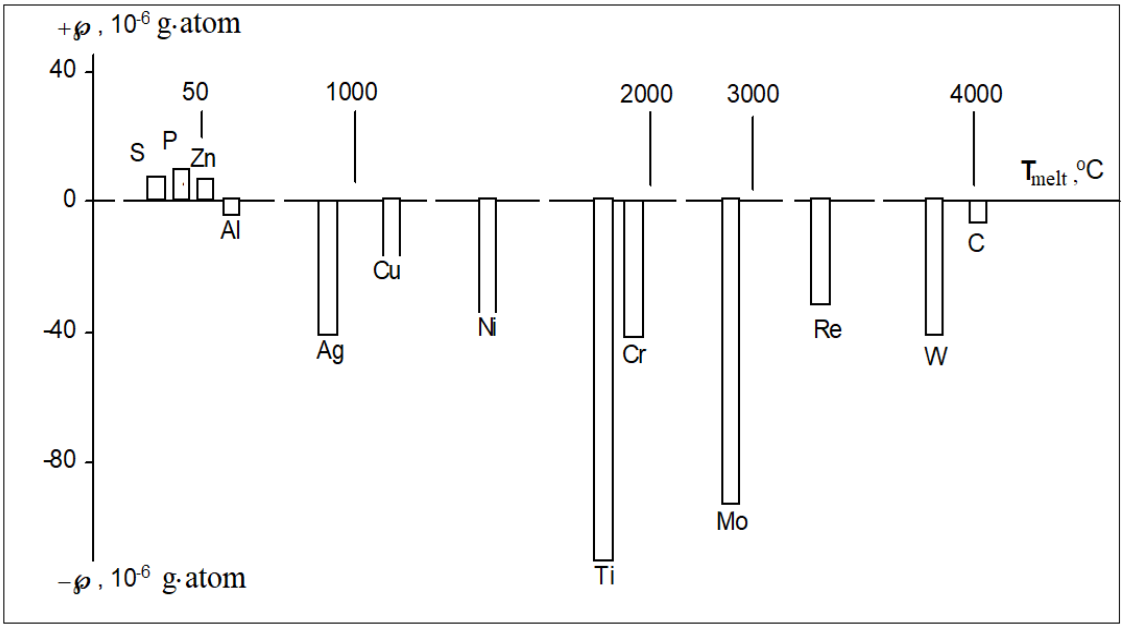

Fig. 2.7. Histogram showing the change in the mass of the aluminum cathode as a function of the melting temperature (T_{melt}) of the anode material (discharge energy 0.3 J, alloying time 1 min/cm²)

Metallographic and X-ray phase analyses of samples alloyed with low-melting-point metals have shown [151–156] that the surface layers consist mainly of electrode material. For example, in the electric spark alloying of aluminum with zinc, the formed coating consists of pure zinc and a small amount (3%) of zinc oxides (ZnO_2), which are formed as a result of the interaction of zinc with oxygen in the air.

During electric spark alloying using electrodes made of metals with higher melting points than aluminum, despite significant erosion of the aluminum cathode, a certain amount of anode material reaches its surface and interacts with it. Thus, on the surface of the aluminum cathode after treatment with chromium, nickel, and copper, the intermetallic compounds $CrAl_7$, NiAl, $NiAl_3$, and $CuAl_2$ were detected. Thus, the obtained data show that during electric spark alloying with compact electrodes on aluminum, layers can be deposited only when using anodes made of low-melting-point metals—lead (Pb), tin (Sn), zinc (Zn), and others—whose melting points are lower than that of aluminum. Processing with electrode materials having a melting point higher than that of aluminum always leads to predominant cathode erosion, and the process may be accompanied by surface modification.

Given the importance of improving the wear resistance of aluminum alloys through their spark alloying with composites based on refractory compounds, attempts were made to reduce the electrical erosion of the aluminum cathode by spark alloying through a layer of metal powder poured onto the cathode surface, which was fed from a hopper equipped with a special metering device [225]. It was anticipated that this would have a shielding effect on the cathode surface and lead to an increase in cathode mass.

2.4.2. Electrospark alloying with powder mixtures

In the works [146, 147] it was established that when powder mixtures are fed into the interelectrode gap by one method or another, under discharges of equal

power, the erosion pits formed on the cathode surface are much smaller in diameter and depth than the pits obtained during electric spark alloying with compact electrodes. At the same time, the erosion pits are filled with electrode material and remelted powder particles.

The data obtained show that when powder material is fed into the interelectrode gap during the electrospark alloying process, cathode erosion decreases sharply. At the same time, regardless of the nature of the powder materials used, the cathode mass increases over time.

The hardness of the formed coatings is close to that of the deposited materials. For example, when feeding TN-20 powder (80% TiC, 20% Ni) into the interelectrode gap, the hardness of the formed coating in certain areas reaches 17–18 GPa [146, 147, 156].

The authors of [151–153] suggested that the sharp reduction in erosion of the aluminum cathode under electrospark alloying conditions when powder materials are fed into the interelectrode gap occurs due to the redistribution of discharge energy in the anode–interelectrode gap–cathode system. As the electrodes approach each other, the electric field increases proportionally to the decrease in the distance between the electrodes. The increasing electric field causes particles located near the electrodes to be drawn into the interelectrode gap. Powder particles that end up in the interelectrode gap initiate a discharge at a distance between the electrodes greater than the breakdown distance [136, 139]. As the distance between the electrodes increases, there is a redistribution of the energy released at the electrodes and in the interelectrode gap [134–136]. The proportion of energy released at the electrodes decreases, while the interelectrode gap increases. With a simultaneous reduction in electrode erosion, intensive melting of powder particles entering the discharge channel occurs, along with the transfer of this material to the substrate (cathode) and the formation of a coating.

The constant component of the short-circuit current when using RC generators, which flows through the powder layer at the moment of electrode

contact, has a positive effect on coating formation. Due to this current, the particles are further heated and interact more intensively with the cathode material.

Using the example of electric spark alloying of the D16T alloy with nickel, it has been shown [134–136, 139, 147, 215, 216, 219] that the hardness of the coatings significantly depends on the electric spark alloying conditions and the composition of the powder mixture.

Since during electro spraying with powder mixtures the temperature of the mixture particles in the microvolume of the substrate reaches the melting and vaporization temperatures of the compounds and elements comprising the mixture, active chemical interaction processes of the electrode materials occur in the substrate; therefore, the composition of the coatings always differs from that of the powder mixture and the base material [138, 139, 146-147, 226].

Electroslag alloying of the D16T aluminum alloy with nickel- and graphite-based powder mixtures significantly increases its wear resistance: the coatings show virtually no wear at a sliding speed of 0.01 m/s and a contact zone pressure of 1... 2 MPa for 10...12 hours [147, 218 and 219].

Electrospark alloying of an aluminum substrate with chromium, copper, and aluminum powders does not lead to an increase in wear resistance, which is attributed to the significant brittleness of the applied coatings [139, 146 and 147].
It should be noted that nickel and graphite are traditionally used to improve the wear resistance of aluminum alloys [158, 218, 219, 220] operating under low load and speed conditions.

The results of [135-139, 146 and 147] indicate that, when powdered materials are fed into the interelectrode gap, it is possible to obtain electro-spark coatings of refractory materials on aluminum and its alloys without loss of cathode mass and to create wear-resistant friction pairs. It should be noted that feeding powders into the interelectrode gap significantly increases the cost of the technology and complicates the automation of the electric spark alloying process. Therefore, the method of electric spark alloying with powder mixtures has not found widespread practical application. However, studies have shown that it is

possible to perform the process of electric spark alloying of aluminum and its alloys with an increase in cathode mass by redistributing energy in the interelectrode gap.

2.5. Factors influencing the formation of electric spark coatings

2.5.1. Selection of Alloying Electrode Material

The literature presents the results of studies on the structure, properties, and kinetics of the formation of electric-spark coatings on iron-carbon and titanium alloys, as reported in the works of Lazarenko B.R., Verkhoturov A.D., Podchernyayeva I.A., Lyashenko B.A., Rutkovsky A.V., Solovykh E.K., Mikosyanchik O.O., and others [130, 131, 215, 133–138, 141–145, 152, 156–158]. However, information on the use of electric spark alloying technology for aluminum and its alloys is very limited due to the high electrical erosion of aluminum caused by its low melting point.

It has been established that electric spark alloying of aluminum and its alloys using traditional electrode materials (metals, their alloys, and metal-like refractory compounds) is accompanied by a loss of cathode mass (the workpiece) that exceeds the mass transfer of the products of electrode (anode) electroerosion and leads to the destruction of the workpiece [135-139, 144, 145, 151, 152, 154, 155]. Positive experience with the electro-spark alloying of aluminum alloys using powder mixtures [139, 146 and 147] has shown that the redistribution of spark discharge energy, achieved through a partial loss of energy in the interelectrode gap, ensures an increase in cathode mass.

A similar effect can be achieved in the process of electric spark alloying with compact electrodes [139] if the electrode material ensures the formation of dielectric components in the interelectrode gap within the electroerosion products in an amount sufficient to suppress the electroerosion of the aluminum cathode. This requirement can be met by composite materials based on aluminum nitride (AlN) [137, 138, 157 and 227]. Under conditions of high-temperature oxidation

during the electric spark alloying process, aluminum nitride will partially oxidize, forming a second dielectric component—aluminum oxide (Al_2O_3)—in the interelectrode gap. A mixture of particles and vapors of aluminum nitride (AlN) and aluminum oxide (Al_2O_3), forming a cloud above the surface of the aluminum cathode, can suppress its electrical erosion.

Given that the doping electrode must be electrically conductive, composites based on aluminum nitride of the AlN-Ti (Zr)B_2 system with Ti (Zr)Si_2, which include electrically conductive boride and silicide phases [135, 137, 138, 142-144, 155, 157, 227, 228]. Surface modification with such composites, which combine the corrosion resistance of aluminum nitride with the hardness and wear resistance of the boride component, ensures a high level of tribological properties in aluminum alloys. A shielding effect can be achieved by using alloying electrodes that do not contain dielectric components but form them in sufficient quantities in the interelectrode gap during the oxidation process. This requirement can be met by electrode materials based on lanthanum hexaboride of the LaB_6-ZrB_2 system [135, 137, 138, 141–143, 154, 155, 157], in which the B_2O_3 oxide phase, formed in sufficient quantities, can perform a shielding function in suppressing the electroerosion of the aluminum cathode.

An important factor in selecting these materials for applying wear-resistant coatings is that they can be classified as self-lubricating materials and coatings designed for operation under dry sliding friction conditions. In high-temperature processes of electric spark alloying of aluminum alloys with these materials, limited solid solutions of the ZrO_2-La_2O_3-Al_2O_3 system, as well as oxide phases of TiO_2, Al_2O_3, SiO_2, ZrO_2, La_2O_3, and corresponding compounds such as β-thialite, mullite, and others, which can act as solid lubricants. At the same time, boron oxide, due to its low melting point (450°C), is capable of functioning as a liquid lubricant up to a temperature of 650°C. This was demonstrated using the example of electric spark alloying of steels and the VT6 alloy with AlN-ZrB_2-$ZrSi_2$ and AlN-TiB_2 materials [135, 137, 138, 141–143, 154, 155, 157].

Thus, the creation of wear-resistant coatings on aluminum alloys without loss of cathode mass during processing, achieved by using composite ceramics based on AlN-Ti (Zr) B_2 and LaB_6-ZrB_2 as electrode materials to strengthen sliding friction pairs made of aluminum alloys, primarily in small-batch production (e.g., crankshaft bearing seats, sliding bearings of gear hydraulic machines, pistons of internal combustion engines, and others), is a pressing task.

2.5.2. Effect of the duration of electric spark alloying

The results of a study on mass transfer kinetics during electric spark alloying of various hardfacing materials (45 steel, AL9 and VT6 alloys) with electrode materials based on aluminum nitride (AlN) of the AlN-TiB_2-$TiSi_2$ (TBSAN) and the AlN-ZrB_2-$ZrSi_2$ (CBSAN) system are presented in Figs. 2.8 and 2.9.

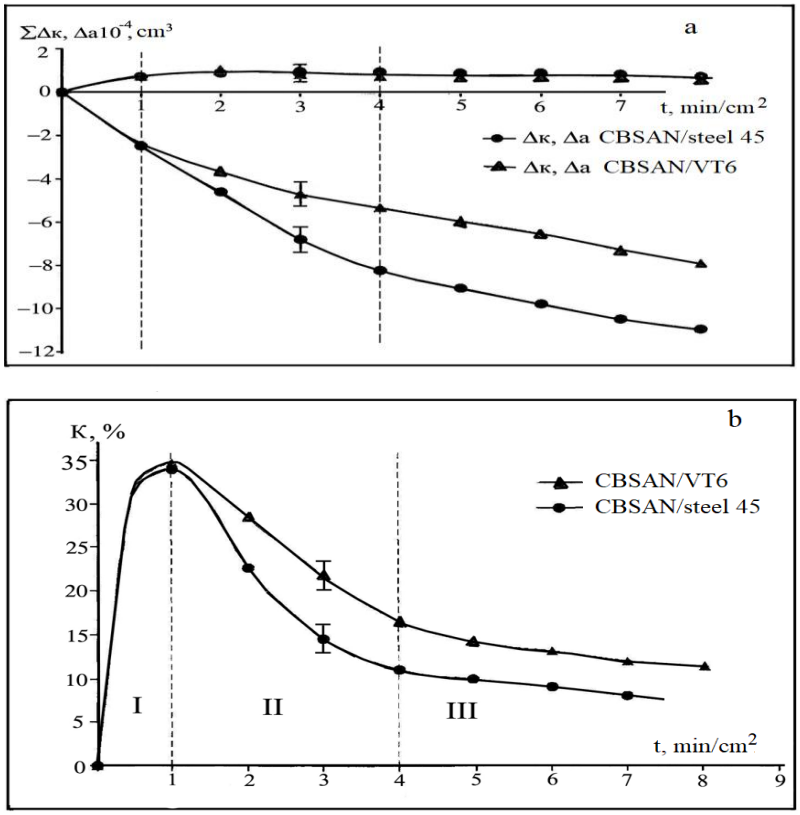

Fig. 2.8. Effect of the substrate material on mass transfer kinetics during electric spark alloying using an AlN-ZrB_2-$ZrSi_2$ electrode (CBSAN): a) cathode weight gain Δk and anode erosion Δa; b) mass transfer coefficient K.

For all the coatings studied, three stages of electric spark alloying can be identified based on the kinetic dependencies of the mass transfer coefficient. During the first stage of the electrospark alloying process (Figs. 2.8, 2.9):

- high efficiency of the electrospark alloying process using an aluminum nitride (AlN) electrode of the AlN-ZrB_2-$ZrSi_2$ system (CBSAN);

- the mass transfer coefficient K of the system "CBSAN coating (AlN-ZrB_2-$ZrSi_2$) – AL9 substrate" is twice as high as the mass transfer coefficient K of the system "CBSAN coating (AlN-ZrB_2-$ZrSi_2$) – substrate (45 steel)" system and three times higher than that of the "TBSAN coating (AlN-TiB_2-$TiSi_2$) – AL9 substrate" system.

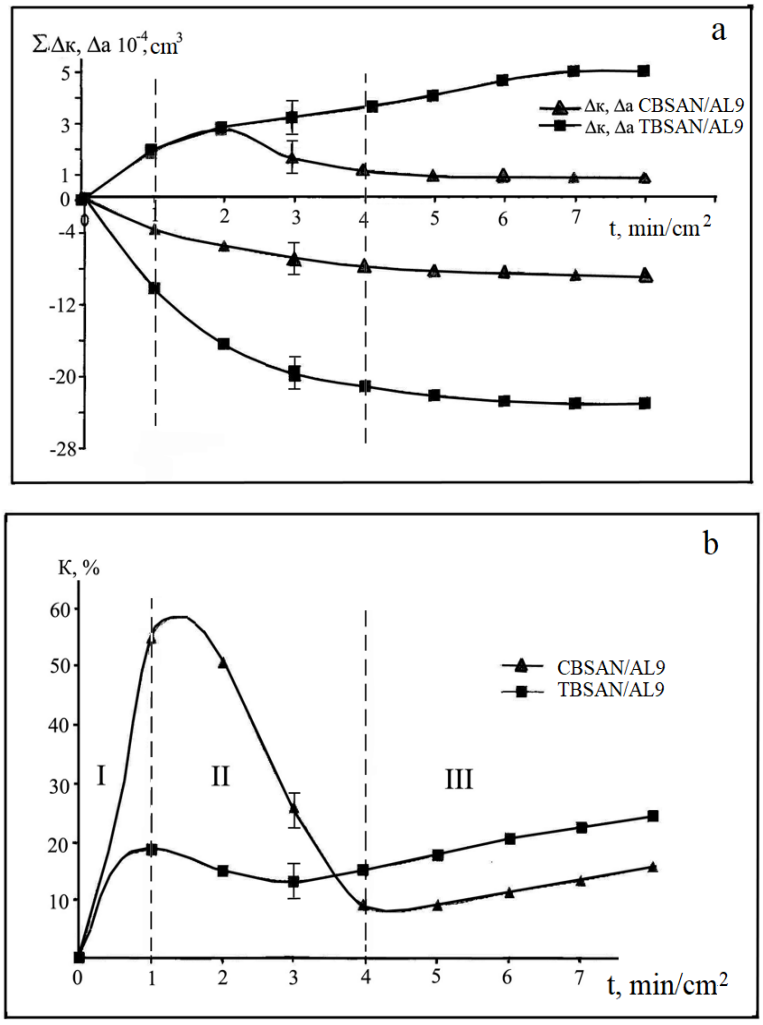

Fig. 2.9. Effect of electrode material on mass transfer kinetics during electric spark alloying of AL-9 alloy:

a) cathode weight gain Δ_k and anode erosion Δ_a;

b) mass transfer coefficient K.

In the initial stage, at duration of ($t \leq 1$ min/cm²) of electric spark alloying, the increase in the mass transfer coefficient (K) is due to the mass transfer of electroerosion products in the absence of a secondary structure on the anode, when the increase in cathode mass (Δ_k) is determined by the amount of eroded anode material (Δ_a).

The absence of a secondary structure is manifested by the coincidence of the values of the mass transfer coefficient K in the range $0 < t \leq 1$ min/cm² during electric spark alloying with the same electrode of different surface materials being strengthened (for electrode materials based on aluminum nitride AlN) of the AlN-ZrB_2-$ZrSi_2$ (CBSAN) system, the mass transfer coefficient K = 135% (Fig. 2.8, b).

In the second stage of the electric spark alloying process ($1 < t < 4$ min/cm²), the cathode weight gain decreases with increasing anode erosion. The reason for this limitation of the cathode weight gain (Δ_k) is the internal stresses that accumulate in the alloyed layer under the action of spark pulses [152, 153 and 158]. The limitation of cathode weight gain and the slowing of the rate of anode erosion (Δa) due to the formation of a secondary structure at $t > 1$ min/cm² leads to a decrease in the mass transfer coefficient K (Fig. 2.8, b; 2.9, b). The formation of a secondary structure during the second stage of the electrospark alloying process ($4 > t > 1$ min/cm²) is evidenced by a decrease in the erosion growth rate with increasing alloying duration (t) and the influence of the reinforced surface material on the erosion resistance of the AlN-ZrB_2-$ZrSi_2$ (CBSAN) system during EIL of substrates made of various materials in the range of alloying process duration $t > 1$ min/cm² (Fig. 2.8, a; 2.9, a), which is associated with the different composition of the secondary structure on the anode.

In the third stage of the electrospark alloying process ($t > 4$ min/cm²), mass transfer occurs in the presence of a secondary structure formed on the working surface of the electrode, which essentially becomes the actual target of electroerosion.

As the duration of the electric spark alloying process increases, the number of oxide phases in the coating increases. At the same time, zirconium dioxide (ZrO_2) is prone to phase transformations, is more brittle compared to titanium dioxide (TiO_2), and is more easily removed from the surface under the thermomechanical influence of repeated spark pulses. This is confirmed by micro- and X-ray structural analysis data, according to which, at the eighth minute of the electric spark alloying process, the Al/Zr (in relative units) in the cross-section of the AlN-ZrB_2-$ZrSi_2$ system C-B-S-AN coating (≈ 42) is several times greater than the Al/Ti ratio in the AlN-TiB_2-$TiSi_2$ system T-B-S-AN coating (≈ 12).

For an electrospark alloying process duration t > 2 min/cm², the cathode weight gain Δk and, accordingly, the mass transfer coefficient K of the system "CBSAN coating (AlN-ZrB_2-$ZrSi_2$) – AL9 substrate" decrease compared to the cathode weight gain Δ_k and the mass transfer coefficient K of the "TBSAN coating (AlN-TiB_2-$TiSi_2$) – AL9 substrate" system (Fig. 2.9).

2.5.3. Stages of alloyed layer formation

It is advisable to organize the electric spark alloying process chronologically, grouping the factors that influence the formation of the alloyed layer at different stages of the process [203, 209 and 214].

The three-stage mechanism of surface layer formation during electric spark alloying of an aluminum alloy with ceramic electrodes is consistent with the concepts [136, 153, 158], developed for the process of electric spark alloying of steel substrates (surfaces to be hardened) with metal alloys and hard alloys of the TK and VK grades [154].

In the first stage, electrical erosion of the anode material occurs under the action of the plasma jet of the spark discharge. As is known [144, 151–153, 158], the particle size distribution of the electrical erosion products includes a liquid-vapor component alongside solid-phase particles.

For electrode materials made of composite ceramics, characterized by increased brittleness and high melting points of the components, the products of electrical erosion should consist predominantly of solid-phase particles in the form of fragments that weakly adhere to the cathode surface. One must also account for the different temperatures of the solid eroded particles of the electrode's composite material due to their varying conductivity.

Dielectric components are not subjected to electron bombardment and are heated on the anode's working surface solely through contact with the conductive phases. Therefore, the reactivity of the electrically conductive components must be higher, and the solid-phase component of the electroerosion products of the electrode is represented predominantly by particles of components with different temperatures – a cold non-conductive phase and a hot electrically conductive phase.

The second stage involves the passage of electroerosion products through the interelectrode gap, accompanied by their interaction with oxygen and nitrogen in the air under conditions of high-temperature oxidation. In this context, four main mechanisms of particle interaction are distinguished [133, 134 and 158]:

- adsorption of gases on the particle surface; chemical interaction leading to the formation of oxide and nitride films;

- dissolution of gases in the liquid phase of the particles;

- diffusion processes and mechanical "mixing" by convective flows of the volume of particles resulting from surface interactions.

These mechanisms fully apply to the interaction of electroerosion products with the spark discharge plasma under conditions of electric spark alloying.

A distinctive feature of the electric spark alloying process is the low particle velocity in the spark discharge plasma (several km/s). This compensates for the small interelectrode gap (≈ several μm), so the duration of the interaction of electroerosion products with the surrounding environment (air) in the spark interelectrode gap is no shorter than in gas-thermal sputtering methods. For this reason, the temperature of the particles in the spark discharge plasma and the effect

of the surrounding environment and phase formation in the interelectrode gap on the structure and properties of the spark-deposited coatings are expected to be significant.

In the third stage of the electrospark alloying process, the leading role is played by factors that determine the physicochemical interaction between the materials of the alloying electrode and the substrate (the surface to be strengthened) in the contact zone.

According to modern concepts [229], the formation of physical contact between the heated particle and the substrate is based on wetting effects and diffusive transport under conditions of plastic deformation with the formation of dislocations, which act as centers for the formation of chemical bonds. These concepts are applicable to the electrospark alloying process, in which, at the moment of electrode contact, high pressure and temperature (close to critical values) are simultaneously generated in a local region of the surface being strengthened due to the high rate of energy input ($\approx 10^3$ J/s), which exceeds the rate of heat removal [133, 134, 158]. As a result, a dislocation structure forms on one side of the surface being strengthened by electric spark alloying, and a molten microzone on the other.

2.5.4. The effect of wetting in the system "electrode material – surface to be strengthened" on the mass transfer coefficient

The mass transfer coefficient is one of the most important technological parameters of the electric spark alloying process, characterizing the process efficiency and the strength of the adhesive bond.

The mass transfer coefficient is equal to the ratio of the cathode weight gain (Δ_k) to the anode erosion (Δ_a):

$$K_m = \Delta_k/\Delta_a \times 100\% \qquad (2.2)$$

In electrospraying, the most active physicochemical interaction occurs between the products of electrode electroerosion and the material of the surface being strengthened (the substrate), which takes place during the micro-spraying of the melt onto the surface of the sample being strengthened. Therefore, along with the extent of electrode erosion, the most important characteristic affecting mass transfer kinetics is the wetting of the electrode material by the metal alloy of the substrate.

The data in Table 2.3 indicate the absence of a direct correlation between the contact wetting angle and the mass transfer coefficient in electrode–substrate metal alloy systems.

In the electric spark alloying of the AL-9 alloy, the mass transfer coefficient (K) when using the AlN-ZrB_2-$ZrSi_2$-based C-type electrode is three times higher than that of the AlN-TiB_2-$TiSi_2$-based T-type electrode (Fig. 2.9, b), although the contact wetting angles in these systems are similar and amount $t_o \sim 50–55°$ (Table 2.3).

Table 2.3

Effect of contact wetting angles on the mass transfer coefficient during electric spark alloying

System Electrode – metal alloy	Contact wetting angle, θ, deg	Mass transfer coefficient at EIL, K_{max}, %
CBSAN - 45 steel	0 (in 7 min)	35
CBSAN - AL9 alloy	55 (in 20 min)	60
TBSAN - AL9 alloy	50 (in 4 min)	20
CLAB-2 - AL9 alloy	35 (in 8 min)	cathode mass loss
CLAB-1 - AL9 alloy	—	30
LaB6 - AL9 alloy	0 (in 3 min)	16
B_6Si - AL9 alloy	—	25

The mass transfer coefficient of the “CBSAN coating (AlN-ZrB_2-$ZrSi_2$) – 45 steel substrate” system is almost half that of the “CBSAN coating (AlN-ZrB_2-$ZrSi_2$) – L-9 substrate” system, although in the first case the contact wetting angle is close to zero. Evidently, mass transfer during electric spark alloying is influenced by the adhesive interaction between the electrode and substrate (the surface being strengthened) materials. The microstructure (Fig. 2.10) and element distribution in the contact interaction zone of the AlN-ZrB_2-$ZrSi_2$ (CBSAN) and AlN-TiB_2-$TiSi_2$ (TBSAN) electrode systems with AL-9 alloy (Fig. 2.11) indicate a significant difference in adhesive interaction in these systems, which accounts for the difference in their mass transfer parameters.

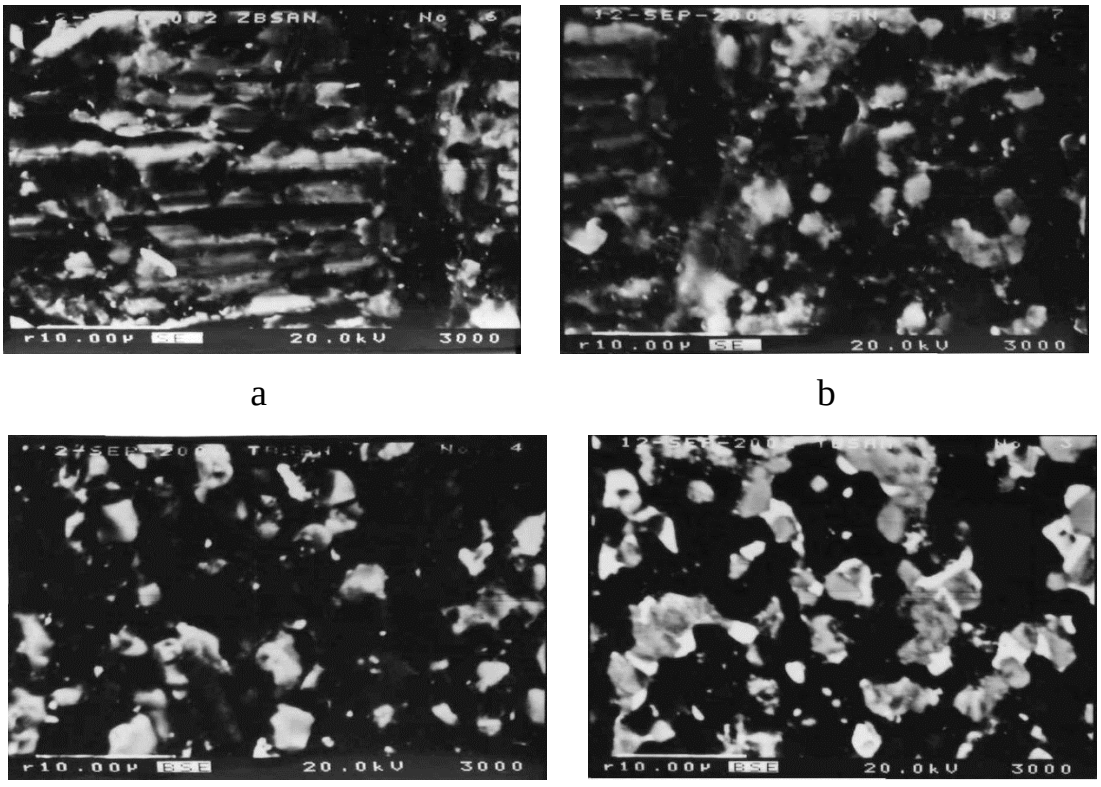

a b

c d

Fig. 2.10. Microstructure of the contact interaction zone between the AL9 alloy and the electrodes:

a, b) AlN-ZrB_2-$ZrSi_2$ system (CBSAN) and c, d) AlN-TiB_2-$TiSi_2$ system (TBSAN);

a) Al-Si alloy on the droplet side (light-colored plates – silicon Si);

b) b, c) transition layer; d) starting material

For both composites, in the contact interaction zone at the “AL-9–ceramic” interface, there is no diffusion of titanium (Ti) or zirconium (Zr) into the AL-9 alloy (Fig. 2.11).

The Si/Al ratio (in relative units) in this zone is high (close to unity), with silicon (Si) segregating at the surface of the aluminum alloy (Fig. 2.11, a). The result of enriching the Al-Si alloy with silicon is its increased microhardness, which is 13.2 GPa; for comparison, the microhardness of the solid phase of the AlN-ZrB_2-$ZrSi_2$ (TBSAN) composite system is 32 ± 1 GPa.

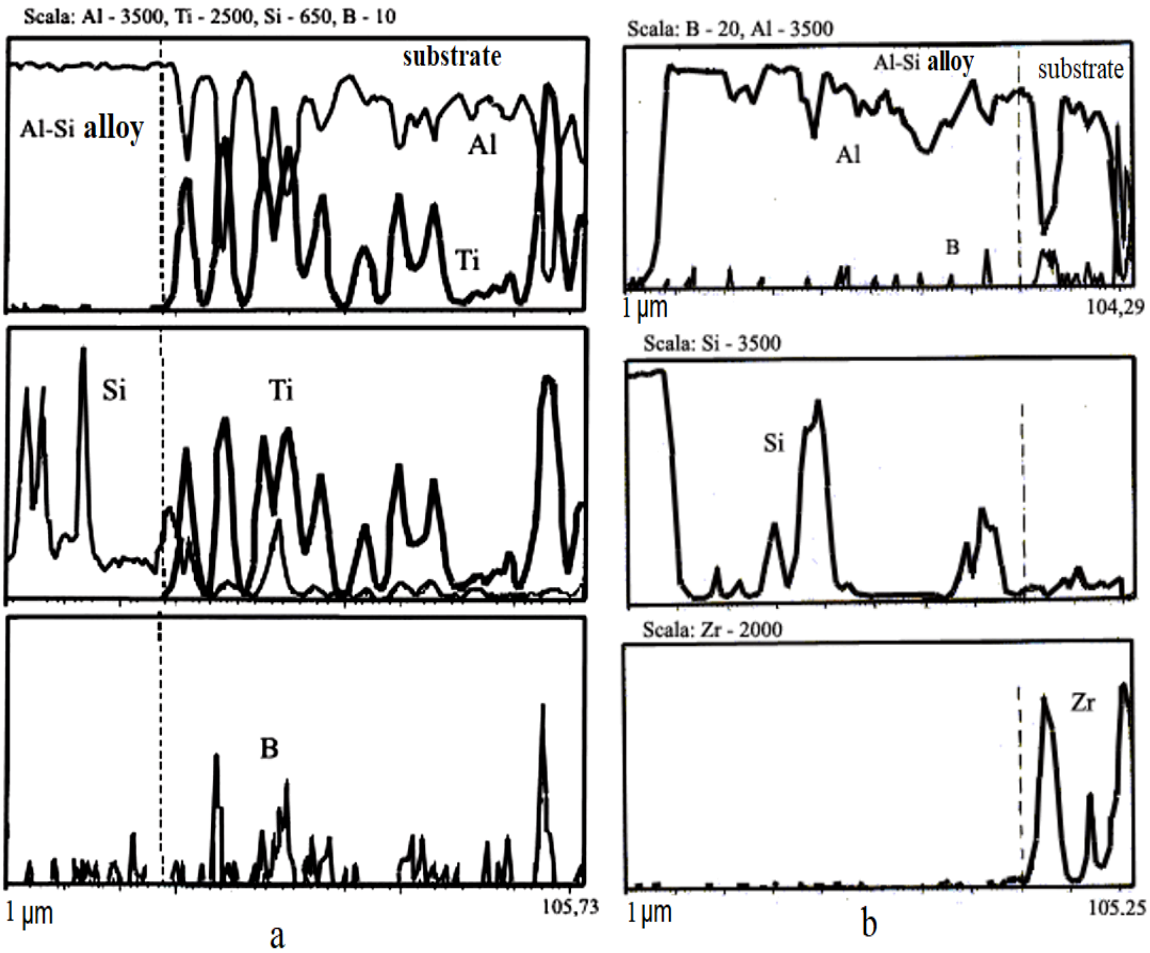

Fig. 2.11. Micro-X-ray spectroscopy (MXRS) spectra in the contact interaction zone of the systems “CBSAN coating (AlN-ZrB_2-$ZrSi_2$) – AL9 substrate” (a) and “TBSAN coating (AlN-TiB_2-$TiSi_2$) – AL9 substrate” (b)

The silicon content on the droplet side in the contact interaction zone between the droplet and the AlN-TiB_2-$TiSi_2$ (TBSAN) system is insignificant (Fig.

2.11, b) and amounts to Si/Al = 0.19, which corresponds to its content in the initial Al9 alloy. This is confirmed by the absence of a dendritic structure and the low hardness of the Al-Si alloy in the contact zone, which is approximately 1 GPa. The presence of boron spikes on the alloy side of the contact zone of both composites indicates the formation of aluminum boride phases.

The more intense interaction of the AlN-ZrB_2-$ZrSi_2$ (CBSAN) ceramic system with the AL9 aluminum melt is manifested in its increased hardness due to the enrichment of the AL9 aluminum alloy with silicon. This leads to the fact that during the process of electric spark alloying with an AlN-ZrB_2-$ZrSi_2$ (CBSAN) electrode, despite its threefold lower electrical erosion compared to the AlN-TiB2-TiSi2 (TBSAN) electrode, the cathode mass does not decrease at the initial stage (t $\leq$ 2 min/cm²) (Fig. 2.9, a). This ensures a significant increase in the mass transfer coefficient (K) (Fig. 2.9, b) and a shift of the maximum mass transfer coefficient (K) toward a longer duration of the electric spark alloying process using the AlN-ZrB_2-$ZrSi_2$ (ZBSAN) [135–137, 154, 155, 157 and 230.

The higher erosion resistance of the AlN-ZrB_2–$ZrSi_2$ (ZBSAN) electrode system compared to that of the AlN-TiB_2–$TiSi_2$ (TBSAN) is due to the lower brittleness of zirconium boride ZrB_2 compared to titanium boride TiB_2, resulting from the specific interaction mechanisms in titanium and zirconium diborides [135-137, 154, 157, 230, 231].

As noted, spark alloying of aluminum and its alloys using compact electrodes is accompanied by a reduction in the part's mass due to its intense erosion caused by aluminum's low melting point [131, 135–139, 215].

From the analysis of the research results presented in Table 2.3, it can be concluded that this negative effect can be reduced by using an AlN-Ti(Zr)B_2 composite as the alloying electrode material, in which the main component—aluminum nitride (AlN)—acts as a dielectric.

The dielectric products of electrical discharge (aluminum nitride AlN and aluminum oxide Al_2O_3) located in the interelectrode gap shield the surface of the

aluminum cathode from the effects of the spark discharge, reducing its erosion, similar to what occurs during spark alloying of aluminum with powder mixtures [26, 205, 206]. In this case, the mass transfer coefficient can range from 20 to 60% (Table 2.3).

2.6. Composition and Structure of Electrospark Coatings

A distinctive feature of electrospark alloying is that the pulsed local impact of spark discharges on the treated surface causes a dynamic distribution of temperature fields in the surface layer. This leads to the simultaneous occurrence of chemical processes and phase formation on the surface at different temperatures, resulting in phase and structural heterogeneity of the electric spark coating.

The most active physicochemical interaction between the products of electrode electroerosion and the base material occurs in the molten pool on the treated surface. Therefore, the wetting of the electrode electroerosion products by the base material plays a leading role in the formation of the electro-spark coating.

Components of the alloying electrode material with small contact wetting angles θ with the base material are entrained by convective flows of the molten pool and modify the surface of the metal alloy, forming globules ("bumps") on the surface. The formation of globules is driven by alloying components with low contact wetting angles θ, which are weakly drawn into the convective flows of the melt, forming hemispherical globules of sintered composite material on the treated surface.

Mass transfer of the base metal into the globule ensures the gradience of its structure and the adhesive strength of the bond. Obviously, the smaller the difference in wettability of the alloying components by the base metal, the lower the probability of globule formation, and, accordingly, the lower the surface roughness.

The idea of selectively incorporating electroerosion products into the molten bath was proposed in [154] based on the results of a study of the electric spark

alloying process of structural alloys: steels, titanium, and Ni-Cr alloys with materials from the Al-Ti (Zr)-B-N system.

It was shown (Table 2.4) that the dielectric components of the electrode's electroerosion products (aluminum nitride AlN, aluminum oxide Al_2O_3), which are not wetted or are poorly wetted by iron and nickel ($\theta \geq 60°$), predominantly enter the composition of the globules, whereas titanium diboride, with a relatively low contact wetting angle ($\theta \leq 40^o$), primarily modifies the surface of the base metal alloy (the surface being strengthened).

Table 2.4

Contact wetting angles θ of refractory metal compounds

Compound	Contact wetting angle θ	
	Iron (Fe)	Nickel-chromium alloy (Ni-Cr)
AlN	non-wetting	62*
Al_2O_3	~ 90	91
TiB_2	39	24
ZrB_2	72	—
$TiN_{0,95}$	98	—

*wetting with the AL5 alloy

This is clearly illustrated (Fig. 2.12) by the distribution of elements on the surface of a nickel-chromium (Ni-Cr) alloy following its electric-spark alloying with a boron nitride–titanium diboride (AlN-TiB_2) system.

Aluminum-containing phases (aluminum nitride AlN, aluminum oxide Al_2O_3) are found predominantly within the globules (Fig. 2.12, c), whereas titanium diboride is mainly located in the interglobular space (Fig. 2.12, b), modifying the nickel-chromium (Ni-Cr) base alloy (hardened surface).

The concept of forming electric-spark coatings on refractory metals, developed in [142, 143, 154, 155], is based on the selectivity of wetting of

electroerosion products by the base material and is, in principle, applicable to low-melting-point metals, in particular aluminum and its alloys.

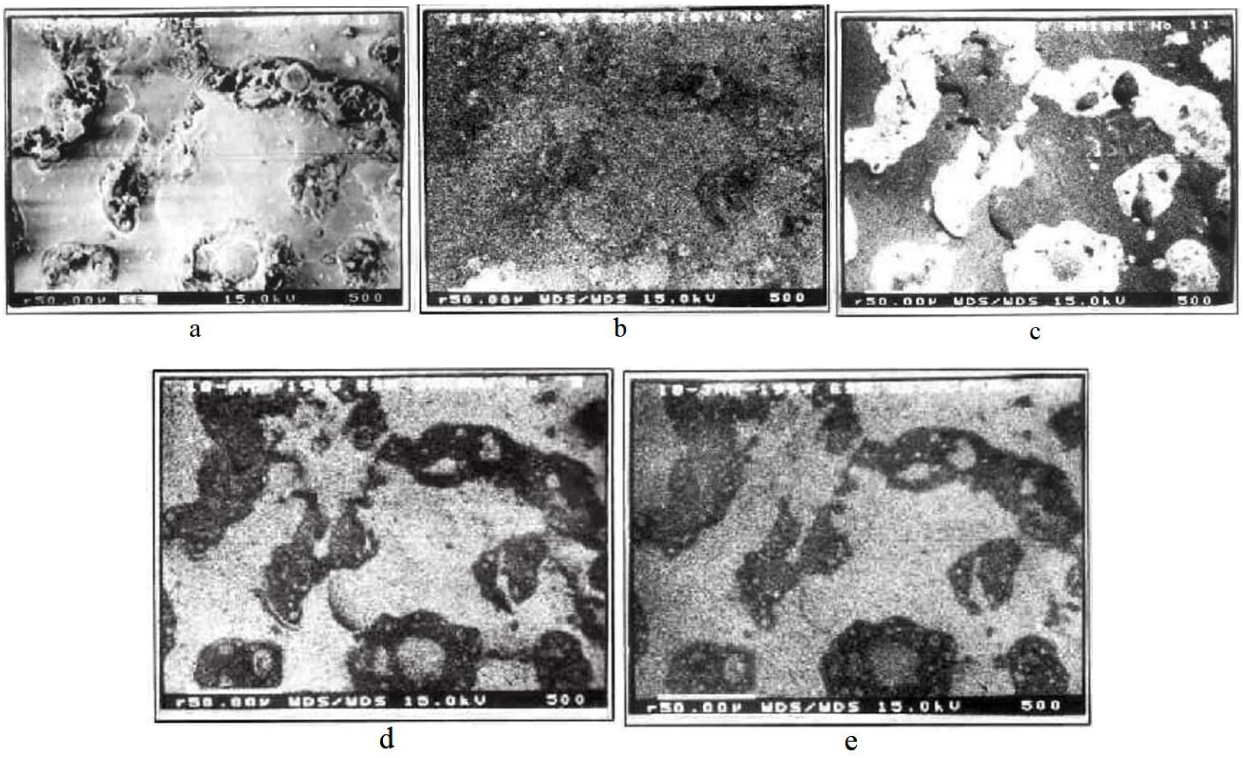

Fig. 2.12. Microstructure of an electric-spark coating on a nickel alloy in secondary electrons (a) and in X-ray radiation: titanium Ti (b), aluminum Al (c), nickel Ni (d), chromium Cr (e)

2.6.1. Globular coating

According to metallographic analysis, during the electrospark alloying of the AL-9 aluminum alloy with the AlN-ZrB_2-$ZrSi_2$ electrode material (CBSAN), a layer with a modified composition and structure, ≤ 10 μm thick, is formed. On the surface of this alloyed layer, hemispherical globules (in the form of "bumps") with a height of 80–100 μm and a diameter of 500–600 μm are formed (Fig. 2.13, a). The area occupied by the globules is ~ 60–70%.

The microstructure of the globule surface and the interglobular space of the "CBSAN coating–AL-9 substrate" system is shown in Fig. 2.13, b, c. In the microphotograph of the globule surface (Fig. 2.13, b), light-colored elongated

grains of oxide and aluminum oxynitride, as well as oval grains of aluminum borate, are clearly visible.

The surface structure of the interglobular space (Fig. 2.13, c) contains spherical aluminum particles formed as a result of the “spraying” of the aluminum alloy under the action of a spark pulse and is characterized by grain refinement due to crystallization processes from the melt.

The difference in the microstructure of the globule surface and the interglobular space (Fig. 2.13, b, c) indicates that the globule is formed as a result of liquid-phase sintering of the electroerosion products of the alloying electrode, whereas the interglobular space is formed as a result of crystallization processes from the molten aluminum alloy, accompanied by surface modification by alloying components, leading to the formation of a composite material based on an aluminum-containing matrix.

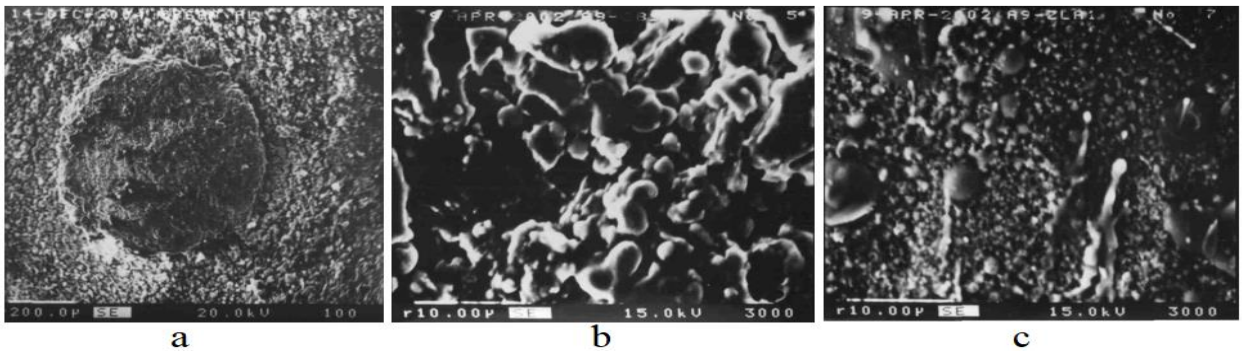

a b c

Fig. 2.13. Microstructure of the electrospark coating of the “CBSAN (AlN-ZrB_2-$ZrSi_2$) - AL9 substrate” coating system: general view (a), globule surface (b), interglobular space (c)

The results of X-ray phase analysis (XPA) of the “CBSAN coating – AL-9 substrate” system (Fig. 2.14) indicate phase formation during the high-temperature oxidation of the electrode’s electroerosion products. At a process duration of t = 2 min/cm², the main components of the coating (in order of decreasing X-ray line intensity) are: zirconium boride ZrB_2 (with a modified lattice period), aluminum oxynitride $Al_{10}N_8O_2$, and aluminum borate $Al_{14}B_2O_3$. Aluminum nitride is not detected by X-ray diffraction due to partial oxidation. With an

increase in treatment time to 8 min/cm², the phase composition of the coating remains virtually unchanged. The absence of aluminum oxide in the diffractograms of the coatings may be associated with partial amorphization. The results of X-ray phase analysis (XPA) are consistent with the spectra of micro-X-ray spectral analysis (MXSA) of the coating surface of the "CBSAN coating – AL-9 substrate" system.

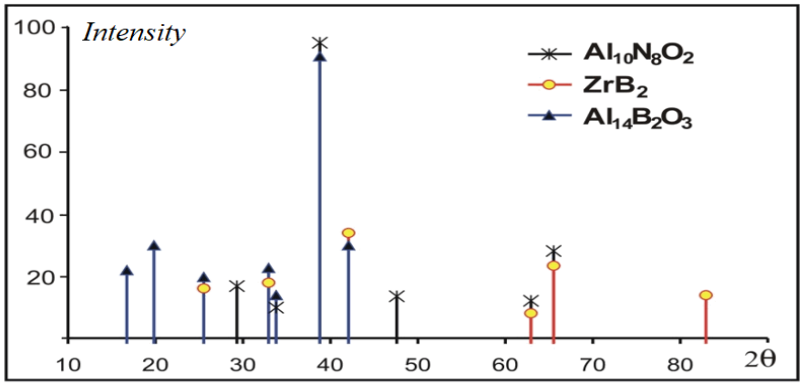

Fig. 2.14. Line diagram of the
"CBSAN electrospark coating – AL-9 substrate" system
(treatment duration: 2 min/cm²)

The distribution of elements at the globule boundaries and in the interglobular space is shown in Fig. 2.15.

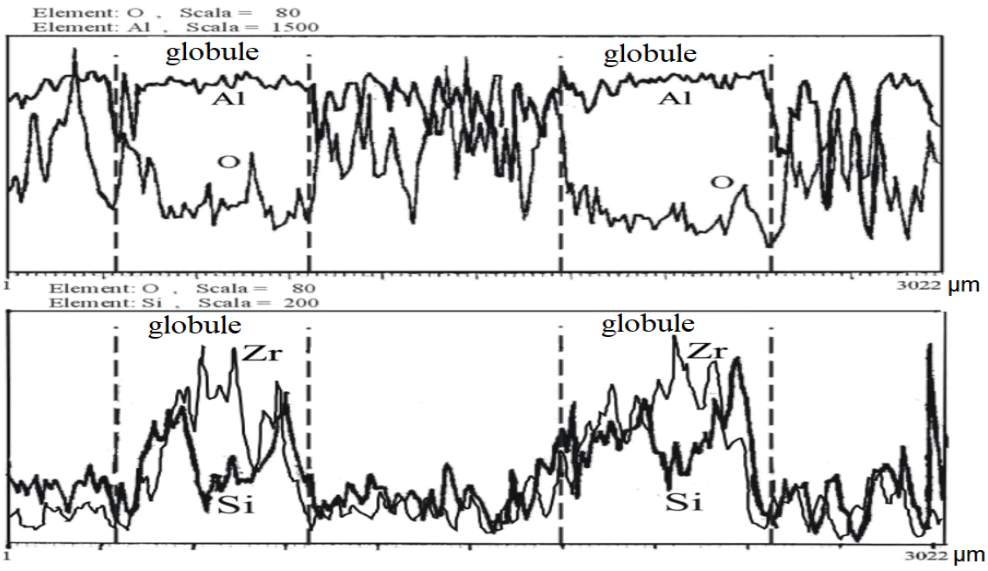

Fig. 2.15. Distribution of elements on the surface of the electrospark coating of the "CBSAN coating – AL-9 substrate" system in the globule region

Concentration peaks of zinc (Zr), silicon (Si), and oxygen depressions in the globule region indicate that it is enriched in zirconium diboride and zirconium borosilicide. The enrichment of oxygen in the interglobular space points to an increased content of aluminum phases of the Al-O-N-B system in that region.

The variation in microhardness across the globule thickness is shown in Fig. 2.16. The gradual decrease in H_μ toward the substrate promotes stress relaxation at the "coating-substrate" interface and, consequently, an increase in the bond strength between the globule and the substrate.

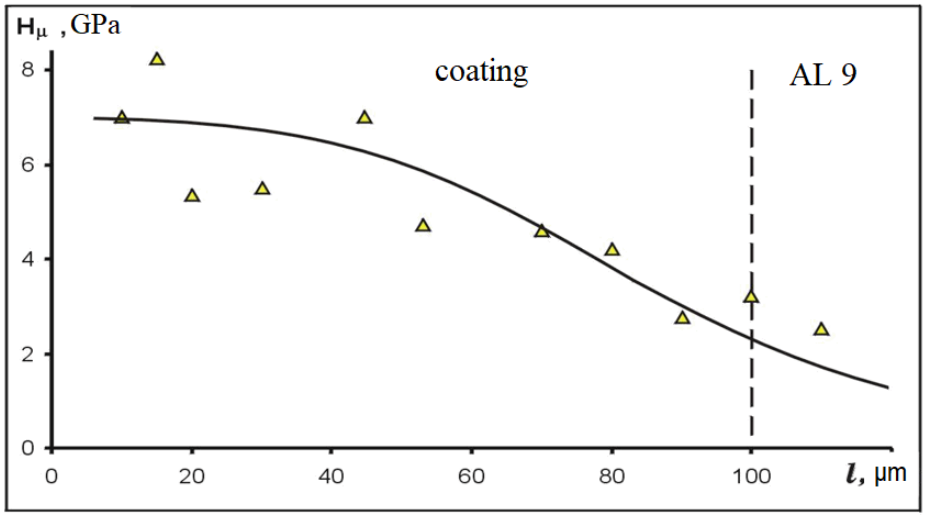

Fig. 2.16. Variation of microhardness Hμ across the thickness of a globule in the "CBSAN electro-spark coating – AL-9 substrate" system

The high adhesive strength of the bond between aluminum oxide and aluminum oxide, nitride, and oxynitride contributes to an increase in the number of aluminum phases toward the substrate. The coincidence of the concentration maxima of silicon (Si) and zirconium (Zr) indicates the presence of zirconium borosilicates in the globule, including in the substrate near the globule-substrate interface, which may be the cause of the increased microhardness at this interface (Fig. 2.16).

This decrease in H_μ is due to the gradient distribution of aluminum across the globule thickness resulting from its diffusion from the substrate (Fig. 2.17).

Noteworthy is the concentration peak of oxygen at the interface with the substrate, indicating the formation of a thin (≈ 11 μm) boundary film of aluminum oxide during the electric spark alloying process.

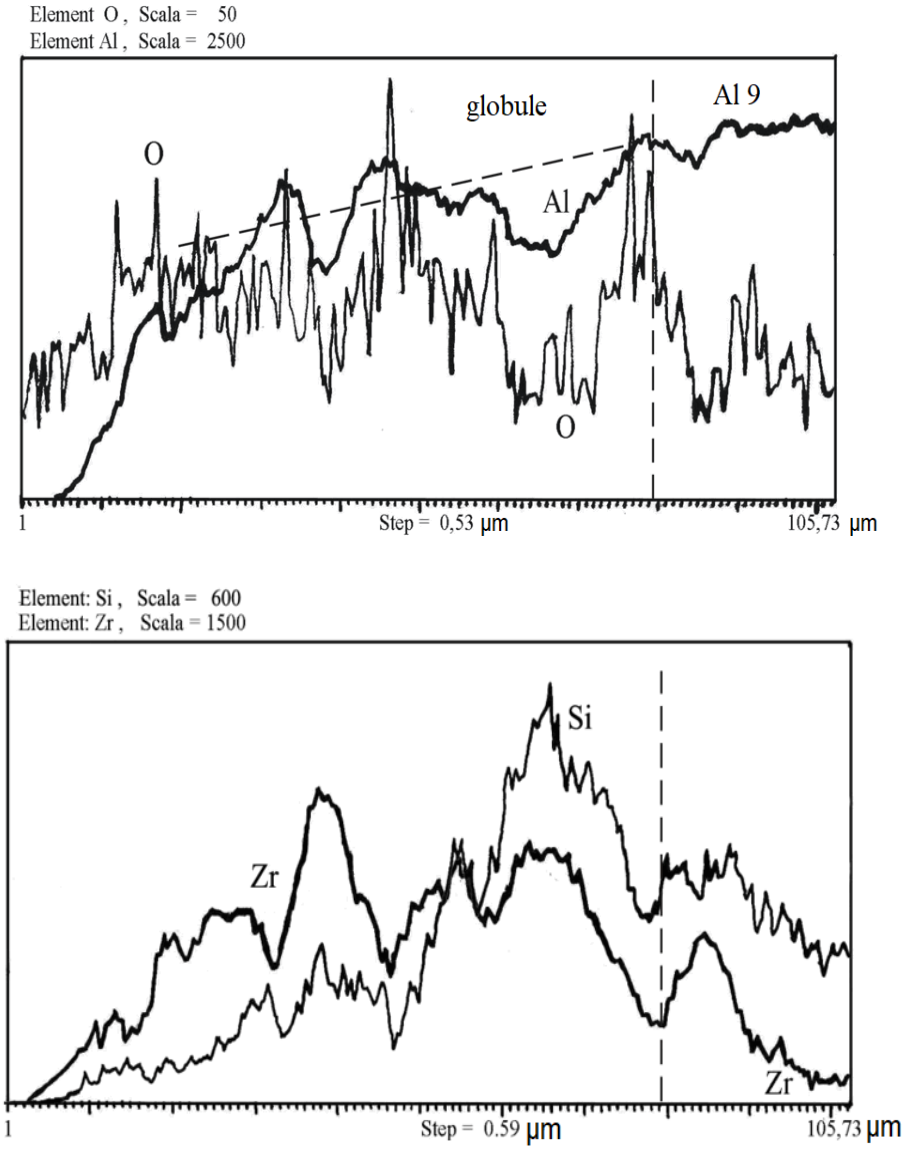

Fig. 2.17. Distribution of elements in the cross-section of the “CBSAN electrospark coating – AL-9 substrate” system

The difference in the structure of the alloyed layer for the “TBSAN coating – AL-9 matrix” and “CBSAN coating – AL-9 matrix” systems is manifested in the different globule heights and the surface area they occupy. This difference is

related to the different wettability of the alloying components by the substrate material—aluminum (Table 2.5).

Table 2.5

Effect of wetting selectivity on the structural characteristics of the "CBSAN coating – AL-9 substrate" and "TBSAN coating – AL-9 substrate" systems

System	Alloying component	Contact angle of aluminum wetting, θ	Structural component of the coating	Globule height *h*, μm	Surface area occupied by globules, *S*, %	Microhardness of globules, H_μ, GPa
TBSAN coating – AL9 base	AlN	15; 30*	aluminum-based matrix	–	–	–
	Al_2O_3	15	same	–	–	–
	TiB_2	38	globule	20…25	40…50	3,99
CBSAN coating – AL9 substrate	AlN	15; 30*	matrix based on aluminum	–	–	–
	Al_2O_3	15	also	–	–	–
	ZrB_2	60	also	80…100	60…70	7,00

* wetting with AL5 alloy

The larger contact wetting angle of zirconium diboride ZrB_2 with aluminum (60°) compared to the wetting angle of titanium diboride TiB_2 (θ = 38°) is the reason why zirconium diboride ZrB_2 particles are less active compared to titanium diboride TiB_2 particles. For this reason, zirconium diboride (ZrB_2) particles are drawn into the convective flows of the melt bath and retained on the surface, forming globules of increased height with a heterophase material structure enriched with zirconium diboride.

Experiments have shown that globule formation (globule height and surface area occupied by them) increases during electrospark alloying of the AL-25 alloy with AlN-TiB_2-$TiSi_2$ (TBSAN) material. This indicates that the contact wetting angle of titanium diboride with the AL-25 alloy is higher than with the AL-9 alloy. It is expected that the roughness of the modified surface will be lower the smaller the difference in wettability of the base material by the alloying components. On the other hand, reinforcing the modified surface of the aluminum alloy with globules of a material of increased hardness should contribute to an increase in the wear resistance of the coating.

Thus, during the electric spark alloying of the AL-9 alloy with electrode materials based on aluminum nitride of the AlN-TiB_2-$TiSi_2$ and AlN-ZrB_2-$ZrSi_2$ systems, a composite coating characterized by a globular structure is formed. The basis of the coatings is a matrix containing the Al–N–O–B system, modified by transition metal (Ti/Zr) boride and silicide, aluminum borates, in which titanium (zirconium) borosilicates, oxide phases, and limited solid solutions of the Ti(Zr)B_2–Ti (Zr)Si_2.

The surface of the aluminum matrix is reinforced with globules of higher hardness (~7 GPa) with an increased boride content and a gradient distribution of phase components, which ensures high adhesion strength between the globules and the matrix. The difference in the structure of the alloyed layer lies in the 4–5 times greater height of the globules and the larger surface area they occupy in the "Ti(Zr)B_2–Ti(Zr)Si_2 coating–AL9 substrate" system compared to the "Ti(Zr)B_2–Ti(Zr)Si_2 coating–AL9 substrate" system (Table 2.5).

This difference is associated with the selectivity of aluminum wetting of the alloying components, which determines the "capture" by convective flows of the molten bath of components with a low contact angle of wetting by aluminum $\theta^o \leq 40°$ (Al_2O_3, AlN, ALON) by convective flows of the melt, and the growth on the surface of globules with an increased content of components having a high wetting angle $\theta^o \geq 40°$ (zirconium boride ZrB_2 and titanium boride TiB_2).

This conclusion is confirmed by the experimentally observed globular structure of the "coating (TiN + 50AlN) – AL9 substrate" system, which is consistent with the high contact wetting angle (58°) of titanium nitride TiN 0.95 by aluminum.

2.6.2. Discrete coating with high boron content

According to metallographic analysis, during the electric spark alloying of the AL-9 alloy with boron silicide B6Si, a continuous coating is formed on the surface without globule formation, with a thickness of up to 30 μm and a microhardness of H_μ = 10.8 ± 0.5 GPa, which is an order of magnitude higher than the microhardness H_μ of the AL-9 metal.

The high coating continuity (≥ 90%) and the absence of globule formation are due to the good wettability of the alloying components by aluminum and the active interaction in the Al-B-O system, in which the formation of aluminum borides and borates is possible due to the partial decomposition of boron silicide. This is confirmed by X-ray phase analysis data, according to which the following are present in the alloyed layer: Al, B_6Si, CaB_6, AlB_2, $AlBO_3$ and Al3BO6 (in order of decreasing X-ray line intensity).

The appearance of new phases is caused by the oxidation of aluminum and calcium-doped boron silicide, leading to the formation of calcium hexaboride and aluminum diboride, which occur under non-equilibrium conditions of high-temperature oxidation under the influence of spark pulses.

The distribution of elements along the depth of the coating (Fig. 2.18) confirms the results of X-ray phase analysis, indicating a gradient distribution of phases due to the diffusion of aluminum into the coating from the substrate. The content of aluminum and oxygen gradually decreases toward the outer surface, which should be accompanied by a decrease in the same direction of the corresponding aluminum-containing phases—AlB_2, $AlBO_3$, Al_3BO_6.

A concentration peak of oxygen at the interface with the substrate indicates the formation of a thin (~7 μm) film of aluminum oxide. At the same time, the content of boron (B), calcium (Ca), and silicon (Si) decreases toward the substrate, indicating a corresponding decrease in the amount of boron silicide and calcium boride. Micro-X-ray diffraction (MXRD) spectra (Fig. 2.18) indicate the possible presence of CaO-SiO_2 calcium silicates in the coating. Thus, during the electric spark alloying of the AL-9 alloy with calcium-doped boron silicide B_6Si, a gradient coating is formed on a matrix containing high-purity aluminum without globule formation.

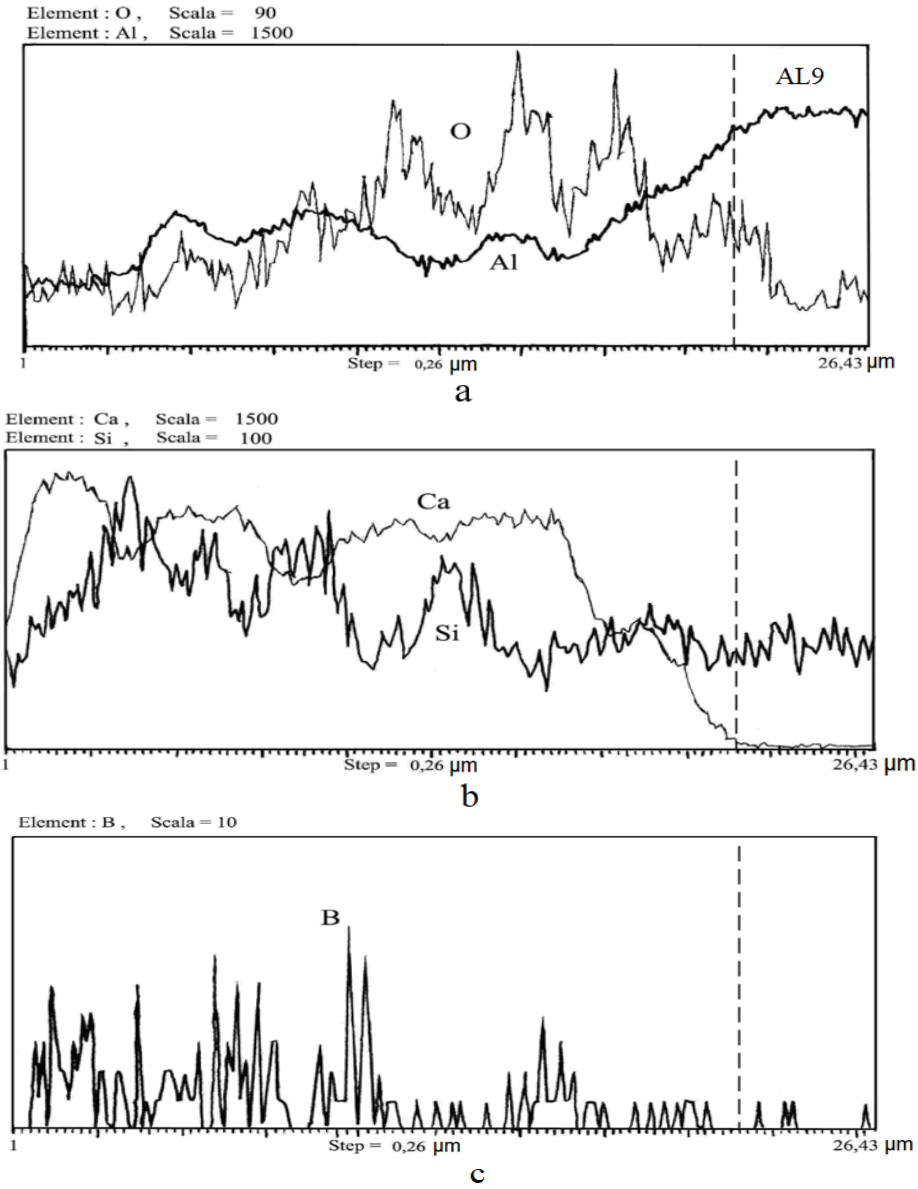

Fig. 2.18. Distribution of elements in the cross-section of the "B_6Si electro-spark coating – AL-9 substrate" system

The coating is characterized by a gradual decrease in the concentration of aluminum-containing phases toward the outer surface and its enrichment with B_6Si and CaB_6 phases. The inner layer of the coating, adjacent to the substrate, is enriched with aluminum phases, with the formation of aluminum oxide at the interface with the substrate (Fig. 2.18, a).

The gradient distribution of phases in the coating determines a gradual decrease in microhardness toward the substrate (Fig. 2.19), associated with an increase in the amount of aluminum in this direction. The microhardness of the coating is nearly an order of magnitude greater than that of the substrate.

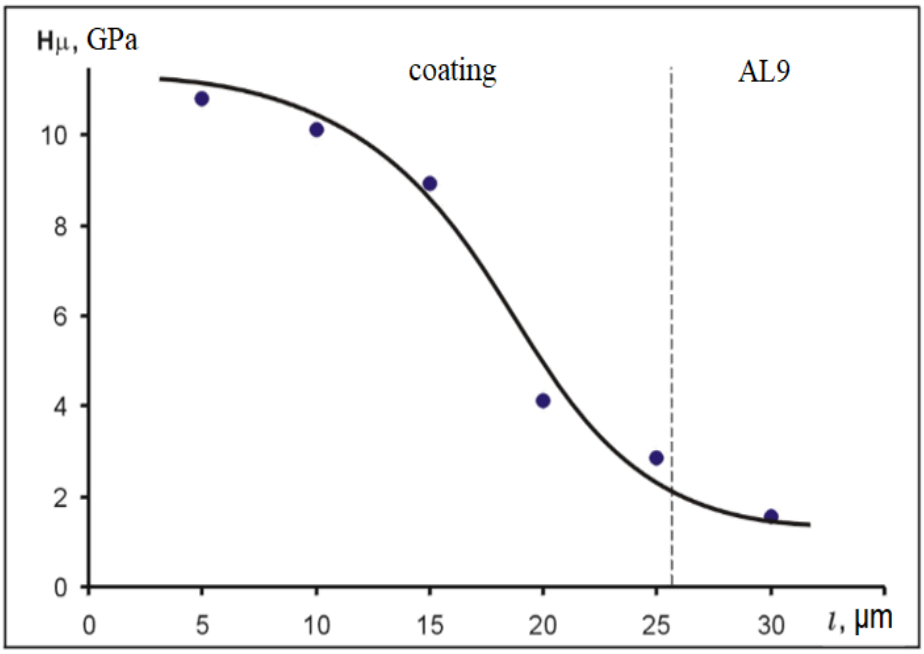

Fig. 2.19. Change in microhardness with coating depth during electric spark alloying of the AL9 alloy with boron silicide B_6Si

On the surface of Al-Si alloys after electric spark alloying with high-boron materials of the LaB_6-ZrB_2 system and boron silicide B_6Si, a modified discrete layer with higher dispersion than the matrix is formed, on the surface of which globules (“bumps”) are practically absent.

The absence of globules in the structure of such high-boron-content coatings is a result of intense chemical interaction between the aluminum matrix and boron,

leading to the formation of aluminum borates and borides, and zero contact angles of wetting of the aluminum cathode surface by the alloying components.

During the process of electric spark alloying of the AL-9 alloy with calcium-doped boron silicide B_6Si, a gradient coating is formed based on a matrix containing high-purity aluminum without globule formation.

The absence of globules in the coating structure may be a consequence of low contact wetting angles θ° and intense chemical interaction in the Al-B-O system due to the B6Si alloying phase with a high boron content.

2.7. Physicochemical model of globular electrospark coating formation

A distinctive feature of electric-spark alloying of low-melting metals, as noted, is their intense liquid-vapor erosion due to evaporation under the influence of the spark discharge, which exceeds the mass gain due to the transport of alloying components.

Based on the results of studies of the phase and elemental composition, structure of the alloyed layer, interphase interaction, and mass transfer kinetics in the systems “TBSAN coating – AL-9 substrate,” “CBSAN coating – AL-9 substrate,” “CLAB-1 coating – AL-25 substrate,” “TsLAB-2 coating – AL-9 substrate,” and “B_6Si coating – AL-9 substrate,” a physicochemical model [23] for the formation of electric-spark coatings on aluminum and its alloys was proposed, which includes:

- selection of components for the alloying material;
- mass transfer processes;
- selectivity of wetting of alloying components by aluminum;
- phase transformations in the interelectrode gap and on the surface being alloyed.

The model is schematically presented in Fig. 2.20.

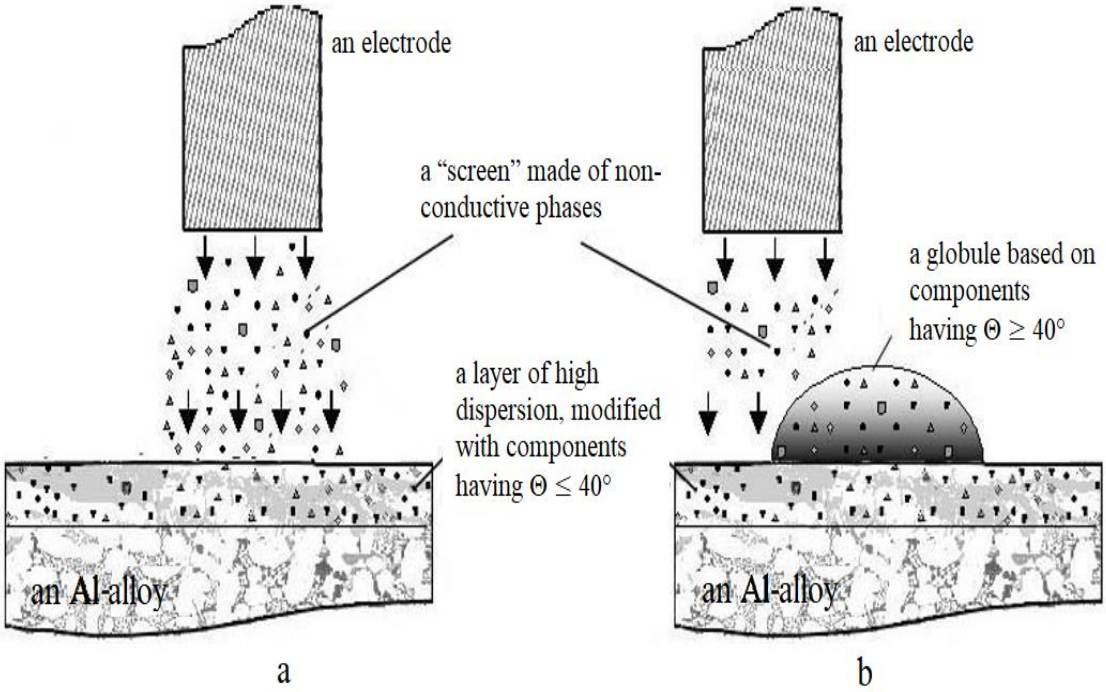

Fig. 2.20. Model of electrospark coating formation on aluminum alloys:
a – for components with a contact wetting angle $\theta << 40°$;
b – for components with a contact wetting angle $\theta \geq 40°$

During the electro-spark alloying process, the positive growth of the aluminum cathode is ensured by the presence in the interelectrode gap of a "screen" consisting of vapor and particles of non-conductive phases of electrode electro-erosion products, which suppress the erosion of the cathode material by redistributing the energy of the spark discharge in the interelectrode gap.

The creation of such a "screen" is achieved by using, as the material of the alloying electrode, a composite ceramic containing, as the main phase (≥ 50 wt. %) a dielectric component (aluminum nitride AlN) or a conductive phase (LaB_6, B_6Si), which has reduced resistance to high-temperature corrosion and oxidizes in the spark discharge plasma to form non-conductive phases (B_2O_3).

Components with high wettability ($\theta^o << 40°$) by aluminum (aluminum nitride AlN and aluminum oxide Al_2O_3), which are intensively drawn into the convective flows of the melt, are responsible for the formation of the matrix structure of a modified layer of increased dispersion based on an Al-N-O-B

aluminum alloy system with a thickness of ≤ 10 μm. The interaction of electrode electroerosion product particles with the cathode surface in the melt microenvironment is determined by their wettability by the aluminum alloy and adhesive interaction and is presented in Table 2.3.

Components with low wettability by aluminum (zirconium boride ZrB_2 and titanium boride TiB_2), characterized by a contact angle $\theta^0 \geq 40°$, are weakly entrained by convective melt flows, forming hemispherical globules of composite material with a height of 40–100 μm and a diameter of up to 60 μm on the modified surface of the aluminum alloy. The globule structure exhibits a compositional gradient due to mass transfer of aluminum from the substrate, which results in a gradual decrease in the microhardness of the coating toward the substrate.

The formation of globules on the modified surface of the "CBSAN coating–AL9 substrate" and "TBSAN coating–AL9 substrate" systems is also facilitated by the increased reactivity of hot boride phase particles compared to non-conductive cold aluminum nitride and oxide particles. Globule growth during the electrospark alloying of aluminum alloys is responsible for the intense increase in cathode mass and explains the threefold higher mass transfer coefficient K for the "CBSAN coating–AL9 substrate" system compared to the "TBSAN coating–AL9 substrate" system (Table 2.3). In general, during the electrospark alloying of aluminum alloys, the three-stage mass transfer kinetics typical of the EIL process is preserved (Fig. 2.8).

In cases where a single-phase electrode material with a low wetting angle (θ^o) and a high boron content (B_6Si, LaB_6)—responsible for intensive phase formation in the Al-B-O system—is used, a coating of high continuity (≥ 90%) is formed, with a thickness of ~ 25 μm and tight adhesion to the substrate, on the surface of which globules are absent (low roughness).

Traditionally, in various coating deposition methods, efforts are made to optimize process conditions in a way that preserves the composition and structure

of the deposited materials, which contain carbides, borides, and other metal-like compounds; this is particularly important for the chromium-cobalt carbide (WC-Co) system and amorphizing alloys [229].

During high-temperature deposition of composite ceramics of the studied compositions in an oxygen-containing environment, intense interaction occurs between the components of the electroerosion products—both with each other and with the substrate material—under oxidizing conditions, accompanied by the formation of new oxide phases.

This enables a predictable change in the coating composition by selecting the components of the deposited material, taking into account the formation of new oxide phases, which are high-temperature corrosion-resistant compounds and can act as a solid lubricant under dry sliding friction conditions. These include mullites, β-thialite, aluminates, and iron titanates [232]. Regarding β-thialite, this is confirmed by model experiments studying the tribological behavior of pre-oxidized ceramics of the titanium nitride-aluminum nitride (TiN-AlN) system [233].

Thus, electric spark alloying is a structure-forming technology controlled by the selection of alloying electrode material components.

2.8. Tribotechnical properties of ceramic electric spark coatings

Currently, researchers are focusing on the development of composite coatings in which variations in structural effects and the selection of phase components allow coatings to be designed in such a way as to combine properties that ensure optimal operating conditions for tribocontact.

The presence of contact loads in friction joints, where significant elastic deformation and even plastic deformation of the substrate is possible, necessitates ensuring the elasticity of the coating material. The requirement to combine high hardness and elastic properties of the coating material has led to the use of finely dispersed heterophase gradient or multilayer structures with alternating hard and soft components [234].

The most important aspect of the problem of wear-resistant coatings lies in the selection of phase components. They must ensure the formation of self-healing secondary structures in the contact zone during tribooxidation, in the form of thin, nanodispersed polyoxide tribofilms that prevent adhesive interaction between friction surfaces, have a low coefficient of friction, a strong adhesive bond with the coating surface to prevent their removal from the working zone [235, 236], increased resistance to high-temperature oxidation, and act as a solid lubricant under dry friction conditions [233].

It is known [237] that during the friction process, the surface layer, due to plastic deformation, transitions into a thermodynamically non-equilibrium active state, from which it tends to transition into a passive state through diffusion and chemical interaction with the surrounding environment. As a result of this interaction, heterophase polyoxide structures are formed, which shield the coating material.

About 90% of the work involved in the plastic deformation of the material is converted into heat, which leads to a local increase in temperature (according to theoretical estimates, up to 1000°C [238]), ensuring the thermal activation of chemical processes and phase transformations. In addition, the process of tribological surface damage is accompanied by triboemission, defined as the emission of electrons, photons, negative and positive ions, phonons, X-rays, and gases, which also initiates chemical reactions [237] that, under friction conditions, can occur at temperatures below equilibrium.

Composite materials based on ZrB_2, LaB_6, and AlN-(Zr/Ti) B_2 systems (Table 2.6), used as alloying electrodes, ensure the formation of a matrix structure of a heterophase coating material based on an aluminum alloy modified with refractory compounds. It should be noted that under non-equilibrium conditions, the process of electric-spark alloying with the studied materials and tribo-oxidation may lead to the formation of oxide solid solutions based on mullite, β-thialite [238], and zirconium oxide ZrO_2 [239]. The presence of solid solutions in the

composition of tribofilms in the tribocontact zone is particularly important, as they increase the system's ability to self-organize dissipative structures and, consequently, enhance the continuity of the secondary polyoxide film, thereby improving its lubricating properties.

Table 2.6

Phase composition and preparation methods of electrode materials used for applying electrospark coatings

Electrode material	Phase composition according to XRF data	Hot pressing temperature, °C	Sintering time, min
TBSAN	AlN, TiB_2, $TiSi_2$	1780…1820	25…35
CBSAN	AlN, ZrB_2, $ZrSi_2$	1820…1860	25…45
CLAB-1	LaB_6, ZrB_2, Ni	1550…1600	25…35
CLAB-2	ZrB_2, LaB_6, $ZrSi_2$	1820…1860	25…35

The oxide phases, which also form in the scale on the oxidized surface of the electrode material, act as a solid lubricant under dry friction conditions and are responsible for the high tribological properties of coatings and electrode materials, especially under elevated load and speed conditions. It should be noted that, when paired with a steel counter face, tribofilms typically contain a phase of iron oxide Fe_3O_4 [240], which acts as a solid lubricant under dry friction conditions [232]. The results of tribological tests presented in the following sections confirm these findings.

Thermodynamic calculations and studies of the sintering process in an air atmosphere of a boron-containing composition have shown [241] that upon heating, boron actively reacts with oxygen and, in the form of boron oxide, migrates to the surface, forming a B_2O_3-based tribofilms during friction. Due to its low melting point (450–470 °C), boron oxide melts under friction conditions and acts as a liquid lubricant up to a temperature of 650 °C, which leads to a significant reduction in friction and wear. On this basis, high tribotechnical characteristics are expected for coatings made of materials with high boron content.

Table 2.7 presents the wear rates of electric spark coatings on AL25 aluminum alloy for LaB_6-ZrB_2 electrode materials depending on the duration (t) of the alloying process and the electric spark treatment scheme, as well as on the composition of the electrode material. The wear rate was determined using the "shaft-insert" scheme on the SMT-2 setup in the "New Technologies" educational and research laboratory of the Department of Applied Mechanics and Materials Engineering based on the change in sample weight according to the formula:

$$I = \frac{(m_0 - m_1)[\text{mg}]}{S[\text{cm}^2] \cdot l[\text{km}]} \qquad (2.3)$$

where l - is the distance traveled; l = V × t = 2 m/s × 3600 s = 7.2 km;

V – sliding friction velocity, t – running time; S – contact area;

m_0 – weight of the initial sample,

m_1 – weight of the sample after tribological testing.

Table 2.7

Wear rate (I) of electric spark coatings of the LaB_6-ZrB_2 system on AL25 aluminum alloy depending on processing conditions (V=2 m/s; P=3 MPa; counterbody – 65G steel)

Material of the electrode	Processing scheme	Duration of EIL, t, min/cm²	I, 10^{-4}±0,5·10^{-4}, mg/km	Relative wear $I_{base}/I_{coating}$
AL-25 alloy (coated)	—	—	2,5	—
TsLAB-1	EIL	2	1,1	2,27
TsLAB-1	EIL	6	0,85	2,94
TsLAB-2	EIL	2	1,4	1,79
TsLAB-2	EIL+ LO	2	0,95	2,63
TsLAB-2	EIL	6	0,95	2,63

The data in Table 2.7 show that the wear rate (I) of the coated AL-25 aluminum alloy decreases by a factor of 2–3 compared to the uncoated sample.

This reduction in wear intensity (I) is facilitated by both an increase in the duration of electric spark alloying (t) and subsequent laser treatment. It can be assumed that the reason for the reduction in wear in both cases is an increase in the number of oxide phases in the coating (with an increase in the duration t of electric spark alloying and during the laser treatment process), which participate in the formation of secondary films that self-heal in the tribocontact zone. In the case of LaB_6-ZrB_2 alloying materials, such phases may include aluminum oxide (Al_2O_3), boron oxide (B_2O_3), zirconium oxide (ZrO_2), and aluminum borates.

These phases form in the coating during electric spark alloying with electrode materials TsLAB-1 (phase composition LaB_6, ZrB_2, Ni) and TsLAB-2 (phase composition ZrB_2, LaB_6, $ZrSi_2$), which explains the similarity in wear values for the "TsLAB-1 coating – AL25 substrate" and "TsLAB-2 coating – AL25 substrate" systems.

The tribotechnical characteristics of the "B_6Si electrospark coating – AL25 substrate" system were obtained using the "shaft-insert" configuration on the SMT-2 setup in the "New Technologies" educational and research laboratory of the Department of Applied Mechanics and Materials Engineering at the National Aviation University.

The coating's coefficient of friction μ decreases sharply to 0.16 (Fig. 2.21, b) as the sliding speed V increases in the range of 1–7 m/s, indicating the formation of a tribofilms in the contact zone during tribooxidation. At the same time, the wear rate of the coating does not exceed 7.5–10 μm/km in the same range of sliding speeds *V* (Fig. 2.21, a).

The most likely main phase of the tribofilms is boron oxide, which melts at a temperature of 450°C and can act as an effective lubricant during the friction process. However, the active evaporation of boron oxide B_2O_3 at a temperature of 900°C leads to the destruction of the protective film at relatively low sliding speeds. This manifests as an increase in wear rate at a sliding speed *V* of 6 m/s (Fig. 2.21, a). During sliding friction of the "B_6Si coating – AL-25 substrate"

system against a 65G steel counter face, a thin film forms on the counter face surface due to reverse transfer of coating material.

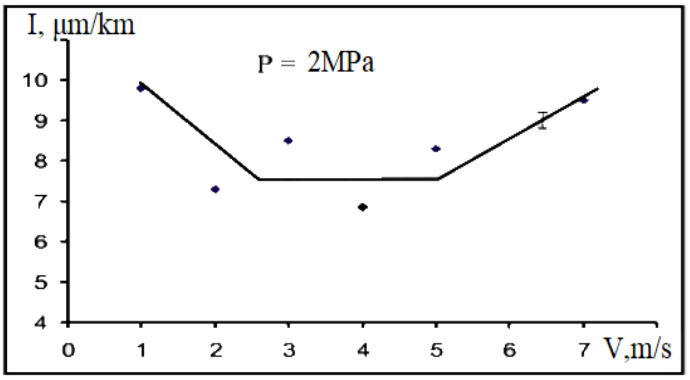

a

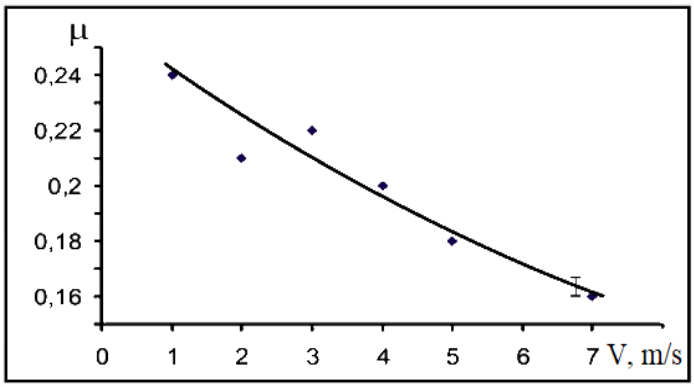

b

Fig. 2.21. Dependence of wear rate I and coefficient of friction μ on sliding speed V for the "B6Si electro-spark coating – AL25 substrate" system

The high lubricating properties of the layer formed on the counter-body surface are evident during friction of the uncoated AL-25 aluminum alloy against a 65G steel counter-body, on the surface of which such a film is preserved. In this case, the uncoated AL-25 aluminum alloy exhibits fairly high wear resistance (~10–15 μm/km), whereas in the absence of a film on the counterbody material, the aluminum alloy wears intensively under the same friction conditions.

Tribotechnical tests were also conducted on the "B_6Si electro-spark coating – AL-9 substrate" system in comparison with the uncoated bronze alloy under dry friction and friction in a kerosene medium. Wear intensity was determined using a

2070 SMT-1 machine in the “New Technologies” educational and research laboratory of the Department of Applied Mechanics and Materials Engineering at the National Aviation University, based on linear wear under a load of P = 10 MPa and a linear speed of V = 0.3 m/s. The test results showed that the wear rate of electrospark coatings on AL-9 aluminum alloy, both under dry friction and in a kerosene environment, is half that of an uncoated bronze alloy, which once again confirms the effectiveness of using electrospark coatings with a high boron content.

According to data from X-ray phase analysis (XPA) and micro-X-ray structural analysis (MXSA), the studied coatings contain oxide phases that form during the formation of the alloyed layer:

- for the CBSAN system (AlN-ZrB_2-$ZrSi_2$) coating—aluminum oxide (Al_2O_3), silicon dioxide (SiO_2), zirconium dioxide (ZrO_2), aluminum oxynitride and borates, as well as mullites;

- for the TBSAN coating system (AlN-TiB_2-$TiSi_2$) – oxides of aluminum (Al_2O_3), silicon (SiO_2), and titanium (TiO_2), aluminum oxynitride and borates, as well as thialite and mullites.

It is assumed that these phases may be present in the composition of tribofilms (in the tribocontact zone), the formation of which is intensified under non-equilibrium tribooxidation conditions and should be accompanied by a reduction in friction and wear with an increase in load and speed parameters under dry friction conditions. The experimental results obtained confirm these assumptions.

As follows from the dependencies of the wear rate of the coatings on the sliding speed $I = f(V)P$=const and the load $I = f(P)V$=const (Fig. 2.22, a, c), at the initial stage of friction, with an increase in load -velocity parameters, the wear rate I decreases to a certain stable value of 4–6 μm/km for the AlN-ZrB_2-$ZrSi_2$ CBSAN coating and to 7–11 μm/km for the AlN-TiB_2-$TiSi_2$ TBSAN coating, respectively.

This indicates the formation of protective tribofilms on the coating surface during the friction process.

With increasing load-speed parameters (sliding speed $V > 0.6$ m/s and load P > 2 MPa), the wear of the AlN-TiB_2-$TiSi_2$ TBSAN coating increases, whereas for the AlN-ZrB_2-$ZrSi_2$ system, the wear intensity I remains consistently low over a wider range of sliding speeds and loads (Fig. 2.22, a, c). This may be the result of thermal protection of the aluminum alloy by zirconium dioxide, which forms as part of the secondary film during the tribooxidation process. Additionally, more pronounced globule formation in the structure of the "AlN-TiB_2-$TiSi_2$ coating–AL-9 substrate" system may have a positive effect on wear intensity. The multilevel heterogeneity of the microstructure of globular electrospark coatings causes a reduction in the effective tribocontact area, which contributes to a significant (up to 103 MPa [241]) increase in pressure and temperature in the friction zone (up to 1000°C and higher) and intensifies the formation of tribofilms.

Fig. 2.22, a and fig. 2.22,b show, for comparison, the dependencies of wear rate $I = f(V)_{P=const}$ and friction coefficient $\mu (V)_{P=const}$ on sliding speed for alloying electrodes. The wear rate of the "CBSAN coating–AL-9 substrate" system approaches that of the CBSAN ceramic of the AlN-ZrB_2–$ZrSi_2$ system at sliding speeds $V > 1$ m/s, which may indicate the formation of a secondary polyoxide film of similar composition on the surface of both the coating and the electrode during the tribooxidation process.

For comparison, Fig. 2.22, a shows the dependence of wear intensity $I = (V)_{P = const}$ for the "CLAB-1 coating – AL9 substrate" system. The similarity of the wear intensity I at sliding speeds ≥ 0.6 m/s for the "CLAB-1 coating - AL9 substrate" and "CBSAN coating – AL9 substrate," both of which contain zirconium dioxide ZrO_2, confirms the possible thermal protection effect of zirconium dioxide on the aluminum alloy. At the same time, the lower wear values of the "TsLAB-1 coating – AL9 substrate" system in the region of low sliding

speeds (V < 0.6 m/s) may indicate a positive effect on wear resistance of the liquid phase of boron oxide B_2O_3.

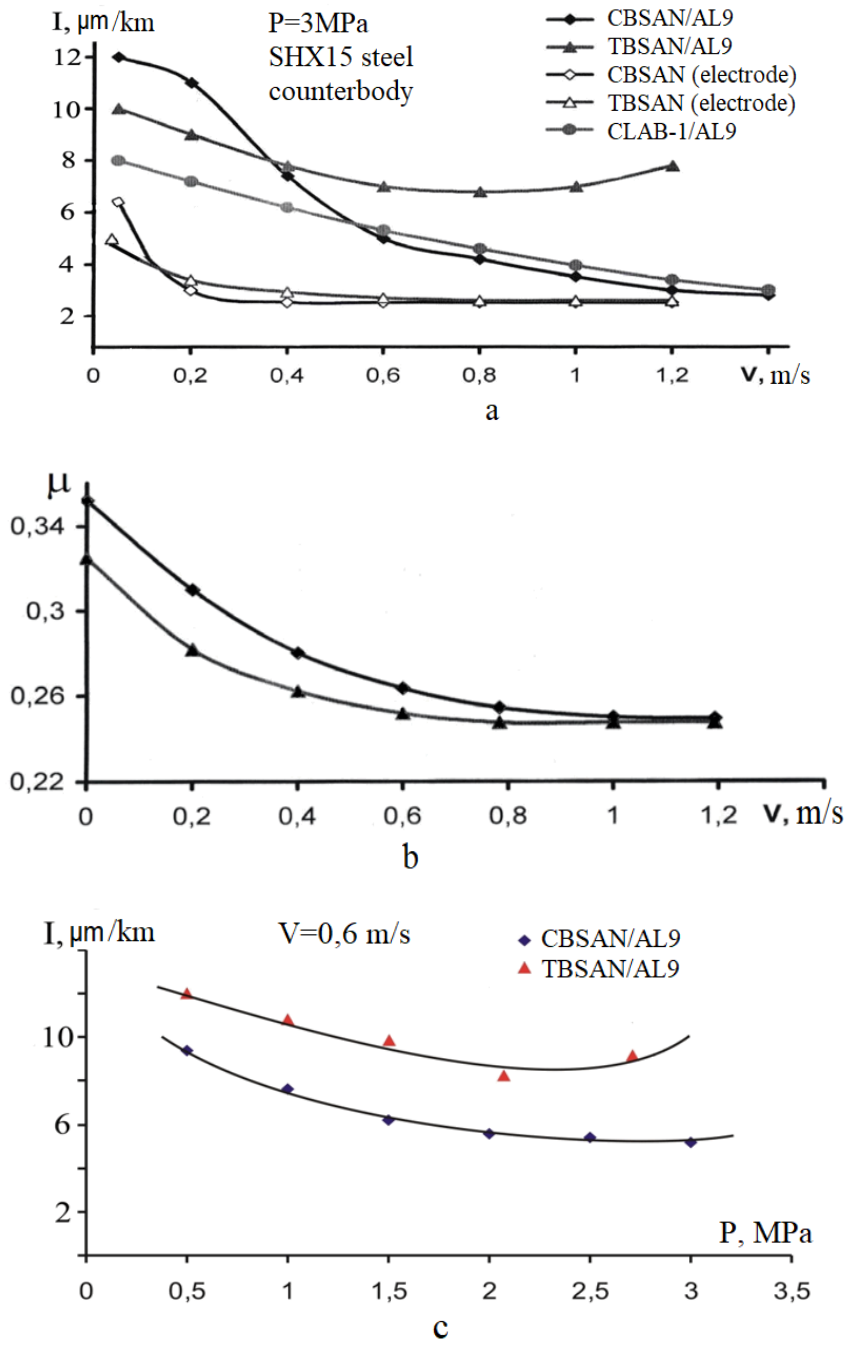

Fig. 2.22. Tribological characteristics of electric-spark coatings and aluminum nitride-based electrodes

The experimentally observed decrease in wear rate I and the coefficient of friction μ with an increase in load and speed parameters (Figs. 2.21, 2.22) indicates

the formation, during sliding friction in air, of a polyoxide tribofilms on the working surface, which acts as a solid lubricant under “dry” friction conditions.

According to micro-X-ray spectral analysis (MXRA) data, its composition includes oxides of aluminum, zirconium, and titanium, mullite, and other composites as promising electrode materials for producing protective coatings on aluminum alloys with adjustable granularity that exhibit high wear resistance.

2.9. Physicochemical criteria for selecting structural components of electrospark coatings

The material of functional high-temperature protective coatings must, as a rule, provide a complex of properties—wear, corrosion, and erosion resistance, resistance to cyclic loads, coating adhesion strength to the substrate, cohesive strength, and others. Therefore, the requirements for coating materials can only be met by using composite materials (CM) through the selection of the composite’s structural components and the coating design method.

These requirements boil down to the following:

1. The composite material (CM) must: have high hardness and strength to withstand mechanical loads; be sufficiently elastic to ensure the coating’s compatibility with the substrate to prevent delamination under impact loads.

This contradiction can be resolved in two ways:

a) by creating a matrix structure of the coating with alternating soft and hard components (a hard ceramic matrix combined with soft metallic inclusions or a soft matrix with hard inclusions);

b) by creating a layered coating structure (“sandwich”) with alternating soft and hard layers. In the case of electric spark coatings, the alloying electrode material may not include a metallic component. This is due to the nature of electric spark coatings, which are discrete (non-continuous) by their nature (continuity ranges from 80–90% for tungsten carbide–cobalt (WC-Co) alloys to 40–60% for tungsten-free ones).

These discontinuities, in the form of patches of base metal alloy modified by alloying components, act as “drainage channels” for residual stresses, limiting the maximum stress level both in the coating itself and in the adhesive interface. Professor B.A. Lyashenko at the G.S. Pysarenko Institute of Strength Problems created controlled discontinuities in the coatings, the size and configuration of which are determined based on the condition of minimizing the stress-strain state under mechanical and thermal influences on the coating [242–251].

2. The composite material (CM) must include structural components that ensure the formation of a tribofilms on the contact surface during tribo-oxidation, which acts as an effective solid lubricant. Such a polyoxide nanoscale tribofilm is formed through phase formation and oxidation of the components comprising the friction surfaces. It is the properties of this film (composition, sintering rate, continuity, and adhesion strength to the substrate) that determine the overall service life of the friction assembly. This allows the composition of the tribofilm in the tribocontact zone to be controlled by varying the coating composition, thereby predicting its service life. Electrospark and gas-thermal coating methods are phase- and structure-forming technologies, since the coating process is carried out at high temperatures in the presence of oxygen/nitrogen. Analysis of literature data and the results of our research show that effective tribofilms are glassy phases, as well as spinel-type oxide systems. Therefore, it is necessary to ensure the presence in the composition of the composite coating of components that would promote the formation of glassy phases, for example, in the form of aluminosilicates (including mullites) and borosilicates (based on boron oxides modified with zirconium and silicon oxides), as well as chromite’s and aluminates of iron, nickel, and titanium. Such tribofilms, acting as high-temperature solid lubricants, contribute to the long-term operation of the friction unit.

3. The selection of structural components for a composite coating (CC) must ensure adhesive strength at the “ceramic-metal binder” and “coating-substrate” interfaces, which is controlled by wetting processes. Adhesive contact is facilitated by the formation of limited solid solutions between the components at the phase

boundary. Thus, the existence of a solid solution of zirconium and titanium borides (Zr, Ti)B_2 suggests that coatings containing zirconium boride ZrB_2 will exhibit enhanced adhesion strength to titanium and hard alloys of the TK grade, which contain titanium carbide. The result of a strong adhesive bond at the phase boundary is intense bidirectional mass transfer of alloying components and matrix/bonding elements, which occurs during the deposition of the composite material (CM). The diffusive, "blurred" nature of element distribution at the "coating-matrix" interface causes a gradient decrease in hardness from the coating into the depth of the matrix (workpiece). Otherwise, microcracks form, the subsequent growth of which leads to delamination and wear.

4. The structural components of the coating must have a similar coefficient of thermal expansion (CTE) or form limited solid solutions to avoid cracking caused by stress due to compressive-tensile effects at the phase boundary. Cracks in electrospark coatings arise as a result of the relaxation of residual stresses that accumulate in the alloyed layer under the influence of pulsed thermomechanical loads from the spark discharge. In this case, the number of cracks can be minimized or even prevented by selecting the optimal processing time topt. The value of the optimal processing time topt is determined from the kinetic dependencies of the electromass transfer parameters and is characterized by a decrease in the rate of cathode mass gain when the processing time exceeds the optimal value $t \geq t_{optimal}$ topt due to mass loss resulting from its brittle fracture.

5. The crack resistance of the cathode material must be higher than the crack resistance of the alloying electrode material to ensure a high electromass transfer coefficient (≥ 60%) of the anode material to the cathode, which is defined as the ratio of the cathode mass gain to the anode erosion during the processing time t. The proposed criteria are generally valid for gas-thermal coatings. For aluminum alloys, the following additional criteria must be considered:

- the electrode material must contain, in an amount of ≥ 50 wt.%, a dielectric component (aluminum nitride AlN) or a conductive phase (LaB_6, B_6Si), which

would form non-conductive compounds (aluminum nitride AlN, aluminum oxide Al_2O_3, and boron oxide B_2O_3) in the interelectrode gap during the high-temperature oxidation of electroerosion products;

- in the case of a composite based on a dielectric component, the phase constituents must ensure electrical conductivity in the anode–interelectrode gap–cathode system;

– the electrode material must chemically interact with the aluminum alloy to ensure adhesive bonding between the coating material and the substrate and, accordingly, to increase the mass transfer coefficient;

– the oxidation products of the electrode material must be high-temperature corrosion-resistant compounds (β-thialite, mullites, solid solutions based on them, and others) that act as a solid lubricant underdry sliding friction conditions;

– to create a structurally heterogeneous globular coating, selective wetting of the main components of the alloying electrode with an aluminum alloy is required, while for a structurally homogeneous coating, there must be no selectivity in the wetting of the alloying components;

- the electrode material must have high hardness and wear resistance to ensure a high level of performance properties of the electric spark coating.

2.10. Strengthening of piston parts of internal combustion engines of vehicles

Aluminum alloys are most widely used in the manufacture of components for various friction assemblies in the automotive and aerospace industries:
pistons for internal combustion engines, compressor pistons, cylinder blocks, crankshaft main bearing housings, electric motor shafts, sliding bearings for hydraulic pumps (131, 244250, 251, , 252-302), gear pump housings (Fig. 2.23, Fig. 2.24).

The entire aircraft control system is a complex hydraulic system that includes various gears and piston pumps. In this regard, it is necessary to improve

the wear resistance of aluminum components in friction assemblies, the most common of which are the plain bearings of pumps, gears, and pistons in internal combustion engines. The most vulnerable areas of the sliding bearings in gear pumps (Fig. 2.24) are the inner surface of the bores, which is worn by the steel shaft, and the surface worn by the gears, which is the side wall of the pump housing.

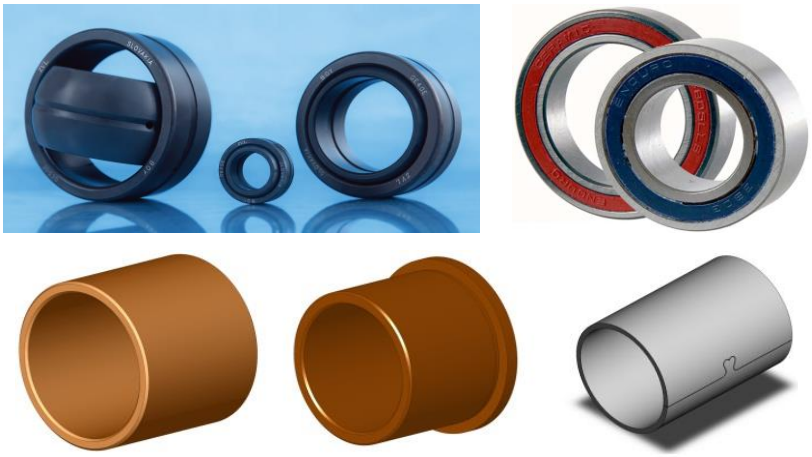

Fig. 2.23. Plain bearings

Fig. 2.24. Plain bearing of the NSh10 gear pump

As for the piston of an internal combustion engine, the following areas require reinforcement: 1) the piston crown, which is subjected to thermal stress due to fuel combustion in the combustion chamber (Fig. 2.25, item 1); 2) the piston skirt (Fig. 2.25, item 4); 3) the ring seats (Fig. 2.25, item 2); 4) the friction

zone between the piston and the pin securing it to the connecting rod (provided that the pin is rigidly fixed to the connecting rod) (Fig. 2.25, item 3).

During tribological tests of the plain bearings of the NSh-10 hydraulic machine gears, whose working surfaces were hardened by the electric spark alloying method using an AlN-TiB_2-$TiSi_2$ electrode material system, it was established at Vinnytsia Tractor Aggregates Plant JSC that the sliding friction coefficients using I-20 oil correspond to those of the anti-friction alloy, and wear resistance increased by 1.5 to 2.5 times. Improving the wear resistance of aluminum alloys through a simple and effective method of electric spark alloying makes them competitive with expensive anti-friction alloys and yields significant economic benefits.

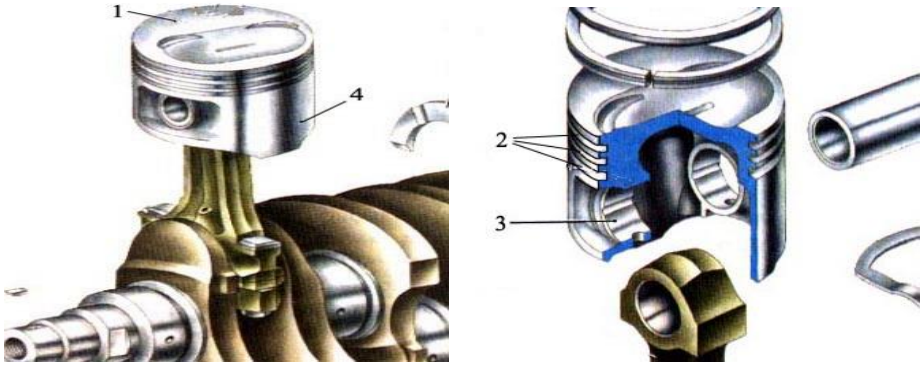

Fig. 2.25. Piston of an internal combustion engine

Conclusions on Chapter 2

In the process of electrospark alloying of alloys, a composite coating system is formed based on an aluminum matrix reinforced with refractory components.

The coatings are characterized by a gradient distribution of phase components across their thickness. The microhardness of the coatings is $H_\mu \sim 4$–10 GPa. The phase composition of the coatings does not change with increasing treatment time.

Taking into account the selectivity of wetting of the electroerosion products by the base material, the factors influencing coating formation have been grouped into three main stages of the electric spark alloying process: anode electroerosion, physicochemical interaction of erosion products in the interelectrode gap, and in the contact zone.

A physicochemical model of electrospark doping with a compact electrode is proposed, which is based on the selection of structural components of the electrode material.

CHAPTER 3

ELECTROSPARK COATINGS WITH A DISCRETE STRUCTURE AND THEIR OPTIMIZATION

The electrospark alloying (ESA) process is discrete in nature [131, 133, 158, 245]. When applying a coating with a discrete structure, the electrospark alloying method offers a number of advantages [242–245, 247–251]:

- the electrical discharge ensures the dimensional stability and properties of individual discrete coating areas;

- by changing the parameters of each individual discharge, discrete areas of various sizes and thicknesses can be deposited. This enables the application of a differential coating (a coating of variable thickness);

- by changing the pulse frequency or the relative movement speed of the electrode and the workpiece, the number of discrete areas on the workpiece's surface, as well as the continuity of the coating, can be adjusted;

- compact and portable equipment, low power consumption;

- the ability to perform a "dry" and "cold" process (without heating the entire workpiece through);

- no need for additional heat treatment;

- the ability to repair workpieces on-site, without disassembling them.

Differential discrete coatings were applied using the electric spark alloying method with the Elitron-22 series of industrial equipment (Fig. 2.1). To restore part surfaces "according to the wear profile" using the electric spark alloying method, electrode materials of the Fe-Ni-Mn-Cu-Al-Si system were used. These materials allow for the application of coatings up to 1 mm thick in a single pass.

The developed technologies and principles for modeling the architecture of discrete-structure electrospark coatings make it possible to select the optimal design for a discrete surface, as well as to choose application modes and coating

materials, taking into account the specific conditions of the friction pair [242, 247, 250, 251 and 258].

The primary goal of discrete-structure electrospark coatings is to ensure a minimal stress-strain state (SSS) of the coating under operational loads. This objective can be achieved by selecting the geometric parameters of the discrete coatings that will minimize stress concentration both in the coating layer and in the plane of adhesive contact. The parameters of discrete coatings are determined based on the stress-strain state (SSS) of the "substrate-coating" composite [235, 238, 240, 241 and 308].

The discrete structure of the electrospark coating allows for a significant increase in its limit state: contact loads—several times over, critical tensile deformations of the substrate—up to two orders of magnitude, and durability—several times greater compared to a continuous coating of the same thickness, composition, and hardness.

The work of researchers at the G.S. Pysarenko Institute for Problems of Strength of the National Academy of Sciences of Ukraine [242–251, 308–310] should be considered the starting point for publications on the creation of coatings with a stress-strain state (SSS)-controlled discrete structure. Subsequently, scientists at the G.S. Pysarenko Institute for Problems of Strength of the National Academy of Sciences of Ukraine further developed this work in collaboration with scientists from the German Aerospace Center (Cologne) [249], the V.N. Bakul Institute for Superhard Materials of the National Academy of Sciences of Ukraine [311], the National Aviation University (Kyiv) [312], and the Zaporizhzhia Automobile Plant [313, 314].

Publications on reinforcing protective coatings (RPCs) with a discrete structure ("Spot-textured coatings") have appeared in distant foreign countries [315, 316]. Thus, the field of developing spot-textured coatings has taken on a global character.

It should be noted that the leading role in the development of spot-textured coatings belongs to the G.S. Pysarenko Institute for Problems of Strength of the

National Academy of Sciences of Ukraine (IPS). The theoretical, technological, and practical foundations of discrete coatings are outlined in a series of master's and doctoral theses supervised by Professor B.A. Lyashenko [245, 250, 251, 308–310]. These works are distinguished by a systematic approach. An analysis of the principles of the methodology for the design, development, and application of discrete coatings shows that success in this area requires solutions to the following problems:

• determining the geometric parameters of a discrete structure based on the conditions for minimizing residual and in-service stresses;

• determining the optimal process parameters for applying discrete coatings.

This section is devoted to addressing these issues.

3.1. Evaluation of the stress-strain state of reinforcing protective electrospun coatings with a discrete structure

Calculating the stress-strain state (SSS) and minimizing its level by selecting the geometric parameters of the discrete structure is the primary goal in enhancing the load-bearing capacity of electrospun coatings. Optimizing the discrete structure to minimize the stress-strain state reduces the scope of experimental research and allows for achieving maximum levels of strength and durability in electrospun coatings.

When analyzing the stress-strain state using numerical methods [245, 250, 251, 308–312, 316-318] for continuous and discrete coatings, a reduction in the stress-strain state and, in particular, in tensile stresses σ+ under contact loads was observed specifically for the discrete structure.

Fig. 3.1 shows the stress-strain diagrams for a traditional continuous coating (a) and a discrete (quasi-continuous) coating (b). In both cases, the coating thicknesses are equal to *h*.

The quasi-continuous layer is modeled by making virtual cuts in the coating at a uniform pitch of *2h*. A Hertzian contact load *P* is applied over a *2h* section,

which is equal to the size of a single discrete section along the X-axis. Cross-section 1 is located parallel to the surface of the “substrate–coating” adhesive bond near the outer surface of the coating. Cross-section 2 is located near the surface of the adhesive bond.

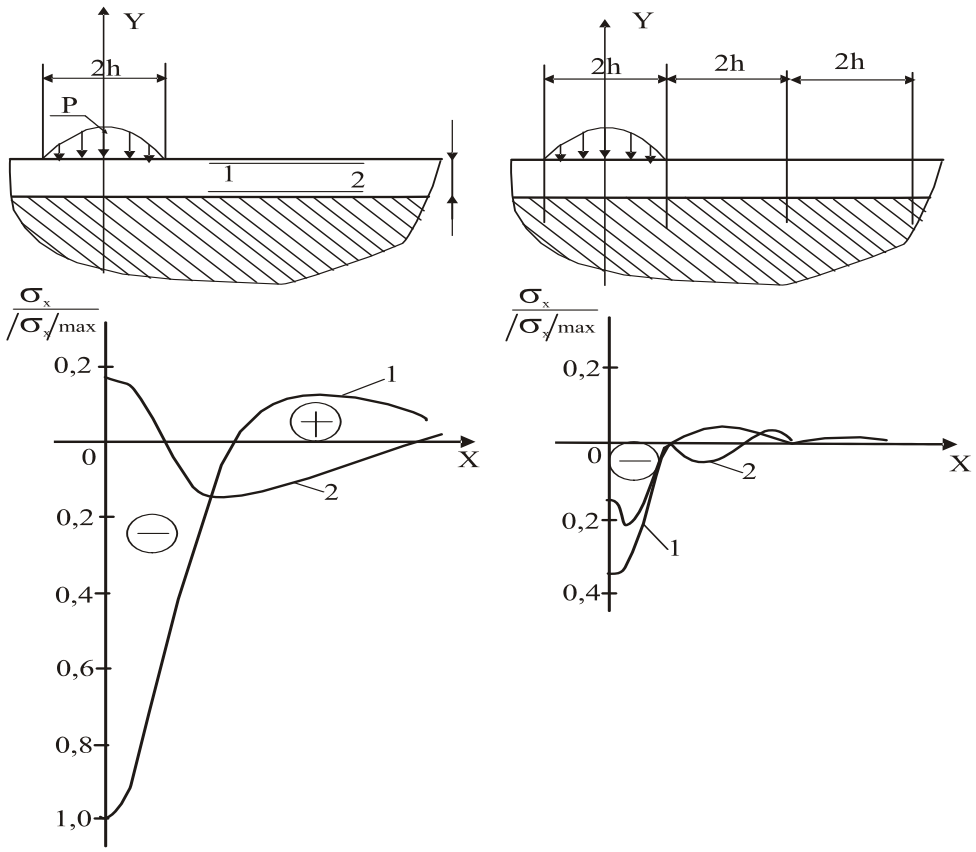

a b

Fig. 3.1. Calculation diagram and stress distribution σ_x under contact load P: a – continuous coating; b – quasi-continuous

Let us compare the stresses σ_x for variants “a” and “b,” as well as for cross-sections 1 and 2 in both cases. The calculation results show that the magnitude of tensile stresses in the critical cross-section is reduced by more than three times, and their maximum value is no more than 5% of the maximum compressive stresses. In the discrete coating near the plane of adhesive contact (cross-section 2), the stresses change sign and transition from tensile stresses to compressive stresses. At

the same time, their magnitude does not exceed 25% of the maximum compressive stresses.

Simulation results show that under contact loads, the discrete structure significantly reduces the stress on the coating. The most significant effect of the discrete structure is a substantial reduction in tensile stresses. This reduces the brittleness of superhard, high-modulus coatings. The Pisarenko-Lebedev strength criterion uses the ratio of the tensile and compressive strength limits of materials as a measure of brittleness [319].

Figure 3.2 shows the calculated values of the ratio of maximum tensile stress to maximum compressive stress on the y-axis. Curve 1 represents a continuous coating, and Curve 2 represents a discrete coating.

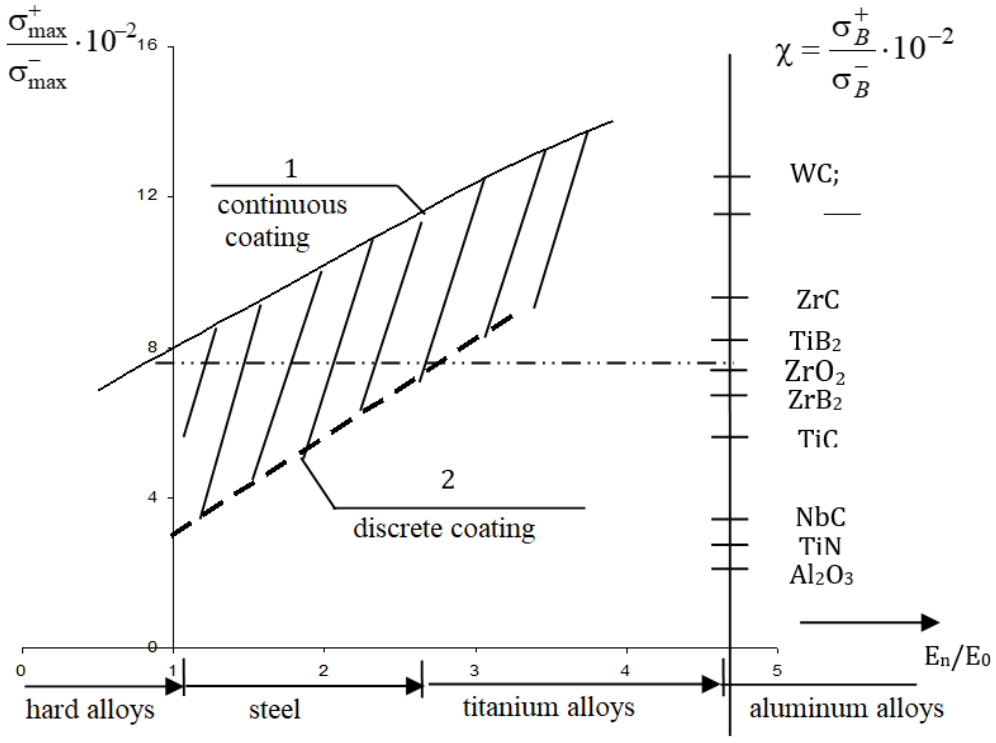

Fig. 3.2. Dependence of the ratio on the modulus of elasticity ratio E_{cover} / E_{base} for continuous (1) and discrete (2) coatings

These curves correspond to calculation schemes “a” and “b” in Fig. 3.1 for equal contact loads. The x-axis shows the ratio of the elastic moduli of the coating E_{cover} and the substrate E_{base}, which models the application of superhard, high-

modulus coatings on hard alloys, steels, Ti alloys, and Al alloys. On the right side of the y-axis is the ratio of the tensile strength to the compressive strength χ for a range of ceramic materials used as coatings [320]. The value $\chi = 0.07$ for zirconia ZrO_2 lies almost entirely below curve 1. This means that in a solid zirconia (ZrO_2) coating, where the ratio of the coating's elastic modulus E to the substrate's elastic modulus E_{coveo} (E_{covep}/E_{baso}) exceeds 0.8 under contact loading according to the selected scheme, tensile stresses reaching critical values will arise.

A discrete coating (curve 2) ensures functionality in this zone. This is consistent with accumulated experience in the use of superhard and brittle coatings on various structural materials.

Fig. 3.1, b shows an idealized calculation scheme in which the distance between adjacent discrete sections is zero. The calculation of the stress distribution for a discrete structure requires consideration of such geometric parameters of the coatings as the distance between discrete sections, the dimensions and shape of the sections in plan view, the thickness (or depth) of the coating, and the shape of the section edges. It is by varying these parameters that the stress-strain state is controlled and minimized under given external loads.

3.2 Wear-Resistant Discrete Coatings

Aluminum alloys are widely used in mechanical engineering, but the challenge of increasing their hardness and wear resistance remains a pressing issue. To this end, virtually all traditional methods of applying hardening protective coatings (HPC) are used. In engine manufacturing, the most common and high-wear components are the piston and cylinder liner of an internal combustion engine. To strengthen pistons and cylinder liners of internal combustion engines made of aluminum alloys, coatings with a discrete structure are used [252, 254, 271, 276, 278].

The “ring–piston groove” tribological interface determines the engine’s service life [278]. Surface strengthening of the piston ring grooves in an internal combustion engine can be achieved by applying discrete coatings.

The electric spark alloying method, which uses rod electrodes, is best suited for strengthening the groove due to its structural feature (height $h = 2…3$ mm with a depth $L > 5$ mm). This feature limits the capabilities of traditional surface hardening technologies. Positive results in strengthening the shoulders of the annular groove have been obtained using electron beam and laser technologies, as well as methods of electrocontact chromium plating and friction-mechanical rubbing, which is a variant of solid-state chemical-thermal treatment [274, 275, 277, 278].

The principle of discrete coatings is implemented using various surface hardening techniques [242–252, 304–316]. However, the most suitable and accessible method for producing discrete coatings is the electric spark alloying method. This method is discrete in nature and offers the following advantages [242–245, 247–251]:

- a single electrical discharge ensures the dimensional stability and properties of an individual discrete coating element, i.e., it ensures reproducibility of properties;

- the effectiveness of electrospark coatings lies in structuring/designing the coating surface in such a way as to create a regular alternation of hard and soft regions in order to minimize the stress-strain state of the surface. Such a regular structure can be realized in the form of globules or islands on the surface;

- a minimal number of controllable process parameters—current intensity, electrode oscillation frequency, and the speed at which the electrode moves across the surface of the workpiece being hardened;

- no prior surface preparation is required;

- by changing the electrical parameters of each individual discharge, it is possible to apply discrete areas of various sizes and thicknesses, which allows for the application of a differential coating, i.e., a coating of variable thickness;

- by changing the pulse frequency or the relative movement speed of the electrode and the part, one can adjust the number of discrete areas on the part's working surface, as well as regulate the coating's integrity;

- the equipment is portable and compact, has low power consumption, and allows for "dry" and "cold" processes (without heating the entire workpiece through).

- there is no need for additional heat treatment, as the treated area remains hardened while the heat from the discharge is dissipated into the workpiece material;

- the ability to locally strengthen and repair large-sized parts, including "in situ," without disassembling them;

- creating a discrete structure in a single pass of the electrode significantly increases the productivity of the electric spark alloying process (part of the part's surface remains uncoated).

Research on electrospark coatings with a discrete structure for strengthening internal combustion engine pistons made of aluminum alloys is presented in [252, 271, 274–276, 277, 278]. The effectiveness and feasibility of further developments in this area of surface strengthening have been demonstrated.

The discrete structure of the coating ensures: 1) high adhesive and cohesive strength of the coating, especially under high contact loads; 2) no cracking or delamination of coating particles under operating conditions.

It is precisely the resistance of the superhard coating to delamination that prevents wear particles from entering the lubrication system of internal combustion engines.

3.2.1 Tribotechnical characteristics of discrete strengthening protective coatings

The test specimens were manufactured from AL25 and AK6 alloys, which were cast in a mold and heat-treated in accordance with DSTU 2839-94.

Specimen preparation involved electric spark alloying using a copper rod electrode, followed by machining. A coating with a discrete structure and 60–65% coverage (Fig. 3.3) was applied on a modernized EFI-25M installation using milling or turning machines. Control samples were made of cast iron. Wear resistance was investigated under reciprocating sliding, simulating the operation of the “ring-piston groove” tribological contact pair.

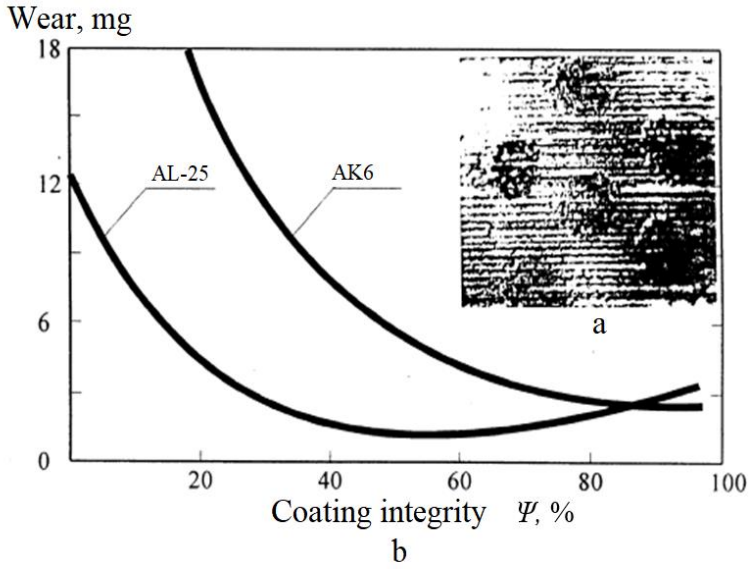

Fig. 3.3. Dependence of the wear resistance of aluminum alloy specimens on the compactness of the hardened layer (b), together with a section of the working surface of the coated specimen (a)

Weight loss diagrams for AL-25 alloy samples in their as-received state and with a discrete-structure coating are shown in Fig. 3.4. Test results at a temperature of 2000°C show that the unhardened AL-25 alloy is serviceable up to specific loads of 8...8.5 MPa (Fig. 3.4, a). As the load increases, fatigue cracks form, leading to the failure of the specimen. AL-25 alloy specimens with a discrete-structure coating paired with cast iron showed a negligible change in weight loss with increasing specific loads across the entire tested range (Fig. 3.4, a), indicating the high wear resistance characteristics of the strengthened surface.

The friction characteristics of the AL-25 alloy do not deteriorate as the load increases; rather, a noticeable decrease in friction force is observed as the amplitude of relative displacement increases. Raising the test temperature to

2000°C (Fig. 3.4, b) results in greater wear of the AL-25 alloy in its as-received condition.

The absence of aluminum transfer from the hardened surface to the cast iron specimens is very important. On the cast iron in contact with the AL-25 alloy, processes of adhesion and sticking occur, which are indicated by a negative weight gain. The alloy is not very sensitive to an increase in the amplitude of relative displacement (Fig. 3.4, c), which indicates good damping properties of the material.

Tests at room temperature showed that the wear resistance of the coated alloy is sensitive to changes in the amplitude of relative displacement. At amplitudes above 35 μm, an increase in the weight loss of the hardened sample surface is observed (Fig. 3.4, c). Cast iron exhibits minimal wear under these conditions.

Metallographic analysis revealed intense oxidation of the alloy at elevated temperatures compared to tests conducted at 200°C. Significant degradation of the cast iron was observed compared to room temperature. However, no adhesion of the aluminum alloy was observed on the cast iron specimens.

The anti-friction properties of the friction pair (AL-25 alloy with coating – cast iron) improve as the load increases to 13 MPa, after which a slight deterioration is observed. An increase in the amplitude of relative displacement leads to an increase in friction force. Raising the test temperature to 2000°C revealed an inversion of certain wear resistance and friction properties of the AL-25 alloy with coating – cast iron pair.

The hardened surface exhibits high wear resistance across the entire studied range of specific loads (Fig. 3.4, b) and relative displacement amplitudes (Fig. 3.4, d), with no sensitivity to increasing amplitude. It has been established that coated samples exhibit high wear resistance at relative displacement amplitudes exceeding 50 μm; however, under these conditions, wear of the cast iron counter face increases.

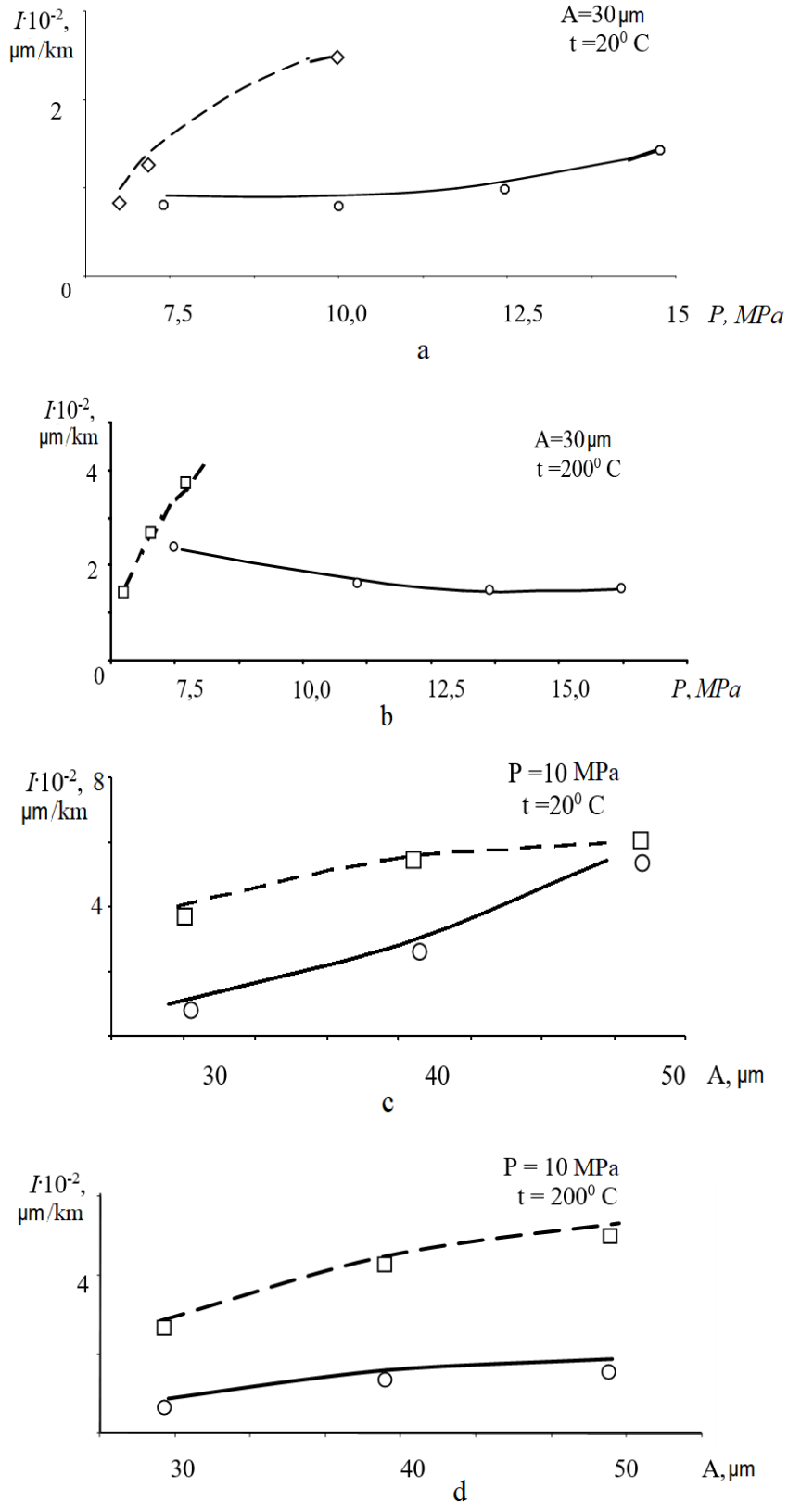

Fig. 3.4. Change in weight loss of AL-25 alloy specimens in their initial state and with a discrete-structure coating as the specific load P (a, b) and the relative displacement amplitude A (c, d) increase.

Test base N = 2,105 cycles, oscillation frequency f = 30 hertz (Hz):

○ - with coating; □ - without coating.

Test results under sliding friction conditions without abrasive lubrication at various temperatures and during reciprocating motion demonstrated high wear resistance of the surfaces of AL-25 alloy samples with a discrete-structure coating.

Fig. 3.5 shows comparative diagrams of the weight loss of the samples over a distance of 7.2×10^3 m at various temperatures under sliding friction conditions without lubrication. As can be seen from the diagrams, the discrete-structure coating significantly increases the wear resistance of the AL-25 alloy, both at normal temperatures and at temperatures close to the operating conditions of pistons in internal combustion engines.

It is worth noting one important feature observed during testing. At small amplitudes under reciprocating motion conditions with an overlap ratio greater than one, zones arise that do not lose contact. In this case, when AL-25 alloy specimens in their as-received state rub against cast iron rollers, a build-up layer forms consistently. The composition of the growth was not studied, but based on our understanding of the processes occurring during the friction of such surfaces, this growth is a consequence of the increased tendency of the Al-25 alloy to seize. Under the same test conditions, no growths were observed on samples with discrete-structure coatings.

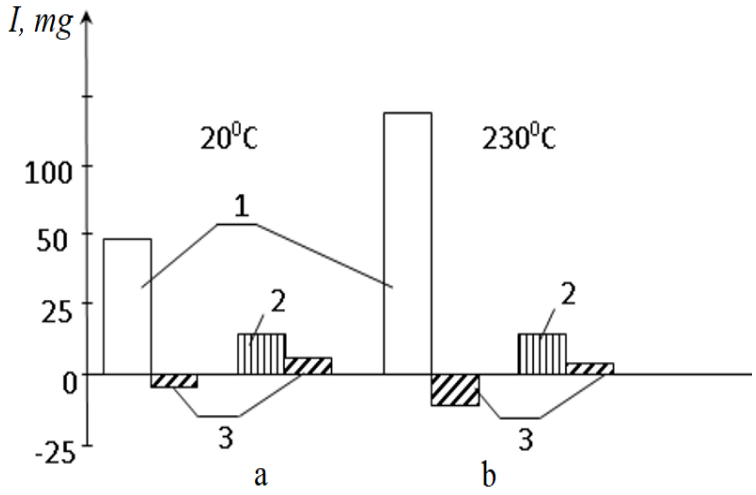

Fig. 3.5. Weight loss diagram for AL-25 (I) samples over a friction distance of 7.2×10^3 m at temperatures of 200°C (a) and 230°C (b):

1 – uncoated; 2 – discontinuous coating; 3 – counterbody

Given the reciprocating nature of the interaction between the ring and the piston, as well as the relatively small amplitude of movement along the surface of the piston groove, reducing the tendency for deposits to form by applying a coating with a discrete structure is a positive factor in improving the performance of the assembly. Test results under sliding friction conditions show that applying coatings with a discrete structure improves the anti-friction properties and wear resistance of AL-25 alloy working surfaces compared to their initial state.

The generalized dependence of the change in the coefficient of friction and the wear rate of the compared materials is shown in Fig. 3.6. The graphs show that the discrete-structure coating increases the pressure at which the catastrophic failure process begins by a factor of 1.5–2.

The laboratory studies concluded with contact fatigue tests. The contact fatigue tests were conducted on an MKV-K test rig under conditions of frictional rolling. The tests involved running-in cylindrical samples with a working diameter of 10 mm between rigid rings using a friction transmission mechanism with a two-cycle load per sample revolution. A normal load was applied to the sample via the driven ring using a spring mechanism. The tests were conducted using M10-G2 oil as lubrication.

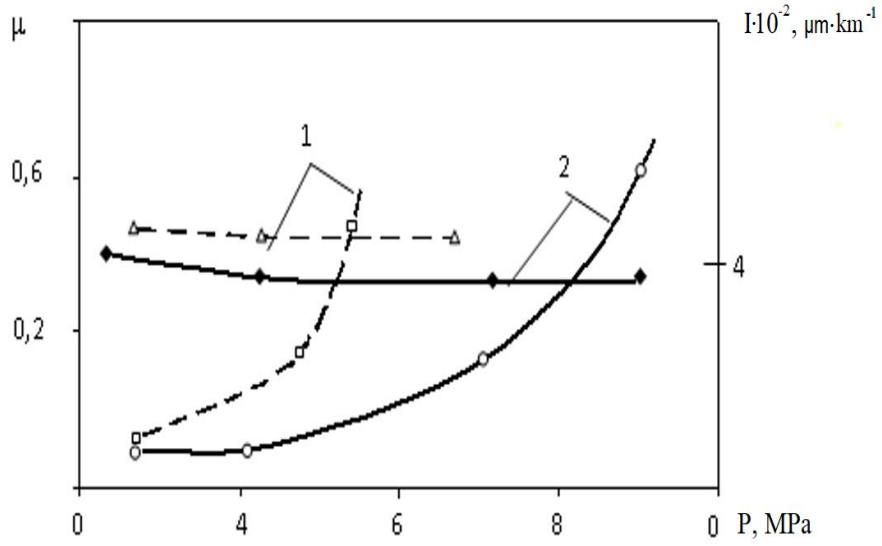

Fig. 3.6. Variation of the coefficient of friction μ and wear rate I as a function of load P (• – μ, ○, □ – I): 1 – uncoated; 2 – discontinuous coating.

The results of the contact fatigue study of the compared sample batches are shown in Fig. 3.7.

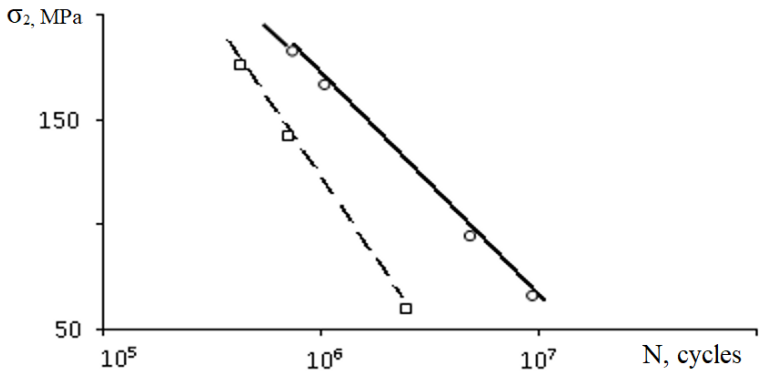

Fig. 3.7. Contact endurance of the AL-25 alloy:
□ - uncoated; ○ - spot-coated

The graphs clearly show that applying discrete coatings to the surface leads to an increase in contact endurance. Since the literature [242, 321] notes the extremely low contact endurance of traditional surface hardening methods, the increase in the contact endurance of the aluminum alloy can be explained by the discrete structure of the coating.

3.2.2. Strengthening of pistons of internal combustion engines of vehicles

The positive results achieved in improving the wear resistance of aluminum alloys through the application of discrete coatings made it possible to move from laboratory testing of samples to bench testing of actual components. The key to success was the absence of cracking and delamination of the discrete coating, i.e., there is no risk of hard wear particles forming that could enter the lubrication system of an internal combustion engine and cause premature failure.

To determine the competitiveness of electrospark discrete coatings, the state of the art was analyzed, as well as trends in improving the wear resistance and durability of internal combustion engine pistons [271]. The need to improve internal combustion engines is linked to enhancing operational characteristics:

pressure in the combustion chamber, crankshaft speed, and specific power per unit of engine mass. Engine performance is also boosted by introducing forced induction into the combustion chamber, specifically turbocharging.

The increasing demands placed on the operation of machines and mechanisms—particularly the rise in dynamic loads—make it necessary to reduce the weight of components. Consequently, there is a growing preference for using lightweight yet strong metals and alloys as structural materials. High specific strength and low specific weight have led to the widespread use of aluminum alloys in engine manufacturing [271]. Recently, titanium alloys have also found application. However, the effectiveness of their use depends on improving the service properties of component surfaces [322].

Defects in pistons of diesel and gasoline internal combustion engines were classified and grouped over three decades ago [323], and the situation has not changed significantly to date. Defects include: damage to the piston crown, the compression ring zone, and the piston bearing surface, as well as damage related to the piston pin and the combustion chamber rim.

For turbocharged diesel engines, wear in the groove beneath the first compression piston ring is the most common issue. The cause of accelerated wear in the ring groove at operating temperatures is the difference in hardness between the mating parts—the piston and the rings. At a temperature of 295°C in the piston groove area for tractor diesel engines, the hardness of the aluminum alloy from which the piston is made is 32 HB, while the high-strength cast iron from which the compression ring is made has a hardness of 140 HB. As the temperature increases, the difference in hardness grows due to the steeper temperature dependence of hardness and its decrease for aluminum alloys.

Thus, the ring’s hardness being nearly four times higher is the main cause of accelerated wear of the piston groove. The nature of the interaction between the components of the cylinder-piston group (CPG) and the variation in hardness between the groove and the ring lead to uneven wear of the lower shoulder of the piston groove, which bears the pressure of the ring during the piston’s power

stroke. Due to the uneven wear of the groove, the ring begins to operate with a misalignment of its supporting end surface.

Positive results from laboratory tests, the absence of cracking and delamination of the discrete-structure coatings under various load conditions, allowed us to proceed to bench and operational tests. The purpose of the bench tests was to determine the effectiveness of strengthening the ledges of the upper ring groove in production pistons of internal combustion engines made of AL-25 alloy by applying discrete-structure electric spark coatings.

The production pistons were hardened using the electric spark alloying method, followed by surface plastic deformation (smoothing). Coatings with a discrete structure were applied with a coverage of 60–65% on a modernized EFI-25M installation, with the pistons mounted in a lathe and the operations of electric spark alloying and smoothing of the ring groove performed under a single operational setup.

The required topography, surface layer properties, and stability of the deposition process were ensured by alloying with a copper rod electrode (DSTU 859-2003) at a working current of 35–40 A.

During bench tests, the pistons with reinforced grooves were fitted with production-grade compression rings and liners without any modifications. The effectiveness of the reinforcement was evaluated by comparing the results with those of tests on mass-produced cylinder-piston group components. The evaluation criteria included both the wear resistance of the friction pair and changes in the engine's key performance characteristics, including oil pressure and consumption, fuel consumption, and engine power.

It should be noted that the most objective method for evaluating the effectiveness of hardening is the results of field tests. And although this approach involves significant costs and time, in global engine manufacturing practice, bench testing is a universally recognized method for evaluating new technical solutions, both in the design of components and in the field of manufacturing technologies.

Bench tests of hardened pistons were conducted on a D-240 engine using the following methods:

- accelerated evaluation of abrasive wear resistance [397];
- accelerated evaluation of ring-groove pair wear resistance;
- reliability testing.

The results of measurements of key technical characteristics during engine tests with production and hardened pistons, based on accelerated tests over 50 hours, are shown in Fig. 3.8 [271, 248].

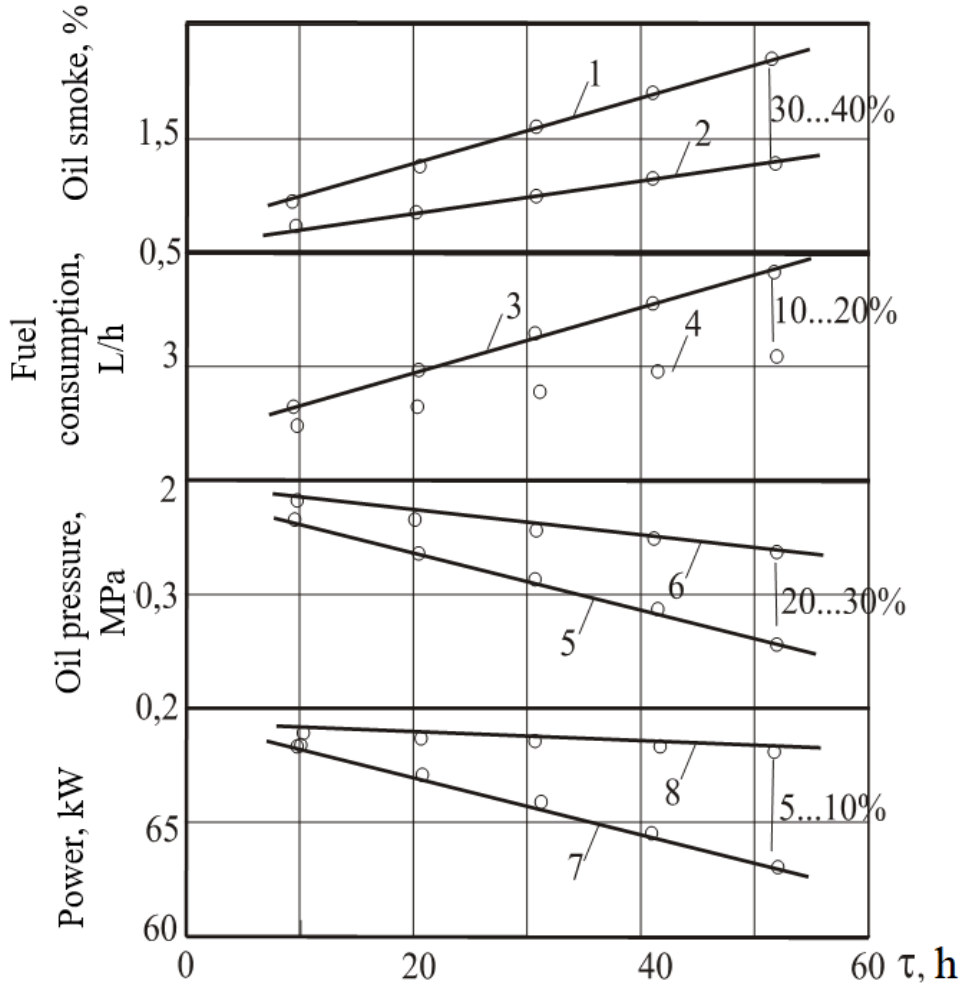

Fig. 3.8. Performance characteristics of engines with standard (1, 3, 5, 7) and reinforced (2, 4, 6, 8) pistons

The performance characteristics of an engine equipped with pistons featuring a reinforced groove increase by an average of 5–40%. The improvement

in engine performance is due to a reduction in the total clearance between the ring and the groove, resulting from reduced wear on both the ring groove and the ring itself.

Figure 3.9 shows the results of bench tests on reinforced pistons. Applying coatings with a discrete structure reduces the total wear of the ring-groove pair by an average of 30–40% (Fig. 3.9, a) and the clearance at the ring joints by 30–40% (Fig. 3.9, b). Stabilization of the piston groove shape with a strengthening coating leads to a 50–60% reduction in engine cylinder liner wear (Fig. 3.9, c).

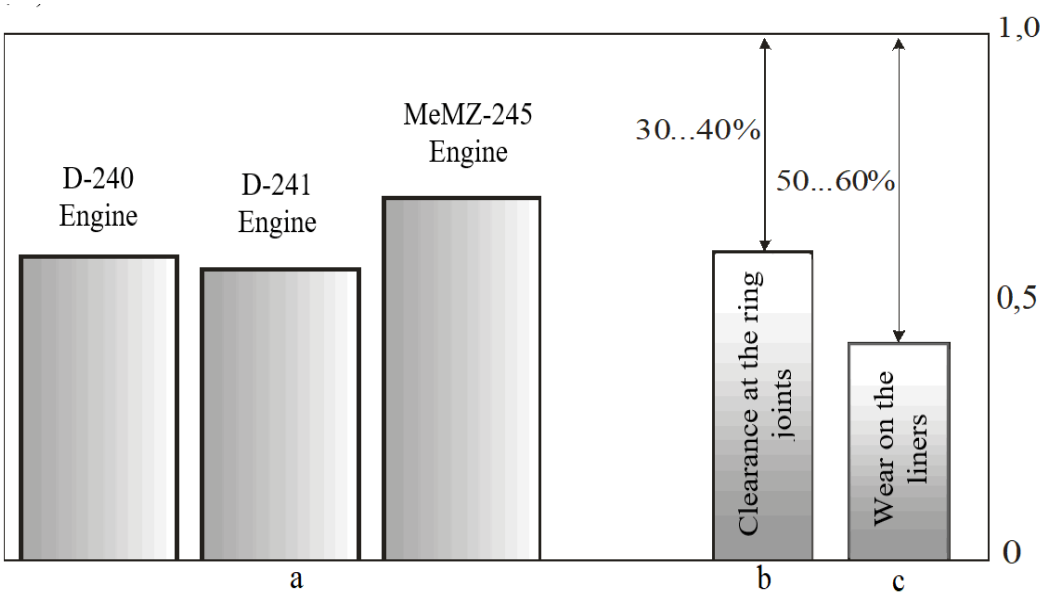

Fig. 3.9. Results of comparative bench tests of cylinder-piston group components with hard-facing coatings. The total wear of the ring-groove pair of a production D-240 engine piston is taken as the unit of measurement.

Visual inspections of the pistons during testing revealed no cracks, chips, or coating delamination on the hardened surface, indicating their high operational reliability. A reduction in total wear in the ring-groove interface by an average of 35% allows for an increase in the engine's overhaul interval, for example, for the D-240 from 6,000 to 8,100 operating hours.

A comparative analysis shows that applying coatings with a discrete structure ensures that the wear resistance of the upper piston groove in turbocharged diesel engines is on par with that of the upper piston groove

reinforced by electric arc remelting or through the use of non-resistive inserts, as employed by a number of foreign companies. However, a technical and economic analysis indicates significant advantages of applying discrete coatings over other methods of improving the performance of piston grooves.

For example, a comparison of the main material and energy costs when performing strengthening processes via electric spark alloying and plasma remelting shows that the use of argon gas is completely eliminated from the technological process, while the consumption of alloying materials is reduced by 90%, electricity consumption by 80 times, and production space by up to 70%.

The effectiveness of coatings with a discrete structure in strengthening the ring grooves of carburetor engine pistons was evaluated based on the results of operational tests.

The increase in wear resistance of the reinforced pistons compared to the production pistons installed on the same engine was determined after 50,000 kilometers of off-road driving in a VAZ-2121. It was determined that, compared to the production piston, the wear resistance of the hardened piston increased:

- by a factor of 2 for the upper ring groove;

- by a factor of 1.5 for the production compression ring operating in contact with the hardened groove.

Wear on the ring-groove pair has been reduced by a factor of 4 [242, 248]. Recent tests of gasoline automotive engines conducted under the European NEDC cycle indicate that approximately 20% of fuel is consumed to overcome friction. For diesel engines, these losses are even higher [324]. The most effective way to reduce these losses is by improving the tribological characteristics of the cylinder-piston group and crankshaft bearings.

Therefore, the technology of applying discrete coatings by the electric spark alloying method is promising in engine manufacturing for reducing friction by strengthening the piston, crankshaft bearings, and cylinder liners. Let us consider in more detail the problem of increasing the service life of cylinder liners in internal combustion engines.

3.2.3 Hardening of Cylinder Liners in Internal Combustion Engines

Positive results from laboratory tests of discrete coatings obtained by the electric spark alloying method on aluminum alloys and results from bench tests of internal combustion engine pistons made it possible to proceed to evaluating the application of discrete coatings to internal combustion engine cylinder liners [294]. Improvements in internal combustion engines are associated with increased power and reduced fuel consumption. These improvements are achieved through direct fuel injection into the cylinders, full variable valve timing, reduced displacement, and the use of high boost pressure [325].

The supercharging of internal combustion engines is associated with an increase in operational parameters: combustion chamber pressure, crankshaft speed, and specific power per unit of engine mass. All of these parameters lead, to varying degrees, to an increase in mechanical and thermal loads on internal combustion engine components.

The problem of reducing friction in the tribological interfaces of internal combustion engines is particularly relevant. Friction losses are directly related to the wear of internal combustion engine components. Converting high-speed diesel engines to “heavy” fuel causes an approximately twofold increase in wear of the cylinder-piston group [271].

The performance of the cylinder liner determines the service life of the cylinder-piston assembly and the entire engine. While the piston in an internal combustion engine is considered a wear part, replacing and rebuilding the cylinder liner involves significant costs. The general trend toward reducing engine weight has led to cylinder heads being most often made of aluminum alloys and a gradual transition from cast iron cylinder blocks to aluminum ones [325].

In addition to the advantages of reduced weight and manufacturing complexity, the benefit of an aluminum block lies in improved cooling conditions for internal combustion engines due to the high thermal conductivity of aluminum alloys. Therefore, there is a growing trend toward the use of lightweight metal

cylinder blocks with various bushings. The need for liners stems from the low wear resistance of aluminum alloys in the cylinder-piston assembly [326].

However, the idea of creating internal combustion engines made entirely of aluminum alloys has not lost its significance [327]. The primary goal of the world's leading engine manufacturers remains the development of a sleeve-less cylinder block made of aluminum alloy [328]. Along with high strength and manufacturability, the main requirements remain wear resistance and anti-seizing properties comparable to those of Fe alloys.

This complex challenge is being addressed through the creation of alloyed aluminum alloys [295–300, 329-333]. Silicon Si (up to 40%) [329–332], lead (up to 8%) [329], magnesium Mg (up to 5%) [329, 332], copper Cu (up to 10%) [329, 332], as well as iron (Fe), nickel (Ni), and chromium (Cr) [295–298, 300, 301 330, 332].

Aluminum alloys may contain varying amounts of zinc Zn, manganese Mn, zirconium Zr, lithium Li, titanium Ti, boron B [292–299, 301], rare earth metals (REM) with a total content of 0.5–10% [250], as well as up to 10% vanadium (V) and cobalt (Co) [301]. In addition to its excellent casting properties, silicon (Si) enhances the alloy's hardness and wear resistance [329, 332]. Lead acts as a solid lubricant on the sliding surface at elevated temperatures [329]. Magnesium (Mg), copper (Cu), and other elements contribute to dispersion strengthening, increasing the corrosion resistance and heat resistance of aluminum alloys [295–309, 329–332].

Alloying additives solve the problem of improving resistance to burning [334]. One of the requirements for alloyed aluminum alloys remains machinability, which is also ensured by alloying additives [332, 333].

A modern high-strength and wear-resistant aluminum alloy for internal combustion engines is produced using powder metallurgy (PM) technology from powders of aluminum (Al), zinc (Zn), magnesium (Mg), copper (Cu), and lead (Pb). Alloyed aluminum alloys are also used in the manufacture of high-pressure compressor blocks [333].

A design for a sleeve-less block made of a bimetallic casting has been developed by sequentially pouring the heat-resistant, wear-resistant alloy $AlCu_5NiCoSbTiZr$, followed by the light alloy $AlSi_6Cu_4$ with good casting properties [300].

One of the emerging trends in the development of aluminum blocks is the use of aluminum-matrix composite materials (CM). Increased wear resistance is achieved by reinforcing the aluminum matrix with hard ceramic particles [327, 335–337]. Dispersed particles are used as fillers at concentrations of 1–30%, including:

- oxides of aluminum (Al_2O_3), magnesium (MgO), zirconium (ZrO_2), and silicon (SiO_2);

- carbides of tungsten (WC), titanium (TiC), silicon (SiC), and boron (B_4C);

- nitrides of titanium (TiN), boron (BN), aluminum (AlN), and silicon (Si_3N_4);

- borides of niobium (NbB), zirconium diboride (ZrB_2), and aluminum diboride (AlB_2).

The average particle size of the ceramic is 0.05–150 μm. The advantage of the composite in terms of wear resistance is attributed to elongated particles [335].

Graphite, molybdenum disulfide (MoS_2), and/or tungsten disulfide (WS_2) are added to the composite as solid lubricants [327, 336].

Graphite additives at a content of 1–8% with an average particle size of 10–50 μm improve sliding properties and reduce the likelihood of seizing between rubbing parts [335].

Nissan's portfolio includes the use of high-alloy aluminum alloys, in which highly filled composite materials are used as the matrix [335, 2336]. The composite is formed through a high-speed crystallization process [327]. In the development of aluminum-matrix composites, Al_2O_3 and carbon fibers are used as reinforcements [338].

The high tribological characteristics of these composites under sliding conditions, especially under "dry" friction, are emphasized. Test results for

cylinder liners of internal combustion engines made from composites containing aluminum oxide (12%) and carbon (9%) fibers demonstrated their operational advantages compared to other materials used for this purpose [338]. It should be noted that sleeve-less blocks made of aluminum-matrix composites have been used in Honda sports motorcycles since 1994 [327].

A compromise solution involves manufacturing an aluminum block with reinforcing components made of steel and cast iron [326, 339]. However, this raises the challenge of forming a strong bond between the cast-iron liner and the aluminum alloy of the cylinder block.

To increase the service life of an automotive engine, General Motors Corp. uses gas-thermal spraying of iron-based (Fe-based) powders onto the bored holes of steel liners in the aluminum block. This ensures the necessary durability of the piston group and reduces engine manufacturing costs [201]. To improve the adhesion of the cast iron liner surface to the aluminum alloy of the cylinder block, a 200-micron-thick AlSi coating is applied via gas-thermal spraying [240].

Methods of securing liners in the cylinder block using ribs are also used [326]. The installation of steel and cast-iron liners into an aluminum block presents a perennial challenge: improving wear resistance. Traditionally, this problem is addressed through final machining.

The process of honing cylinder working surfaces is widespread in engine manufacturing in various technological variants. In mass production, a domestic method is used to improve the anti-friction and anti-wear properties of cast iron cylinder liners—flat-top anti-friction honing [341, 342]. A regular micro-relief is applied using diamond lapping methods [343].

Audi has launched a 3.0-liter turbocharged high-output diesel engine into series production.

Leading engine manufacturers use laser honing for the surface hardening of cast iron cylinder liners [344]. The working surfaces of cast iron cylinder liners were subjected to laser honing, which reduced piston ring wear by a factor of 2, oil

consumption by 25%, and fuel consumption by 3%. The outer layer of the working surface was melted to a depth of 2 μm, forming metal vapors, under the action of which atmospheric nitrogen entered the melted layer.

After the laser pulse ended, the layer of the working surface formed a nanocrystalline structure with a nitrogen content of up to 18% during cooling. As a result, the coating, approximately 200 nm thick, consists of iron nitrides and carbides and exhibits high hardness and ceramic-like properties [342]. According to Opel, laser honing of the liners halved the wear of the cylinders and piston rings. Laser treatment of cast iron liners increases their wear resistance to the level of a production liner with a nichrome insert [344].

It is worth noting a trend in engine manufacturing toward replacing steel and cast iron liners in aluminum blocks with aluminum liners. For this purpose, aluminum matrix composites containing dispersed particles of Ni-coated graphite are used.

Compared to cast iron liners, aluminum alloy liners exhibit less wear and contribute to increased engine power [344]. A liner made of a high-alloy aluminum alloy with 3% graphite possesses all the positive qualities of cast iron while being significantly lighter. The use of aluminum liners instead of cast iron ones provides an increase in engine power of 11–27%, fuel savings of 4–28%, and a reduction in friction losses of 18%, along with a significant reduction in piston ring wear and improved dimensional stability of the pistons.

Honda has patented a wear-resistant, heat-resistant, and durable aluminum-based composite material for cylinder liners. The aluminum matrix contains inclusions of aluminum oxide (Al_2O_3) (3–5%) and graphite (0.5–3%). A two-layer liner is also offered, the inner working layer of which consists of the patented composite [345], and the outer layer of a deformable aluminum alloy.

Peak Werkstoff GmbH supplies Daimler-Chrysler with aluminum alloy cylinder liners for high-load turbocharged engines [346]. The use of aluminum liners eliminates the problem of ensuring a strong bond between the liner and the block. The power of internal combustion engines with aluminum cylinders

increases by up to 10% while fuel consumption decreases by the same amount [296].

An aluminum alloy sleeve solves the problem of reliable heat dissipation, which is particularly important for modern air-cooled internal combustion motorcycle engines. This allows for an increase in specific power output to a level of 37–52 kW/L [347].

For aluminum liners, improving wear resistance remains a challenge. Therefore, the most promising approach is the use of strengthening coatings capable of increasing surface hardness and reducing the coefficient of friction. In addition, these coatings solve the “cold start” problem that occurs when using uncoated aluminum liners.

In the field of engine manufacturing, electroplating methods are the most common technique for applying wear-resistant coatings to aluminum liners. The most frequently used coatings are traditional hard chrome (Cr) [348] and nickel (Ni) coatings with boron and silicon carbide (SiC) additives [349, 350]. BMW has developed and implemented an industrial technology for the electrolytic deposition of a nickel-silicon carbide (Ni-SiC) coating system with a deposition rate of 100 μm in 16 minutes [351]. Additionally, this technology enables the restoration of worn aluminum cylinders.

Anodizing [349, 352] and micro-arc oxidation [353] are also used. Increased wear resistance is achieved by etching the surface of the aluminum-matrix composite, after which hard silicon (Si) particles form protrusions above the liner surface [350].

One of the most common coating methods in practice is thermal gas spraying, which is widely used in engine manufacturing. For plasma spraying of aluminum cylinder surfaces, mixtures of aluminum (Al), iron (Fe), and molybdenum (Mo) powders, as well as mixtures of aluminum and cast iron powders, are used. Gas-flame spraying is used to apply a coating made of wire consisting of iron-containing material to aluminum cylinders. A wide range of powder materials is used for gas-thermal spraying on aluminum cylinders. The

main component of the mixtures is iron. The powders contain chromium (Cr) and manganese (Mn) in various weight ratios, and other elements may also be added. All elements are incorporated into the powders in their pure form or as compounds [353].

In addition to honing [342, 343], laser technologies are used to alloy the surfaces of aluminum cylinders. Silicon is effectively diffused into the surface layer to a depth of 1 mm [354].

The wear resistance of aluminum cylinders is increased by rolling a regular micro-relief in the form of depressions 10–50 μm deep.

A bimetallic aluminum liner is formed by pouring molten aluminum over a cladding layer consisting of iron (Fe) and copper (Cu) powders. Particles of the sintered cladding layer diffuse into the molten aluminum, ensuring a strong bond at the layer interfaces [355].

The wear resistance of Al cylinders is improved by rolling a regular micro-relief with indentations of 10–50 μm [356].

Combinations of different technologies are also used. AUDI AG has patented a technology for applying an electroplated coating composed of silicon Si (1.8–2.8%), manganese Mn (0.3–1.0%), chromium Cr (0.15–0.4%), cobalt Co (10–20%), copper Cu (0.1%), iron Fe, and other elements. The electroplated coating is treated with short laser pulses.

A widely recognized drawback of hardening protective coatings is their cracking and delamination under extreme operating conditions. As contact loads increase, the strengthening effect of the coatings decreases [357? 358]. Large particles of the superhard coating that have delaminated and entered the engine's lubrication system pose a particular danger.

For a cylinder made of any material, this leads to catastrophic wear. Therefore, the engine manufacturing industry, particularly components of the cylinder-piston group, is the least receptive to new technologies for hardening coatings. To date, the problem of selecting materials for hardfacing coatings and the technologies for their application for rotary internal combustion engines

remains unresolved. A series of patents by Ford Motor Co. and other leading firms has not made it possible to ensure the required service life of the rotary engine [359, 360].

A new phase in the development of hardfacing coatings began with the application of the principle of coatings with a discrete structure and enhanced thermomechanical stability [242, 248].

A tractor compressor sleeve manufactured by the Khmelnytskyi Tractor Aggregates Plant was selected as the test specimen with a discrete coating for bench testing. The compressor model is A29.03.00B. Along with the compressor equipped with a standard cast iron sleeve, a compressor with an AL-25 alloy sleeve, reinforced with a discrete electric spark coating, was supplied for bench testing.

Using the electric spark alloying method with a 3.0 mm diameter copper rod electrode at an operating current of 35–40 A, a discrete coating with 60% coverage was applied on the EFI-25 machine. After coating application, the sleeve underwent finishing turning to the required surface roughness. The allowance for finishing was 0.15–0.20 mm. The appearance of the sample after electric spark alloying and stepwise finishing turning is shown in Fig. 3.10.

Fig. 3.10. Fragment of a sleeve with discrete coatings after step turning

Bench tests of the aluminum liner with a discrete coating showed a threefold increase in its durability compared to a standard cast iron liner under equal linear

wear conditions. Moreover, and very importantly, replacing the cast iron liner allowed for an 18% reduction in the compressor's weight.

Finally, it should be noted that the current trend in engine manufacturing is a shift toward aluminum alloys in the production of cylinder blocks. The main challenge remains increasing the wear resistance of the cylinders. In sleeve-less blocks, this problem is solved by using high-alloy aluminum alloys, aluminum-matrix composites, and bimetallic technologies. Cast iron inserts are also used in aluminum blocks.

A realistic, alternative solution to this problem, in our opinion, should be sought in the development of new, modern types of coatings capable, in principle, of avoiding the traditional (classic) shortcomings in the operation of heavily loaded friction units in mechanisms and machines.

3.3. Optimization of the electric spark alloying process for discrete coatings based on wear resistance criteria

A conceptual approach to the comprehensive structural and technological improvement of the load-bearing capacity of reinforcing protective coatings involves the following sequential stages:

- optimization of technologies and structural designs for traditional solid coatings using methods of multifactorial planning and multi-criteria optimization. The goal of this stage is to determine the maximum potential of a specific technology and structural configuration of the coating;

- further increasing the load-bearing capacity of reinforcing surfaces by forming coatings with a discrete structure. The goal of this stage is to determine the relationship between the geometric parameters of the structure and the elastic properties that ensure a minimum stress-strain state under operational conditions. Particular attention is paid to reducing tensile stresses by selecting the parameters of the discrete structure. This reduces the brittleness of superhard, high-modulus coatings;

- selection of the parameters of the discrete structure of the coatings and transition to the optimization of the coating application technology based on strength and wear resistance criteria. To this end, mathematical modeling, multifactorial planning, and multi-criteria optimization are employed. The objective of this stage is to determine the maximum potential of strengthening protective coatings with a discrete structure.

In experimental studies, anti-friction coatings were applied to D1T aluminum alloy. Steel 30ХГСН2А is used as the counterface in this tribological pair. Three variants of the structural configuration of the coatings were tested:

- single-layer copper (Cu) coating;
- two-layer coating consisting of copper (Cu) + SP-1 alloy;
- two-layer coating consisting of copper (Cu) + SP-2 alloy.

The compositions of the SP-1 and SP-2 electrodes are given in Table 3.1.

Table 3.1

Chemical composition of the electrodes

Electrode material grade	Composition, %					
	Al	Si	Mn	Fe	Ni	Cu
SP-1 alloy	3-5	1	38-40	1-2	34-35	16-17
SP-2 alloy	-	8-9	36-37	1-2	33-34	1

A standard Elitron-22 setup was used to apply the coating via the electric spark alloying method. To form a new anti-friction, wear-resistant coating using the electric spark alloying method, the base components manganese (Mn) and nickel (Ni) were used in the composition of the SP-1 and SP-2 electrodes.

Manganese, as is well known [222, 361, 362], improves strength, ductility, and corrosion resistance. Nickel enhances mechanical properties and increases the heat resistance and corrosion resistance of materials.

The tribological characteristics of the electrode material were improved by introducing alloying additives of aluminum (Al), silicon (Si), iron (Fe), and copper (Cu). To achieve optimal tribological characteristics, the aluminum content should be more than 5%, and the silicon content more than 8%. The introduction of silicon ensures the heterogeneity and fine dispersion of the coating structure, which in turn contributes to the optimal distribution of stresses acting on the friction surface. The loads are absorbed by the hard components of the coating structure, which ensure the material's wear resistance [362].

The alloying elements aluminum (Al), silicon (Si), and iron (Fe), interacting with oxygen in the air, form oxides from a mixture of elements in the form of "spinels," which improve tribological characteristics.

3.3.1 Multifactorial planning of tribological tests

Regular multifactorial designs were used to plan the experiment [363], on the basis of which a general experimental design was developed. The controlled design, process, and operational factors, as well as their levels of variation, are presented in Table 3.2.

Table 3.2

Factors and their levels of variation

Factors	Code	Variation Levels		
Coating Material	X_1	0(Cu)	1(Cu+ SP-1)	2(Cu+ SP-2)
Lubricant	X_2	N_o (AMG-10)	N_1 (CYATIM-201)	N_2 (Svinol-01)
Operating current, A	X_3	1...4		
Electrode oscillation amplitude, mm	X_4	0,2...0,5		
Sliding speed, m/s	X_5	0,1...0,5		
Specific load, MPa	X_6	0...20		

The design matrix in actual values is shown in Table 3.3.

The main tribological characteristics—wear rate I_c and coefficient of friction μ—were taken as response variables. As a result of friction and wear experiments, the tribological characteristics of the coatings were determined as a function of design, manufacturing, and operational factors.

Table 3.3

Working design matrix

X_1	X_2	X_3	X_4	X_5	X_6
1	N_1	2,5	0,35	0,3	10
0	N_2	1,75	0,45	0,2	15
2	N_0	3,25	0,25	0,4	5
0	N_1	3,75	0,5	0,4	2
1	N_0	2	0,3	0,1	13
1	N_1	3	0,2	0,5	18
2	N_2	1,25	0,4	0.2	7
0	N_2	3	0,3	0,1	1
1	N_1	1,5	0,45	0,4	11
0	N_0	4	0,35	0,3	17
2	N_1	2,25	0,2	0,5	6
0	N_0	2	0,4	0,3	3
2	N_2	3,5	0,25	0,1	14
1	N_2	1	0,35	0,5	19
2	N_0	2,75	0,5	0.2	9
0	N_1	2,25	0,25	0,3	5

Based on the results of the experiment, the best tribological characteristics of the copper coating were observed in the CYATIM-201 lubricant at a specific load of P_{spec} = 2 MPa. A further increase in the specific load to P_{spec} = 10 MPa demonstrates the effectiveness of the Cu+SP-2 coating.

With an increase in the specific load to P_{spec} = 10...18 MPa, the use of the Cu+SP-1 coating is recommended. In AMG-10 and Svintoli-01 lubricant media, the Cu+SP-2 coating exhibits the best tribological characteristics as the specific load increases across various sliding speeds. The friction surface of this coating is

free of scratches, cracks, and wear marks due to the formation of wear-resistant zones based on manganese and nickel, as confirmed by micro-X-ray diffraction analysis. The research results are presented in Figures 3.11–3.17 and Table 3.4.

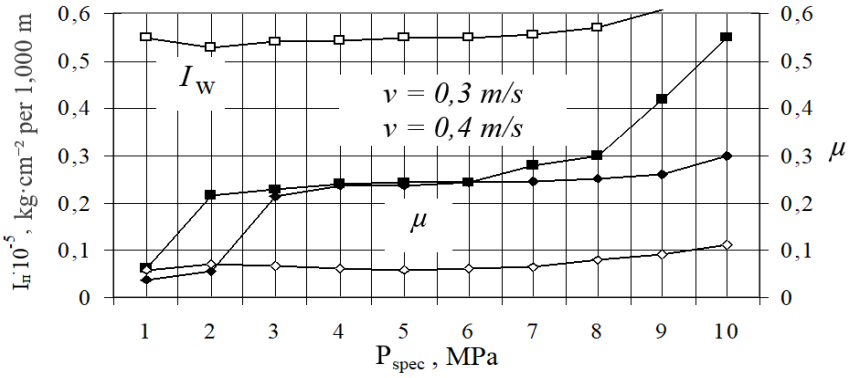

Fig. 3.11. Dependence of wear rate I_c and friction coefficient μ for a Cu coating on the specific load P_{spec}. (AMG-10)

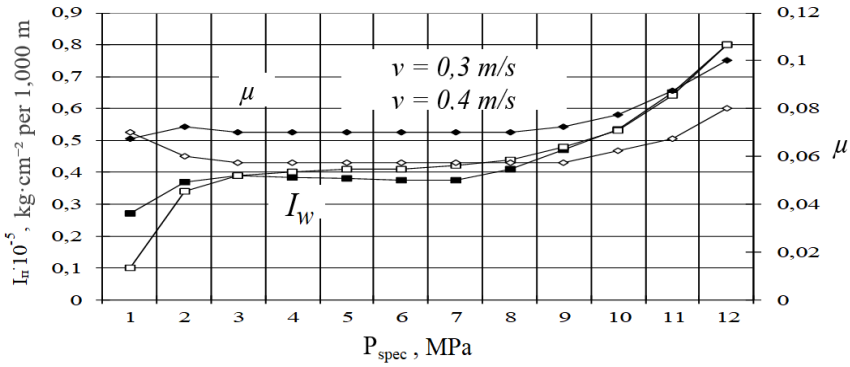

Fig. 3.12. Dependence of wear rate I_w and friction coefficient μ for the Cu+SP-1 coating on the specific load P_{spec}. (CYATIM-201)

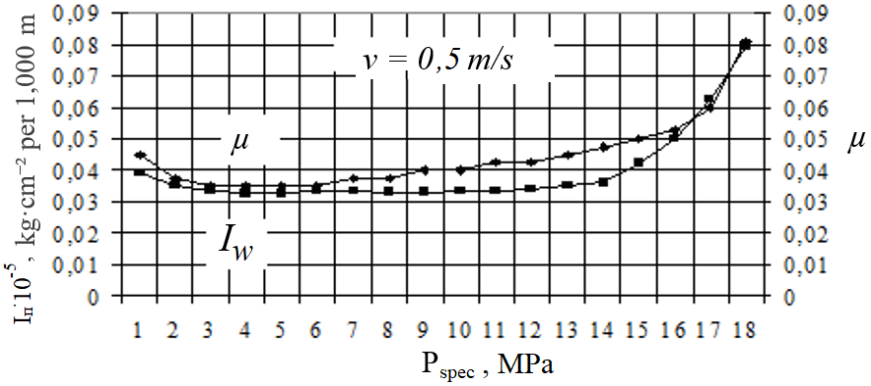

Fig. 3.13 Dependence of wear rate I_w and friction coefficient μ for the Cu+SP-1 coating on specific load $P_{spec.}$ (CYATIM-201)

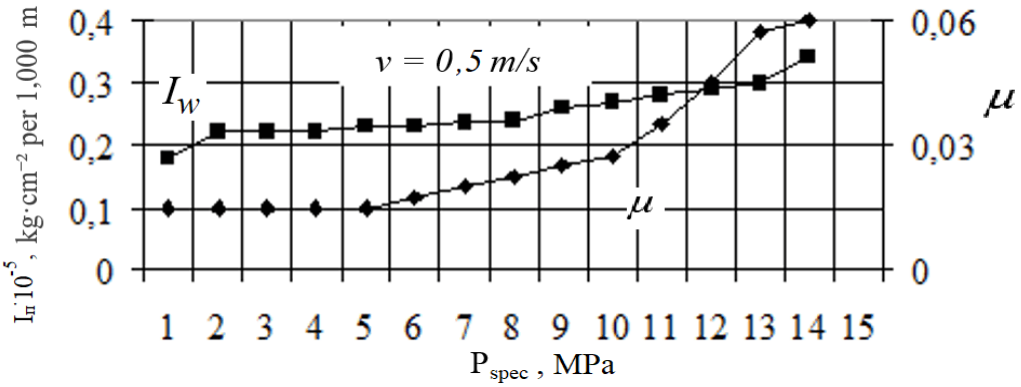

Fig. 3.14. Dependence of wear rate I_w and friction coefficient μ for the Cu+SP-2 coating on specific load P_{spec} (Svintoli -01)

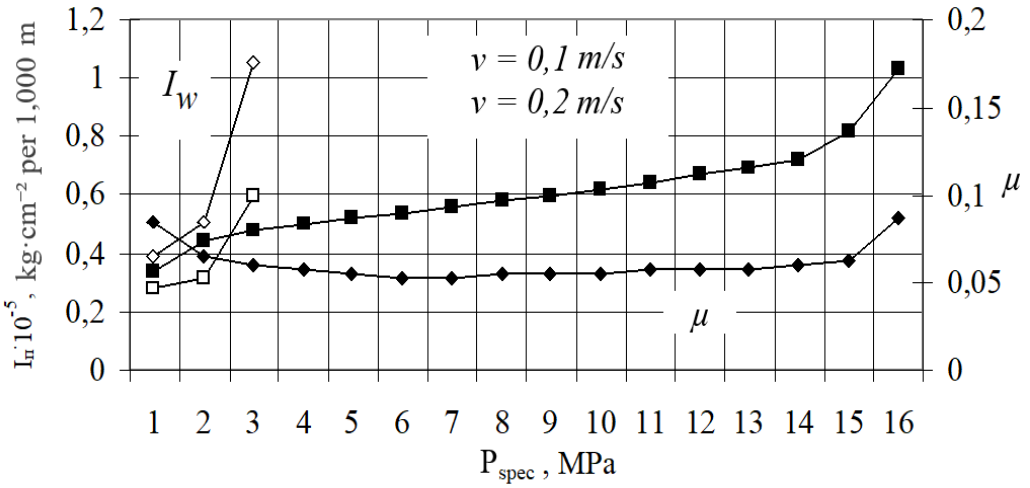

Fig. 3.15. Dependence of wear rate I_w and friction coefficient μ for a Cu coating on the specific load P_{spec} (AMG-10)

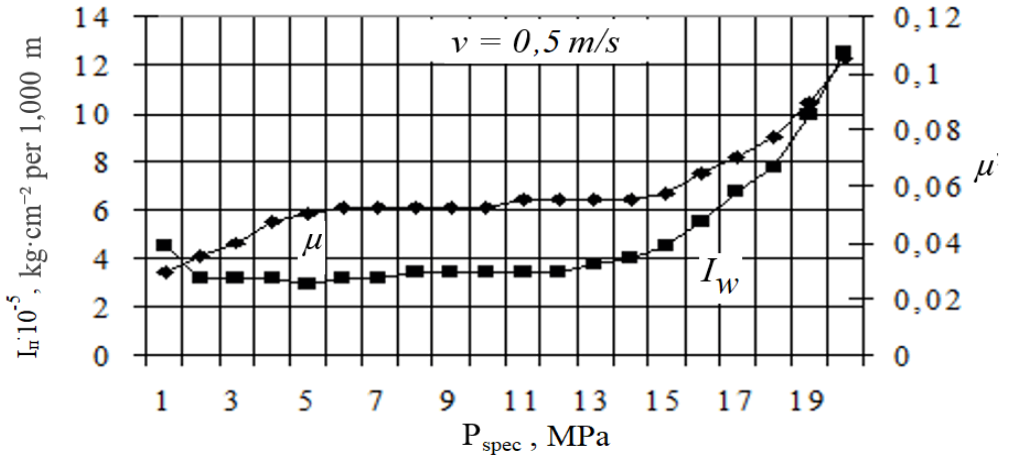

Fig. 3.16. Dependence of wear rate I_w and friction coefficient μ for the Cu+SP-1 coating on specific load P_{spec} (CYATIM-201)

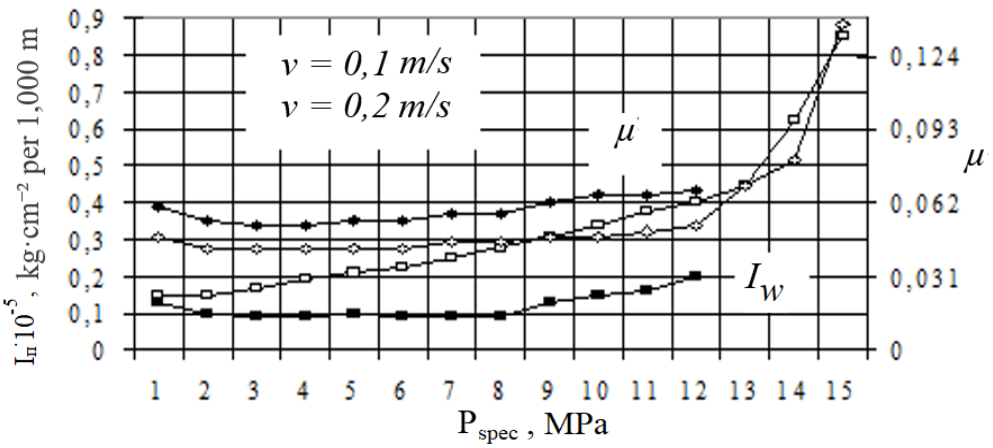

Fig. 3.17. Dependence of wear rate I_w and friction coefficient μ for the Cu+SP-2 coating on specific load P_{spec} (Svintoli -01)

Table 3.4

Test Results

Wear rate of the coatings, I = 10^{-5} kg·cm^{-2} per 1,000 m		Coefficient of friction, μ	
Y_{11}	Y_{12}	Y_{21}	Y_{22}
0,540	0,490	0,077	0,0752
0,910	0,895	0,0658	0,0623
0,70	0,752	0,082	0,0853
0,210	0,303	0,055	0,0571
14,70	12,60	0,138	0,124
0,079	0,12	0,081	0,083
0,09	0,138	0,058	0,061
0,275	0,284	0,067	0,0688
0,70	0,93	0,07	0,085
1	1,2	0,17	0,185
0,1	0,08	0,06	0,0574
0,330	0,42	0,0728	0,0758
0,53	0,62	0,0907	0,0923
10,2	9,84	0,091	0,0874
2,80	1,7	0,193	0,182
0,47	0,54	0,058	0,063

3.3.2. Regression Analysis of Test Results

Regression analysis and validation of the resulting mathematical models provide a more accurate quantitative interpretation of the experimental results [364, 365]. The models were calculated using the PRIAAM software package [366, 367].

Based on the results of the regression statistical analysis, the dependencies of the wear rate of coatings Y_1 and the coefficient of friction Y_2 on design, manufacturing, and operational factors were obtained, which are as follows:

$$Y_1 = 1{,}79779 + 5{,}87766\,x_2x_5 + 0{,}681912\,x_3^2x_6^3 - 2{,}49064\,x_5 + \\ + 1{,}72778\,x_5^2 + 1{,}81677\,x_2x_5^3 + 2{,}2649\,x_1^2x_3 + 1{,}47827\,x_3^3x_3^5; \quad (3.1)$$

$$Y_2 = 0{,}0827649 + 0{,}113278\,x_1^2x_3 - 0{,}0504034\,x_3 + 0{,}0232166\,x_1^2 + \\ + 0{,}0611406\,x_4^3x_6 + 0{,}104833\,x_3^3x_4 + 0{,}0728096\,x_1x_3^3 + 0{,}0465043\,x_6 - \\ - 0{,}0590069\,x_2x_5^3 + 0{,}0979191\,x_3x_5 + 0{,}041559\,x_3^2x_6^3 + 0{,}022658\,x_2^2x_6^2. \quad (3.2)$$

where Y_1 and Y_2 are mathematical models in encoded coordinates for the coating wear rate and the coefficient of friction.

Formulas for converting from encoded coordinates to natural coordinates:

$x_1 = 0{,}941176(X_1 - 0{,}9375);$

$x_1^2 = 1{,}64632(X_1^2 - 0{,}0907563\,X_1 - 0{,}605536);$

$x_2 = 1(X_2 - 1);$

$x_2^2 = 1{,}6(X_2^2 - 0{,}625);$

$x_3 = 0{,}659794(X_3 - 2{,}48438);$

$x_3^2 = 1{,}50615(X_3^2 - 0{,}0300673\,X_3 - 0{,}324689);$

$x_3^3 = 3{,}04649(X_3^3 - 0{,}0129029\,X_3^2 - 0{,}653277\,X_3 - 0{,}0055731);$

$x_4 = 6{,}4(X_4 - 0{,}34375);$

$x_4^3 = 4{,}38694(X_4^3 - 0{,}122458\,X_4^2 - 0{,}69253\,X_4 + 0{,}0172601);$

$x_5 = 5(X_5 - 0{,}3);$

$$x_5^2 = 1{,}88235(X_5^2 + 5{,}16884 \cdot 10^{-8} X_5 - 0{,}46875);$$

$$x_5^3 = 3{,}33333(X_5^3 + 4{,}25889 \cdot 10^{-8} X_5^2 - 0{,}85 X_5 + 4{,}26538);$$

$$x_6 = 0{,}107383(X_6 - 9{,}6875);$$

$$x_6^2 = 1{,}75479(X_6^2 - 0{,}0746302 X_6 - 0{,}370028).$$

The obtained relationships were tested for adequacy, reproducibility, and the informativeness of the results using criteria from mathematical statistics [367].

The wear intensity model I_w is adequate:

$F_{\text{extra charge}} = 1.90 < F_{\text{crit}}. = 3.55$; $\alpha = 0.05$; $V_1 = 5$; $V_2 = 7$ explains 96.47% of the total variance.

The multiple correlation coefficients $R = 0.982$ is statistically significant:

$F_R = 38.31 > F_{crit} = 2.71$, $\alpha = 0.05$; $V_1 = 5$; $V_2 = 20$.

The multiple correlation coefficients R characterize the strength of the statistical relationship between the multiple regression equation Y_i and the initial experimental results.

The Box-Wetstein criterion for informativeness is $\gamma = 2$, i.e., the model is robust: the coefficient of determination COND = 1.35.

The friction coefficient μ model is adequate:

$F_{\text{extra charge}} = 2.993 < F_{crit}. = 3.5$; $\alpha = 0.05$; $V_1 = 7$; $V_2 = 8$ and explains 97.15% of the total variance.

The multiple correlation coefficients $R = 0.986$ is statistically significant:

$F_R = 39.03 > F_{crit}. = 2.42$, $\alpha = 0.05$; $V_1 = 7$; $V_2 = 24$.

The Box-Wetstein criterion for informativeness is $\gamma = 3$.

The model is robust: the coefficient of determination COND = 2.83.

Based on these results, a visual representation of the geometric images of the response functions was obtained by constructing the corresponding geometric surfaces (Figs. 3.18–3.20).

It should be noted that there is a break in the surface $Y_1 = f(X_1, X_6)$ (Fig. 3.19), which is associated with a change in the wear mechanism as the contact load X_6 increases

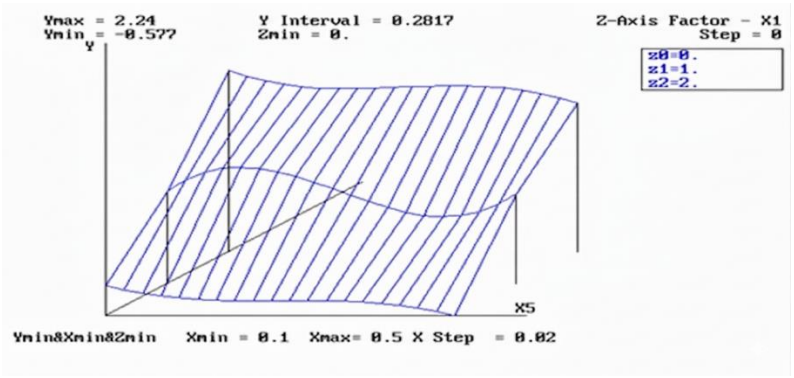

Fig. 3.18. Response surface $Y_1 = f(X_1, X_5)$:

Y_1 – coating wear rate (Table 3.4);

X_1 – coating material (Table 3.2); X_5 – sliding speed, m/s (Table 3.2).

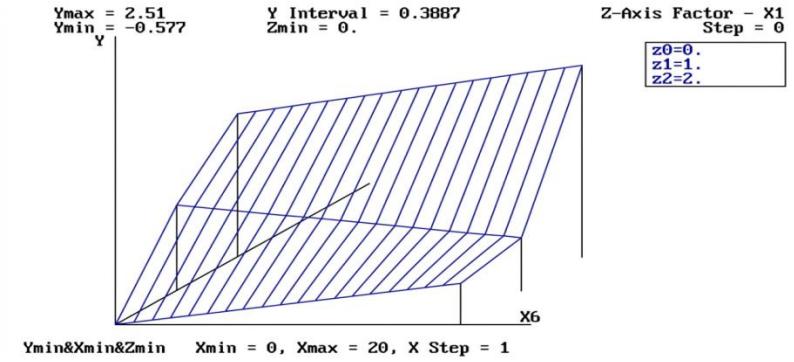

Fig. 3.19. Response surface $Y_1 = f(X_1, X_6)$:

Y_1 – coating wear rate (Table 3.4);

X_1 – coating material (Table 3.2); X_6 – specific load, MPa (Table 3.2).

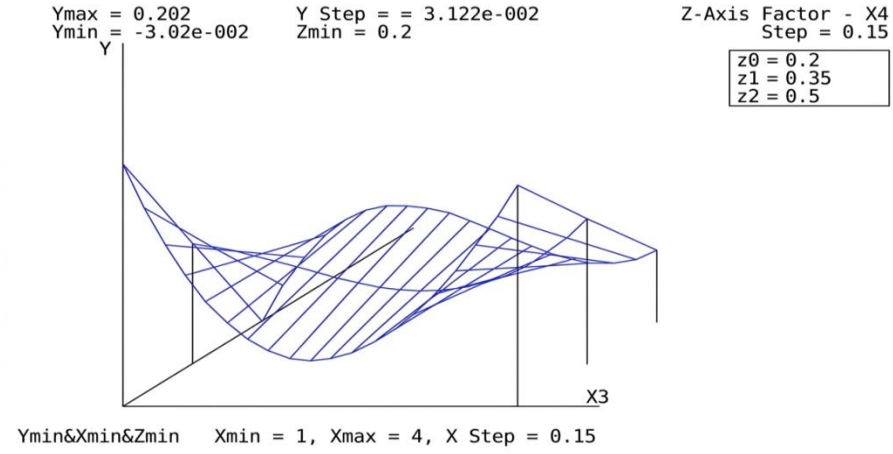

Fig. 3.20. Response surface $Y_2 = f(X_3, X_4)$:

Y_2 – coefficient of friction (Table 3.4); X_3 – operating current (Table 3.2);

X_4 – electrode oscillation amplitude, mm (Table 3.2).

3.3.3. Multi-criteria optimization of coating application technology using the electric spark alloying method

The electric spark alloying process is characterized by several key quality indicators, including wear rate and coefficient of friction. When optimizing these parameters, the requirements can be quite contradictory; that is, improving one criterion may lead to deterioration in another. Consequently, there is a need for multi-criteria optimization by determining a specific compromise point that must satisfy the desired requirements (a Pareto compromise) [362, 363 and 368]. As a rule, the results for each individual indicator will be worse than in the case of single-criteria optimization for that parameter. In this case, a more complex situation arises, where the pursuit of individual goals leads to their inequality relative to one another.

The ability to assign relative weights to multiple quality criteria is complex, and the PRIAAM software package offers a practical solution by allowing the user to compare criteria in pairs to determine which criterion is better (or if they are equivalent). After analysis, the criteria are constructed automatically [366, 367].
To optimize the electric spark alloying technology, a random search method based on uniformly distributed random points was used [368]. The results of the multi-criteria optimization are presented in Table 3.5.

Table 3.5

Results of multi-criteria optimization

Factor values						Criterion values		Relative efficiency
X_1	X_2	X_3	X_4	X_5	X_6	$I_n \cdot 10^{-6}$	μ	δ
Cu+ SP-2	CYATIM 201	2,25	0,5	0,2	6	0,08	0,0574	0,9857
Cu+ SP-2	Svinzol-01	1,25	0,2	0,4	7	0,09	0,058	0,98139
Cu+ SP-1	CIATIM-201	3	0,5	0,2	18	0,07	0,081	0,86078
Cu+ SP-2	AMG-10	3,25	0,4	0,25	5	0,7	0,082	0,8478

Based on the results of the multi-criteria optimization presented in Table 3.5, it can be concluded that the Cu+SP-2 coating achieves the highest relative efficiency for various lubricants, and the implemented process parameters for its application are optimal.

Multicriteria optimization of electric spark alloying allows determining the combination of design and technological factors that ensure the formation of coatings with high operational properties.

The obtained mathematical models for ensuring optimal tribological characteristics of strengthening protective coatings can serve as a basis for developing control programs for the automated technological process of electric spark alloying.

3.4. Optimization of discrete coating technology for parts restoration

An analysis of the results of defect detection in bronze components during theoverhaul of modern aircraft shows that 82% of components are rejected due to excessive wear [131].

This is caused by high specific loads at low sliding speeds, contamination of contacting friction surfaces with abrasives, dust, and condensate, as well as the non-additive nature of the lubrication.

Such assemblies include plain bearings, bolted joints, ball-bearing joints, and others. Parts made of bronze are among the most common sliding elements in bearings, which undoubtedly limit the service life of the entire unit.

It should be noted that the coating application methods traditionally used in aircraft repair manufacturing clearly do not allow for the effective restoration of steel-bronze tri-component parts.

Our search for advanced coating technologies to restore worn parts operating under extreme friction and wear conditions has shown that one of the most effective and economical methods for eliminating wear, particularly in bronze parts, is the electric spark alloying method [131].

3.4.1. Electrode Materials and Coating Designs

BrAZhMts10-3-1.5 bronze was selected as the substrate material for coating application; this material is used in aviation equipment assemblies in contact with 30KhGSN2A steel. A standard Elitron-22 installation was used to apply coatings via the electric spark alloying method. Alloys SP-1 and SP-2 were used as electrode materials; their compositions are given in Table 3.1. Friction and wear tests of the experimental coatings were conducted on the SMT-1 universal friction machine using a disc-block configuration in the "New Technologies" educational and research laboratory of the Department of Applied Mechanics and Materials Engineering at the National Aviation University. To rationally select the parameters of the coating's discrete structure, preliminary experiments were conducted to determine the dependence of wear resistance on the continuity coefficient ψ. The continuity coefficient ψ is defined as the ratio of the area of the discrete coatings to the total area. Fig. 3.21 shows the dependence of weight loss on coating continuity. The accuracy of determining coating continuity was ±5% and was determined using the method described in [244].

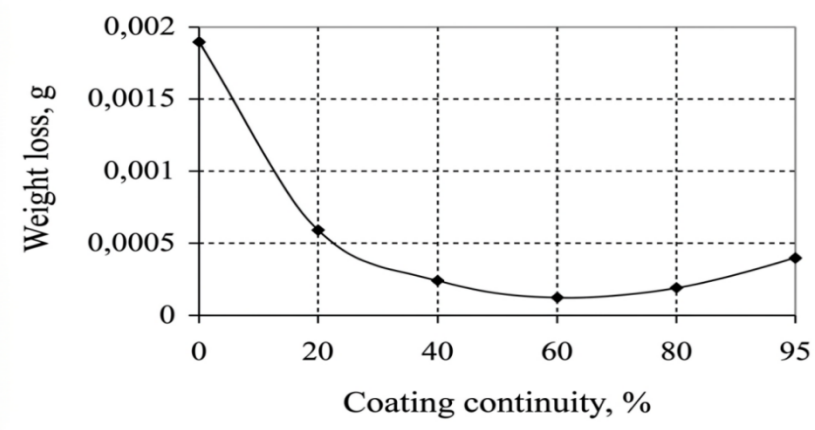

Fig. 3.21. Dependence of wear on coating integrity

The coating density was adjusted by varying the electrode's travel speed relative to the sample. The research results presented in Figure 3.21 confirm the

effectiveness of using discrete coatings [242, 244]. Minimal coating wear is observed at a coverage of ψ = 55...65 %. In all subsequent studies, a coverage of ψ = 0.6 was used. Tests were conducted on three coating variants: 1) a coating made of electrode material SP-1; 2) a coating made of electrode material SP-2; 3) a two-layer coating M2 with a first layer of SP-2 and an outer layer of base material—bronze BrAZhMts 10-3-1.5. The composition of the M2 coating is justified by the fact that, for high anti-galling resistance, it is advisable to apply a thin layer of softer material to a hard surface, which acts as a solid lubricant and prevents the formation of surface defects in the form of gouges, which almost always render the tribological contact inoperable. The surface plastic deformation method was used as a finishing treatment for the coatings prior to testing. Hardening the surface layers by surface plastic deformation ensures the required surface finish and part dimensions without machining [369], as well as an increase in hardness and wear resistance [370]. The main tribotechnical characteristics—wear rate and coefficient of friction—were selected as criteria for optimizing the electric spark alloying process.

3.4.2 Selection of Controllable Parameters and Optimization Criteria

Design, technological, and operational factors were selected as the input control variables. To solve the optimization problem in practice, we selected precisely those factors that have the greatest influence on the optimization criteria and can be controlled. The use of expert assessment methods [131] and a series of screening experiments allowed us to obtain an average a priori ranking of the factors influencing the electric spark alloying process (Fig. 3.22). The discretization parameter (Fig. 3.22, item 9) is taken as a constant (ψ = 0.60).

Modeling the coating application process based on the analysis of the conducted ranking allowed us to identify a group of parameters that have the greatest influence on the values of the optimization criteria; therefore, the following were included in the design matrix as controllable factors: coating

material and lubricant material; working current of the electric spark alloying process; electrode oscillation amplitude; sliding speed; and specific load.

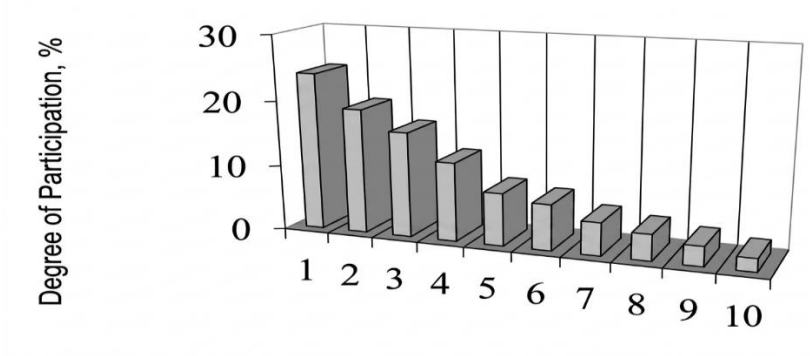

Fig. 3.22. Ranked list of factors: 1 – coating material; 2 – EIL operating current; 3 – electrode oscillation amplitude; 4 – sliding speed; 5 – specific load; 6 – lubricant; 7 – coating thickness; 8 – electrode diameter; 9 – discretization parameter ψ; 10 – deposition time

Tests on the SMT-1 universal friction machine under boundary friction conditions were conducted in a special sealed chamber. CYATIM-201, AMG-10, and Svinol-01 were used as lubricants [370]. The anti-friction grease CYATIM-201 is used to reduce friction and wear in aircraft control assemblies and their engines, landing gear mounting assemblies and retraction mechanisms, wheel bearings and various electrical units, weapon systems, special equipment, and instruments [370]. In the operation of hydraulic systems in aviation equipment, where sealing parts and hoses are made of oil-resistant rubber, AMG-10 oil) is currently used as the working fluid. “Svynol-01” grease is characterized by high anti-wear properties and is a product of combining CYATIM-201 grease with 10% lead powder. This grease is used in aviation equipment in assemblies with high specific pressure due to the high stability of the boundary lubrication film. Due to the presence of lead powder, which acts as a solid lubricant, this film protects contacting surfaces from scoring, for example, in the swing-wing assemblies with variable sweep. Table 3.6 presents the controlled factors and their levels of variation. Based on the data in Table 3.6, an experimental design was generated in this study and is presented in Table 3.7 in the form of a design matrix.

Table 3.6

Controlled factors and their levels of variation

Factors	Code	Variation Levels		
Coating Material	X_1	SP-1	SP-2	M_2
Lubricant	X_2	N_o (AMG-10)	N_1 (Svinol-01)	N_2 (CYATIM-201)
Operating Current, A	X_3	1…4		
Electrode oscillation amplitude, mm	X_4	0,2…0,5		
Sliding speed, m/s	X_5	0,1…0,5		
Specific load, MPa	X_6	0…20		

Table 3.7

Design matrix for the experimental design

X_1	X_2	X_3	X_4	X_5	X_6
SP -1	N_o	2,25	0,35	0,3	10,53
SP -1	N_1	1,63	0,28	0,4	12,5
SP -1	N_2	2,88	0,43	0,2	8,55
SP -1	N_o	3,19	0,39	0,45	7,57
SP -1	N_1	1,94	0,24	0,25	11,51
SP -2	N_2	2,56	0,46	0,15	13,49
SP -2	N_o	1,31	0,31	0,35	9,54
SP -2	N_1	2,72	0,26	0,23	7,07
SP -2	N_2	1,47	0,41	0,43	11,02
SP -2	N_o	3,34	0,33	0,33	12,99
M_2	N_1	2,09	0,48	0,13	9,05
M_2	N_2	1,78	0,37	0,38	8,06
M_2	N_o	3,03	0,22	0,18	12,01
M_2	N_1	1,16	0,44	0,28	13,98
M_2	N_2	2,41	0,29	0,48	10,03
M_2	N_o	2,02	0,34	0,19	8,80

3.4.3 Regression Analysis of Research Results on Tribological Characteristics

Experimental studies yielded the tribological characteristics of coatings with a discrete structure as structural, technological, and operational factors were varied in accordance with the experimental design (Table 3.6).

Based on the obtained results, dependencies of wear rate and coefficient of friction were plotted in accordance with the working matrix of the experimental design.

The experimental results are presented in Figs. 3.23–3.31 as dependencies of wear rate and coefficient of friction for various coating materials, sliding speeds, and lubrication conditions.

The dependence of wear intensity I_w on specific load for the SP-1 coating in AMG-10 lubricant (Fig. 3.23) exhibits a “threshold” character. According to X-ray structural analysis, a stable secondary structure forms on the surface during friction, the tribological characteristics of which change sharply at $P_{crit} \geq 3.5$ MPa.

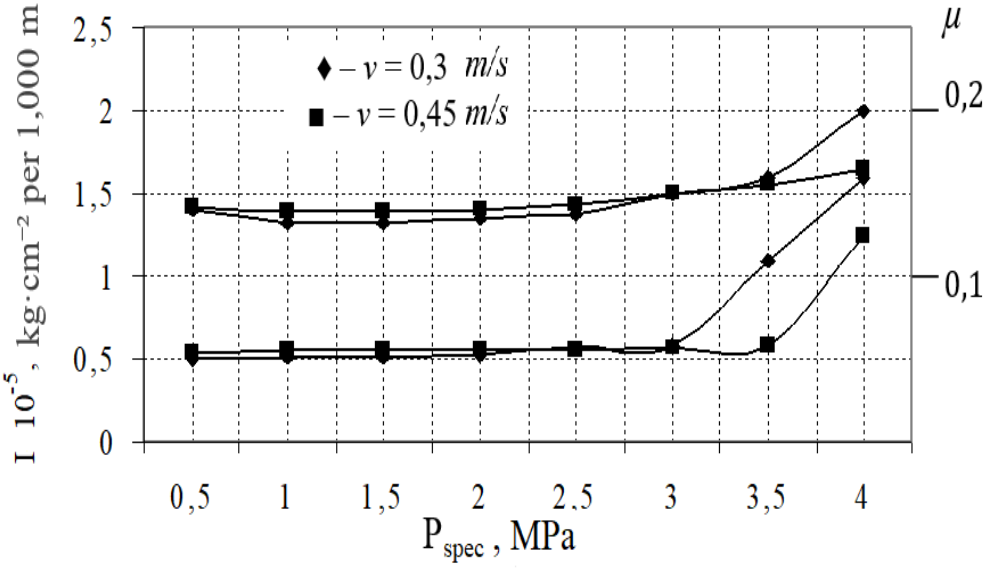

Fig. 3.23. Dependence of wear rate I_w and coefficient of friction μ for the SP-1 coating on specific load P_{spec}, MPa (AMG-10 lubricant)

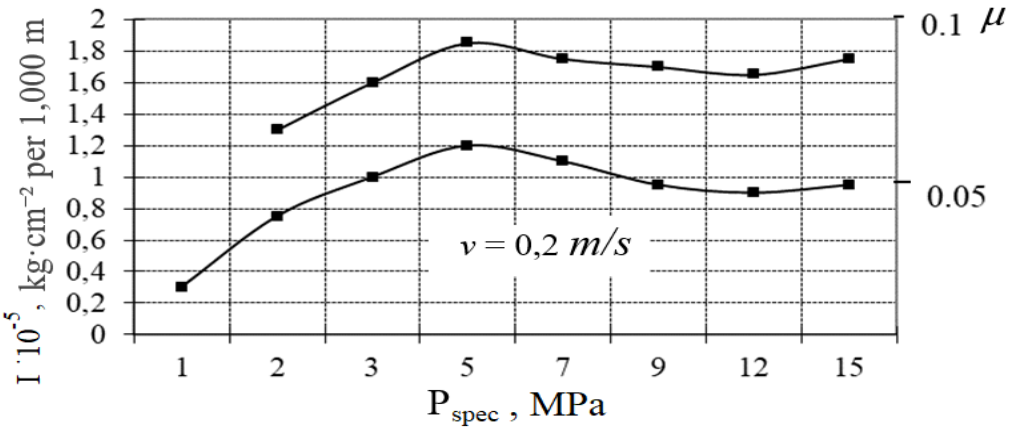

Fig. 3.24 Dependence of wear rate I_w and coefficient of friction μ for SP-1 coating on specific load P_{spec} (CIATIM-201 lubricant)

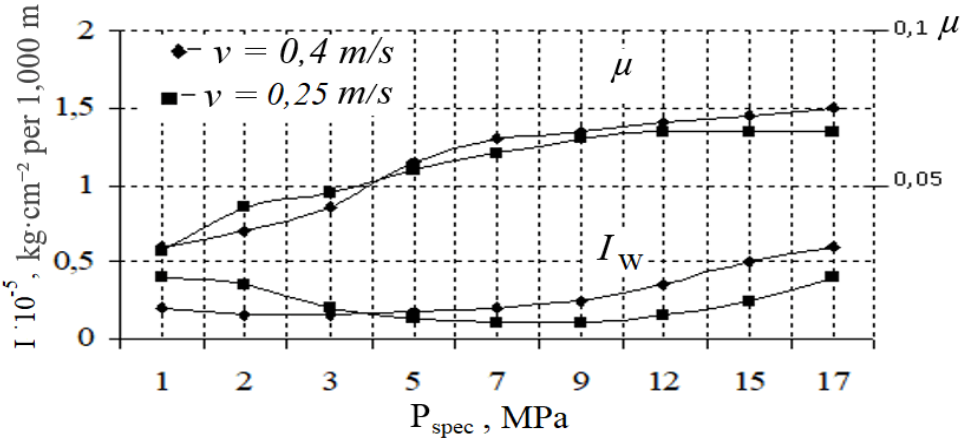

Fig. 3.25. Dependence of wear rate I_w and coefficient of friction μ on specific load P_{spec} for coating SP-1 (Svinzol-01 lubricant)

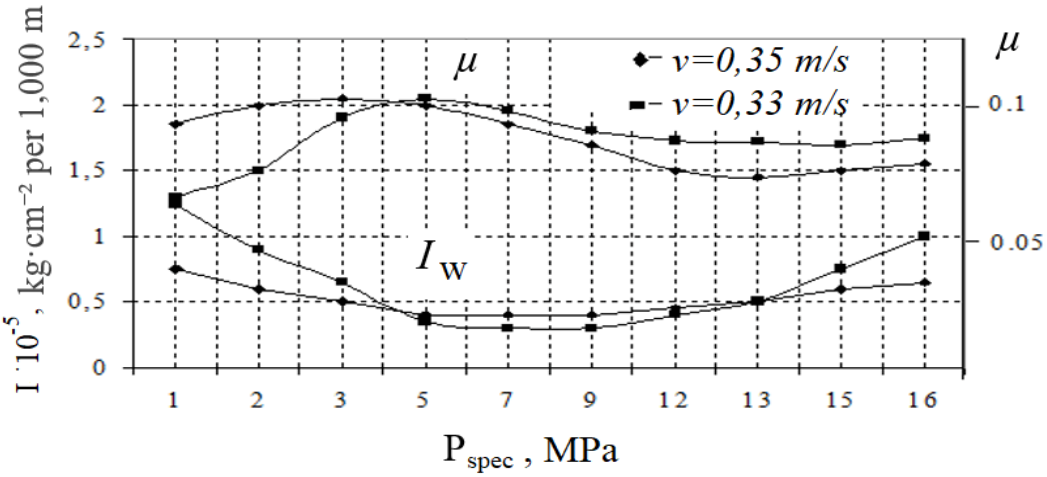

Fig. 3.26. Dependence of wear rate I_w and coefficient of friction μ for SP-2 coating on specific load P_{spec} (AMG-10 lubricant)

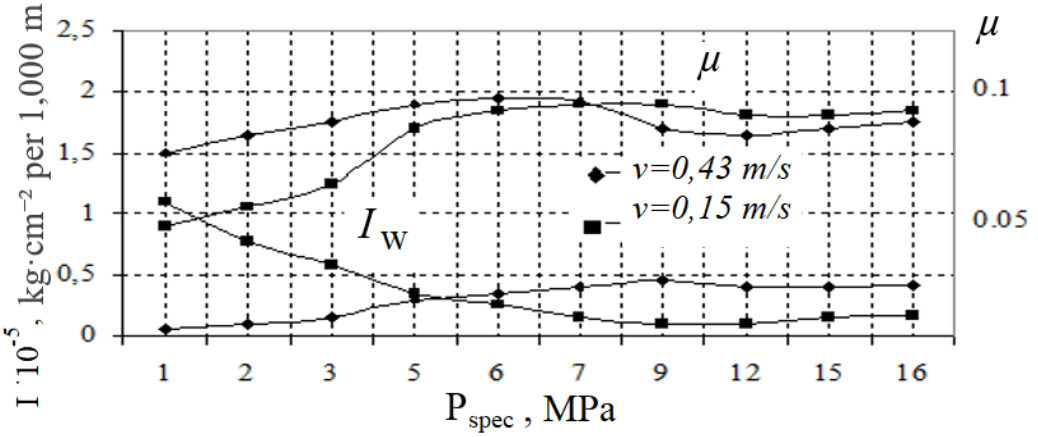

Fig. 3.27. Dependence of wear rate I_w and coefficient of friction μ for SP-2 coating on specific load P_{spec} (CIATIM-201 lubricant)

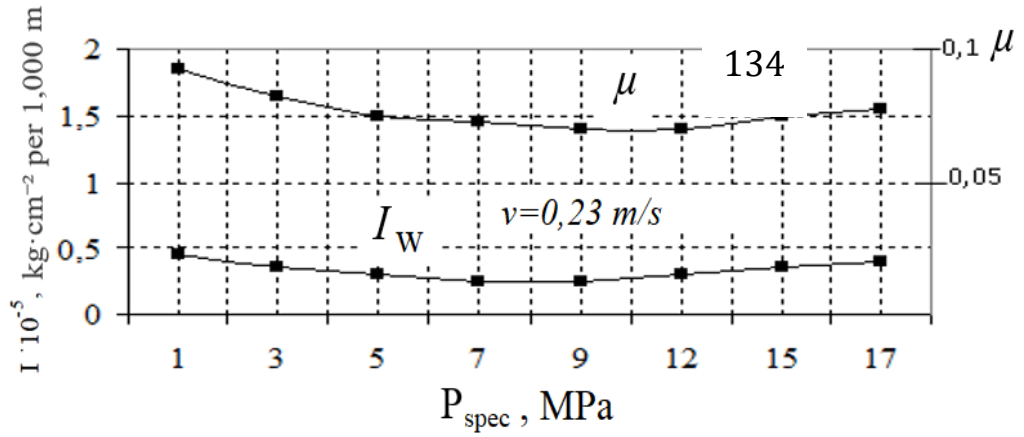

Fig. 3.28. Dependence of wear rate I_w and coefficient of friction μ for SP-2 coating on specific load P_{spec} (Svinzol-01 lubricant)

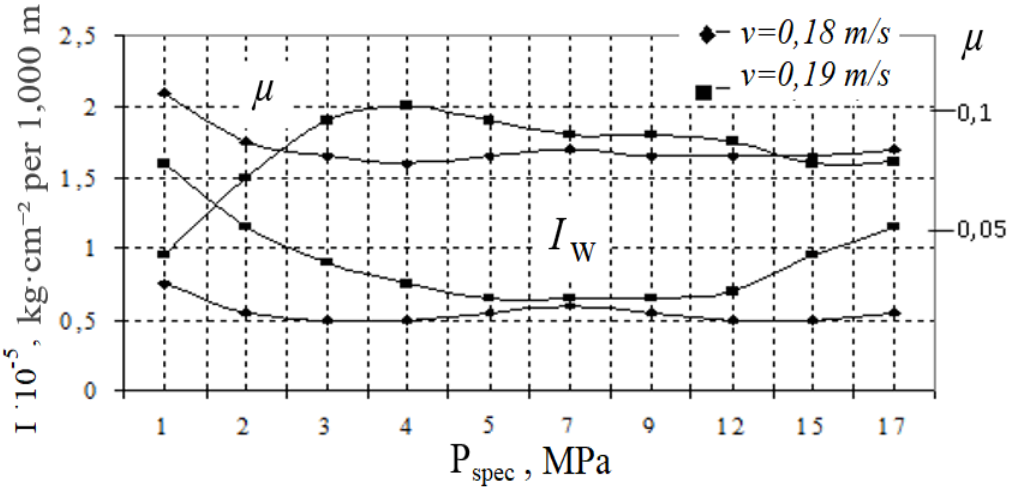

Fig. 3.29. Dependence of wear rate I_w and coefficient of friction μ for coating M_2 on specific load P_{spec} (AMG-10 lubricant)

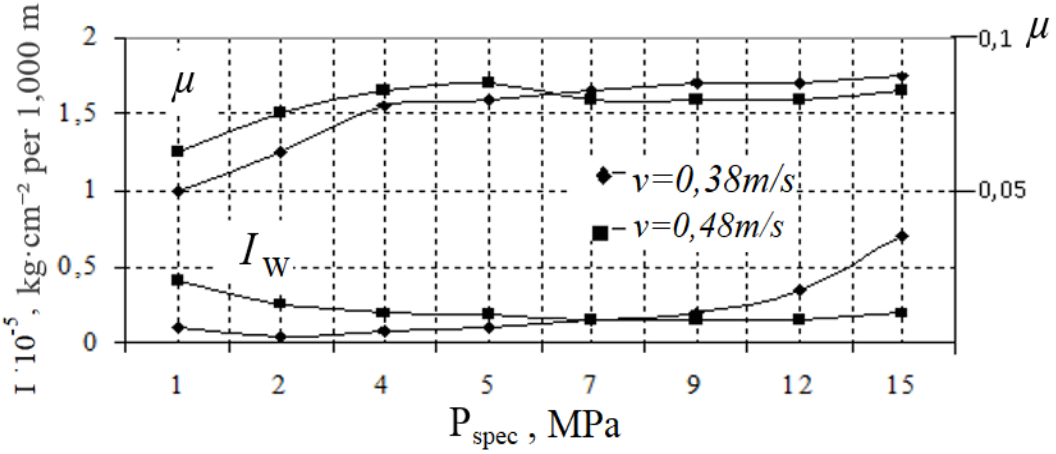

Fig. 3.30. Dependence of wear rate I_w and coefficient of friction μ for coating M_2 on specific load P_{spec} (CYATIM-201 lubricant).

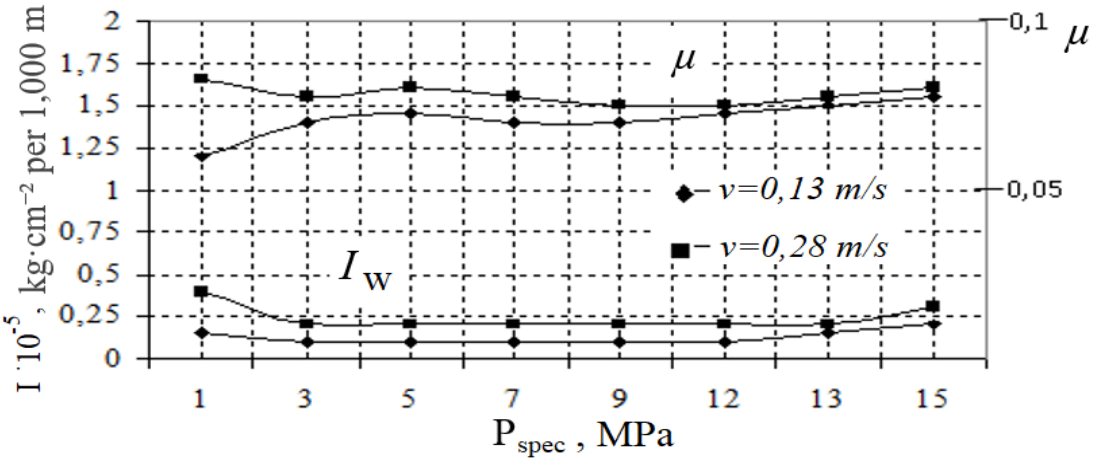

Fig. 3.31. Dependence of wear rate I_w and coefficient of friction μ for coating M_2 on specific load P_{spec} (Svinzol-01 lubricant)

The tribological characteristics of the coatings were determined for various lubricants, sliding speeds, and specific loads. Of the coatings studied, coating M_2 showed the best results (Figs. 3.27–3.31). The two-layer M2 coating consists of a first layer of SP-2 and an outer layer made of the base material—BrAZhMts 10-3-1.5 bronze. The friction surface of this coating is free of gouges, cracks, and wear marks, which, in our opinion, is the result of the formation of wear-resistant zones based on manganese (Mn) and nickel (Ni) and is confirmed by micro-X-ray structural analysis data. The values of tribotechnical characteristics according to the experimental plan are given in Table 3.8. A more complete and accurate assessment of the relationship between tribotechnical characteristics and design,

technological, and operational factors is provided by regression analysis of the experimental results. The models were calculated using the PRIAM software package [367]. Based on the results of the regression statistical analysis, the dependencies of wear rate and coefficient of friction on the variable factors were obtained (Table 3.6, Table 3.7):

$$Y_1 = 0,0670 - 0,0984x_5^3 + 0,1369x_1x_5^2 - 0,0775x_5^2x_6^3 - 0,0653x_3^2x_2^3 + \\ +0,0449x_3^3x_6 + 0,0326x_1x_4^3 - 0,0384x_3^3x_4; \quad (3.3)$$

$$Y_2 = 0,0805 + 0,-141x_4^2 + 0,0081x_6^2x_2, \quad (3.4)$$

Table 3.8

Tribological characteristics

Intensity of wear of coatings, $I_w = 10^{-5}$ kg·cm^{-2} per 1,000 m of track		Coefficient of friction, μ	
Y_{11}	Y_{12}	Y_{21}	Y_{22}
4,02	4,081	0,312	0,299
0,038	0,046	0,0684	0,0715
0,160	0,134	0,0921	0,0973
4,05	4,102	0,29	0,32
0,0180	0,0130	0,0715	0,0705
0,0182	0,0131	0,0926	0,0957
0,054	0,058	0,087	0,0852
0,024	0,034	0,0763	0,071
0,130	0,146	0,08	0,085
0,10	0,094	0,09	0,086
0,0089	0,011	0,0571	0,055
0,02	0,018	0,0882	0,0863
0,304	0,296	0,0842	0,0865
0,024	0,03	0,0623	0,0658
0,016	0,021	0,0871	0,085
0,052	0,044	0,091	0,0907

Formulas for converting from encoded coordinates to natural coordinates:

$$x_1 = 0,8235(X_1 - 1,2143);$$

$$x_2 = 0,9333(X_2 - 1,07143);$$

$$x_2^3 = 3,448(X_2^3 - 0,1576X_2^2 - 0,5361X_2 - 0,0385);$$

$$x_3^3 = 3,5272(X_3^3 - 0,1749X_3^2 - 0,5661X_3 + 0,2462);$$

$$x_4 = 5,1603(X_4 - 0,2812);$$

$$x_4^2 = 1,7976(X_4^2 - 0,1387X_4 - 0,3049);$$

$$x_4^3 = 3,9117(X_4^3 - 0,2789X_4^2 - 0,5082X_4 + 0,0427);$$

$$x_5^2 = 1,6942(X_5^2 - 0,0704X_5 - 0,3815);$$

$$x_5^3 = 3,344(X_5^3 - 0,0264X_5^2 - 0,6578X_5 - 0,0167);$$

$$x_6^2 = 1,5037(X_6^2 - 0,0197X_6 - 0,3546);$$

$$x_6^3 = 2,9362(X_6^3 + 0,0745X_6^2 - 0,6183X_6 - 0,0334).$$

The obtained relationships were tested for validity, reproducibility, and informativeness using criteria from mathematical statistics [368]. A graphical analysis of the response surface reveals a significant influence of the factors on the dependent variables (Figs. 3.32 and 3.33).

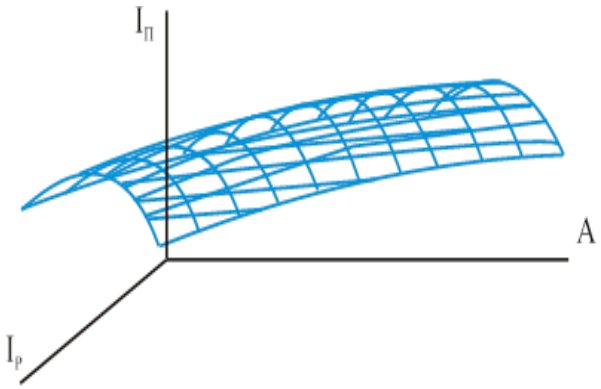

Fig. 3.32. Response curve of wear rate Iw as a function of operating current I_w and electrode oscillation amplitude A

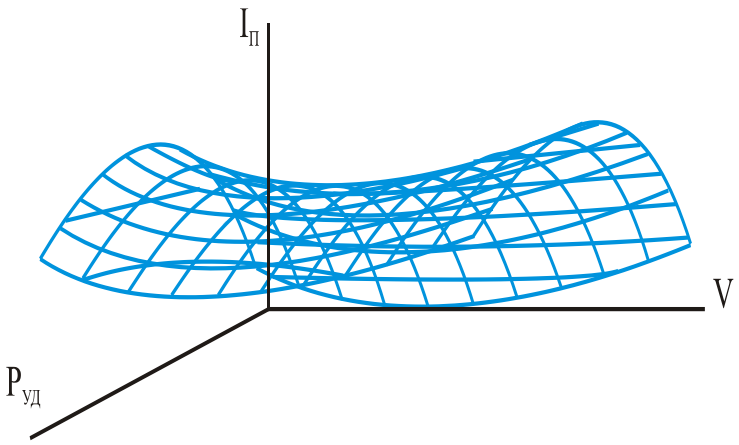

Fig. 3.33. Response curve of wear rate Iw as a function of sliding speed *V* and specific load $P_{spec/}$

3.4.4. Multi-criteria optimization of electric spark alloying and the role of coating thickness

The task is to perform multi-criteria optimization by determining a specific compromise point that will equally satisfy all requirements (a Pareto optimal solution). Coating thickness plays a significant role in the optimization of the electric spark alloying process. Analysis of the results of defect detection in bronze components of aviation equipment during major repairs showed that in most cases, the wear value lies within the range of 0.2–0.4 mm [131]. Therefore, it is necessary to assess the role of coating thickness h_{coat} in ensuring tribological characteristics under operating conditions.

Coating thickness h_{coat} ranks seventh among the ranked factors (Fig. 3.22). Including coating thickness h_{coat} in the design matrix increased the number of required experiments. Therefore, a separate experiment was conducted to determine the dependence of wear rate I_w on coating thickness h_{coat} while holding other ranked factors constant. The results are shown in Fig. 3.34. For SP-1 and SP-2 coatings to function properly, their thickness must not exceed 0.6 mm. The M_2 coating exhibits high scratch resistance due to its outer plastic layer. This allows

the M_2 coating to be applied at a thickness of up to 0.8 mm without compromising performance.

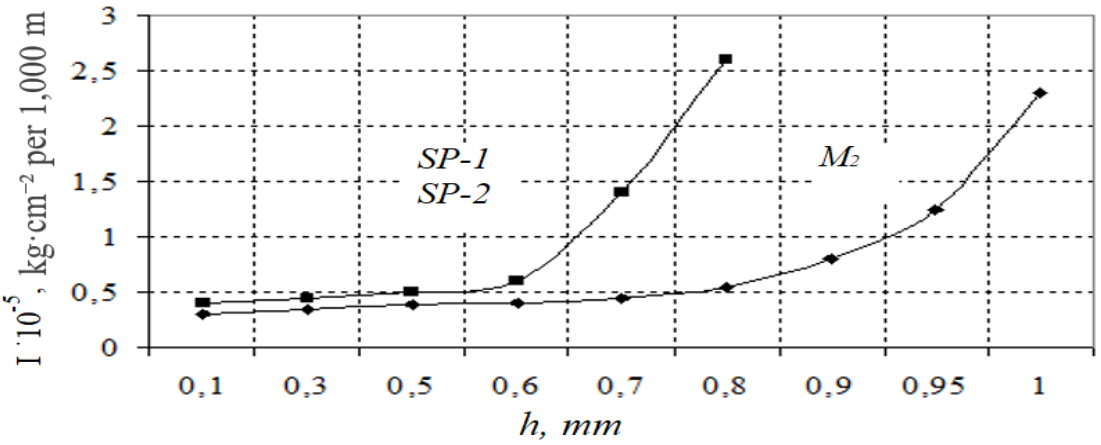

Fig. 3.34. Relationship between wear rate I_w and coating thickness h_{coat} (V = 0.2 m/s, P_{spec} = 15 MPa, lubricant – Svinzol -01)

Table 3.9 presents the results of multi-criteria optimization.

Table 3.9

Results of multi-criteria optimization

Independent variables						Dependent variables	
Coating material	Lubricant	I_r, A	V, m/s	A, mm	P_{spec}, MPa	I, 10^{-5} kg·cm^{-2} per 1000 m	μ
M_2	N_o	1,31	0,35	0,31	4	0,43	0,1025
M_2	N_1	2,09	0,2	0,48	15	0,18	0,075
M_2	N_2	2,41	0,3	0,3	12	0,2	0,08

3.5. Using electrospark coatings in the restoration of bronze parts of vehicles

Significant savings in bronze consumption can be achieved by using electro-spark coatings both in the restoration of worn bronze parts and in the manufacture of new parts. The previous section (Section 3.2) demonstrated the effectiveness of

using EIL coatings. Further expansion of the scope of application of electro-spark coatings opens up opportunities for the use of composite electrode materials.

Fig. 3.35 shows the results of microhardness measurements of electric spark coatings on BrAZ-type bronze.

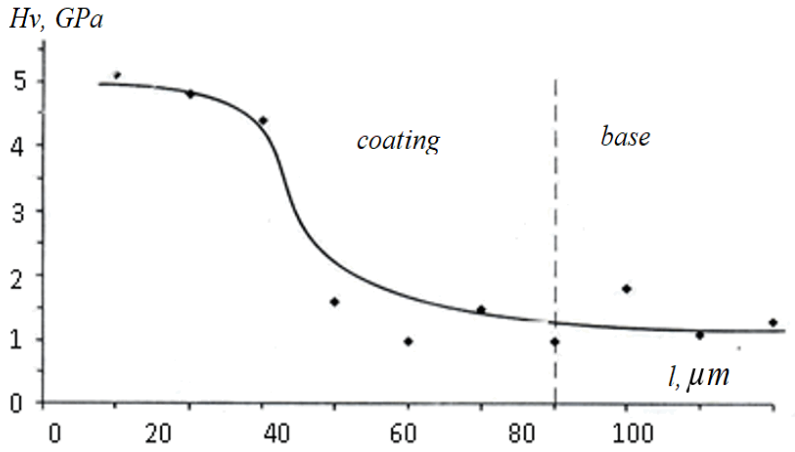

Fig. 3.35. Variation in microhardness with coating thickness

A composite electrode material with the composition (TiB_2+TiC)+NiCr was used. However, a more radical solution is to replace the bronze with an aluminum alloy with a discrete coating.

Fig. 3.36 shows the results of comparative friction and wear tests of commercial bronze and two industrial aluminum alloys. The latter were tested in two variants: in their as-received condition (uncoated) and with a discrete coating applied using a copper electrode via the electric spark alloying method. The coverage of the discrete coating is 65%.

The friction test conditions are identical (pressure, speed, duration, lubrication, counterbody—cast iron). Standard bronze is used as the reference for wear and friction coefficient.

As shown in Fig. 3.36, discrete coatings on Al alloys reduce wear by 30% compared to bronze, and the coefficient of friction by a factor of 2. It should be noted that replacing bronze with a coated Al alloy results in a threefold reduction in part weight. With a reduced coefficient of friction, Al alloys with discrete coatings can operate without lubrication.

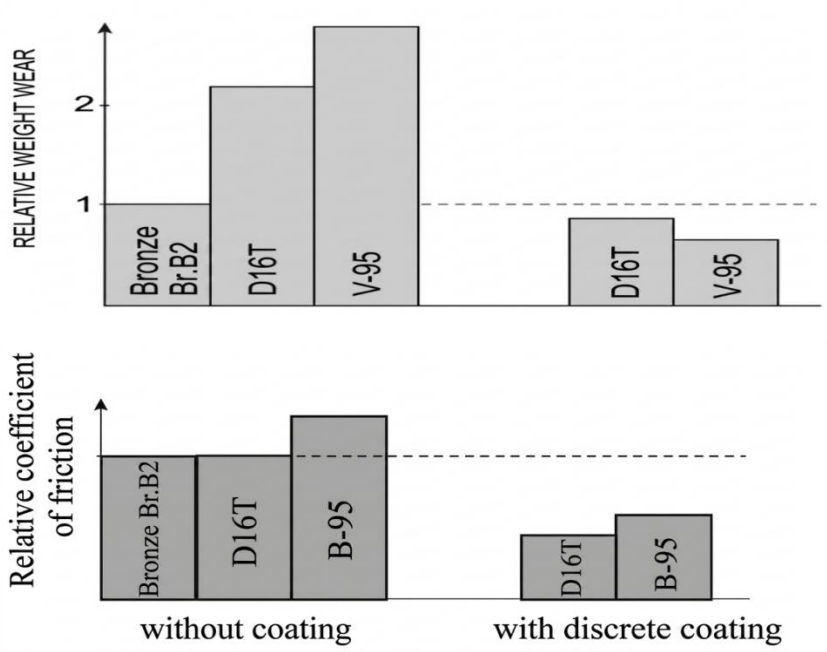

Fig. 3.36. Results of comparative friction and wear tests of standard bronze and industrial aluminum alloys without coatings and with discrete-structure coatings

Future development prospects include the application of solid lubricant coatings on aluminum alloys and the creation of “dry” friction units that do not require the costs associated with a continuous liquid lubrication system. This is a promising solution for the machine-building industry.

Conclusions on Chapter 3

Surface coating design is a promising area of surface engineering. A classic example of a structured surface in the form of natural discontinuities in the coating is the electrospark alloying (ESA) technology, which provides a change in continuity in the range of 40–100% depending on the ESA process parameters and the composition of the electrode material.

Another variant of a structured surface for an electrospark coating is the creation of a globular structure formed on the surface of structural alloys during electrospark alloying with a composite ceramic, the main component of which is

poorly wetted by the material of the surface being strengthened (the substrate) and enriches the globule. Globules of increased hardness (5...10 GPa) up to 50...100 μm in height occupy 30...50% of the surface, depending on the spark alloying mode and the composition of the alloying electrode material.

The discreteness of the surface structure can be achieved not only in the form of globules or an intermittent electrospark layer with adjustable discontinuity, but also in the form of depressions (pores) created on the coated surface (e.g., by laser treatment), the depth of which exceeds the thickness of the deposited layer.
In all cases, the discreteness of the structure of electro-spark coatings ensures a significant improvement in their tribological characteristics compared to continuous coatings.

There is a complex of reasons for the significant improvement in the tribological characteristics of discrete coatings compared to continuous ones: minimization of the stress-strain state; increased adhesive and cohesive strength of coatings, especially under high contact loads; reduced tensile stresses; the presence of reservoirs in the form of discontinuities, intergranular regions, and pores for trapping solid lubricants, including abrasive wear particles; improved heat dissipation from the sliding surface.

A new promising direction in the development of discrete coatings with enhanced wear resistance under “dry” friction conditions is the electric spark alloying of alloys with composite ceramics. By selecting the composition of the electrode material, it is possible not only to suppress the electro-erosion of the cathode during the coating process, but also to significantly (by a factor of 5 to 10) increase its hardness compared to the surface being strengthened (the substrate), as well as control the composition (and, accordingly, the properties) of the polyoxide tribofilm on the wear surface, which acts as a solid lubricant.

Surface structuring for the purpose of strengthening it is the main direction of research in the field of technology for creating various types of coatings.

CONCLUSION

The improvement of internal combustion engines of vehicles is associated with an increase in operational characteristics: pressure in the combustion chamber, crankshaft speed, and specific power per unit of engine mass.

Boosting internal combustion engines is also possible through the use of forced induction in the combustion chamber, particularly turbocharging. The increasing complexity and severity of operating conditions, particularly the rise in dynamic loads, necessitates a reduction in component weight. Therefore, preference is given to the use of lightweight and high-strength metals and alloys as structural materials. High specific strength and low specific weight have led to the widespread use of aluminum alloys in engine manufacturing. However, the effectiveness of their use depends on improving the functional properties of component surfaces.

The requirements for high technological performance in the production of internal combustion engines for vehicles are determined by: the optimal selection of structural materials and processing technologies; a favorable combination of anti-friction and mechanical properties, manufacturability, and cost.

Given the market economy and Ukraine's dependence on imports, electric spark alloying is the most suitable technology for industrial use. It is most effective for applying coatings with a discrete structure and enhanced thermomechanical stability to aluminum alloys in the manufacture of internal combustion engine pistons and plain bearings. For Ukraine, the replacement of bronzes and babbit with aluminum alloys featuring coatings in sliding bearings is a pressing issue.

A review of the literature indicates the potential of using electric spark alloying technology to improve the performance of pistons and other internal combustion engine components.

Taking into account the selectivity of wetting of the electroerosion products by the base material, the factors influencing coating formation have been grouped into three main stages of the electric spark alloying process: anode electroerosion,

physicochemical interaction of erosion products in the interelectrode gap, and in the contact zone.

A physicochemical model of electric spark alloying of aluminum alloys using a compact electrode is proposed, based on the selection of the structural components of the electrode material and on the selectivity of wetting by the aluminum alloy of the alloying components responsible for the microstructure formation of the alloyed layer.

The design of coating surfaces during the electrospark alloying process is a promising area of surface engineering. Electrospark alloying technology is a classic example of creating a structured surface in the form of natural discontinuities in the coating. In electrospark alloying, the change in coating continuity ranges from 40% to 100%, depending on the process parameters and the composition of the electrode material.

Another option for structured electrospark coating surfaces is to create a globular structure, Globules of increased hardness (5...10 GPa) with a height of up to 50...100 μm occupy 30...50% of the surface being strengthened, depending on the spark alloying mode and the composition of the alloying electrode material.

The discrete nature of the surface structure can be achieved not only in the form of globules or an intermittent electrospun layer with adjustable discontinuity, but also in the form of depressions (pores) created on the coated surface (for example, by laser treatment), the depth of which exceeds the thickness of the deposited layer. In all cases, the discrete nature of the structure of electrospark coatings ensures a significant improvement in their tribological characteristics compared to continuous coatings.

There is a complex set of reasons for the significant improvement in the tribological characteristics of discrete coatings compared to continuous ones: minimization of the stress-strain state; increased adhesive and cohesive strength of the coatings, especially under high contact loads; reduction of tensile stresses/

Surface structuring for the purpose of strengthening it is the main focus of research in the field of coating technology.

REFERENCES

1. A.G. Fesenko K.V. Bechke, S.V. Manzheliyivskij Metodi poverhnevogo zmicnennya u procesi vigotovlennya detalej mashin [Tekst]: navch. posib. D.: RVV DNU. 2015. 104 s.

2. Golloch R., Merker G.P., Ressen U. та ін. Benefits of laser – structured cylinder liners for internal combustion engines. *Tribology and Lubrication Engineering:* 14 Intern. Colloq. Tribology (Jan. 13-15 2004, Ostfildern). Vol. 1. Ostfildern: Techn. Akad. Esslingen. 2004. S. 321-328.

3. Schwaderlapp M., Dohmen Y., Andraos N. Base engine design improves fuel efficiency. *Ing. Automob.* 2003. №762. S. 44-46.

4. Sako Takahiro, Nakai Shunsaku, Moriya Koji et al. Дослідження роботи двигуна HCCI на природному газі. *B=Trans. Jap. Soc. Mech. Eng. B.* 2004. 70. №694. P. 1583-1589.

5. Agarwal A.K., Bijwe Y., Das L.M. Effect of biodiesel utilization of wear of vital parts in compression ignition engine. *Trans. ASME. J. Eng. Gas Turbines and Power*. 2003. 125. №2. P. 604-611.

6. Elleuch K., Fouvry S. Experimental and modelling aspects of abrasive weark of a A357 aluminium alloy under gross slip fretting conditions. *Wear*. 2005 258. №1-4. P. 40-49.

7. Kuroda Yoshikazu, Iga Atsuro, Seo Kenji. Eksperimentalni doslidzhennya termichnih napruzhen i deformaciyi v golovci cilindra dizelya.*B=Trans. Jap. Soc. Mech. Eng. B.* 2003. 69. №686. P. 2388-2395.

8. Iga A., Kuroda Y. The investigation of the thermal behaviour for the high-speed diesel engine cylinder head. *Schiff und Hafen.* 2004. 56. №4. P. 29-30.

9. Lyashenko B.A. Nesucha zdatnist materialiv i konstruktivnih elementiv iz zahisnimi pokrittyami v ekstremalnih umovah ekspluataciyi. Avtoref. dokt. dis., IPP AN U. Kiyiv. 1976. 55 s.

10. Canumalla A., Dynan S.A., Green D.J. et al. Mechanical behavior of mullite fiber reinforced aluminum alloy compostes. *J. Compos. Mater.* 1995. 29. №5. P.

653-670.

11. Agarwala V.S. Fatigue and corrosion. *Nav. Res. Rev*. 1998. 50. №4. P. 16-24.

12. Splav dlya detalej, pracyuyuchih v umovah kovzannya. Zayavka 60-63344. Yaponiya. S22S 21/02. Opubl. 11.04.85.

13. Heat resistant aluminum alloy powder, heat resistant aluminum alloy and heat wear resistant aluminum alloy-based composite material. Pat. 5374295 USA. C22C 21/02. Опубл. 20.12.94.

14. Das S., Prasad S.V., Ramachandran T.R. Microstructure and wear of cast (Al-Si alloy) – graphite composites. *Wear*. 1989. 133, №1. P. 173-187.

15. Visokomicnij zharomicnij i znosostijkij Al-splav, zmicnenij dispersnimi chastinkami, i jogo otrimannya. Zayavka 60-50137. Yaponiya. S22S 21/02. Opubl. 19.03.85.

16. Kompozicijnij material dlya znosostijkih detalej i sposib jogo vigotovlennya. Zayavka 58-58243, Yaponiya, S22S 21/00, opubl. 06.04.83.

17. Aoyagi N., Takahashi S., Maeda M. et al. Mechanical and wear properties of SiC Whisker/ADC 12 aluminum alloy composites fabricated by die casting. *Met. Abstr. Light Met. and Alloys.* Vol. 24 (1990-1991). Osaka. 1991. P. 58.

18. Heat resistant aluminum alloy powder, heat resistant aluminum alloy and heat wear resistant aluminum alloy-based composite material. Pat. 5374295 USA. C22C 21/02. Опубл. 20.12.94.

19. Prasad S.V., Rohatgi P.K. Tribological properties of Al alloy particle composites *J. Metals.* 1987. 39, №11. P. 22-26.

20. Visokomicnij kompozicijnij na osnovi Al-splava dlya detalej mashin. Zayavka 63-42343, Yaponiya, S22S 21/02, opubl. 23.02.88.

21. Detali par kovzannya, vigotovleni z Al-splava. Zayavka 62-89833. Yaponiya. S22S 21/00. Opubl. 24.04.87.

22. Wilson S., Ball A. Wear resistance of an aluminum matrix composite. *Tribol. Compos. Mater.:* Proc. [ASM Int.] Conf., Oak Ridge (Tenn., 1-3 May, 1990). Materials Park (Ohio). 1990. P. 103-112.

23. Pratt G.C. Aluminum alloys for automotive crankshaft bearings: *Proc. Jap. Int. Tribol. Conf.* (Oct . 29 - Nov.1 1990, Nagoya). Vol.1. Tokyo. 1990. P. 125-130.
24. Tung S.C., McMillan M.L. Automotive tribology overview of current advances and challenges for the future. *Tribol. Int.* 2004. 37. № 7. P. 517-536.
25. M.F. Dmitrichenko, R.G. Mnacakanov, O.O. Mikosyanchik Tribotehnika ta osnovi nadijnosti mashin: Navch. posibnik. K.: Informavtodr, 2006. 216 s.
26. M.V. Kindrachuk, V.F. Labunec, M.I. Pashechko, Ye.V. Korbut Tribologiya: pidruchnik Kiyiv, vidavnictvo Nacionalnogo aviacijnogo universitetu "NAU-druk". 2009. 410 s.
27. Zakalov O.V., Zakalov I.O. Osnovi tertya i znoshuvannya v mashinah: Navchalnij posibnik Ternopil: Vidavnictvo TNTU im. I. Pulyuya, 2011. 322 s.
28. Konspekt lekcij z disciplini "Tribotehnika ta osnovi nadijnosti mashin" dlya zdobuvachiv pershogo (bakalavrskogo) rivnya specialnosti 131 "Prikladna mehanika" / Ukl. k.t.n., doc. O.V. Nikulin. Kamyanske: DDTU, 2017. r. 84 s.
29. Kragelsky I.V., Demkin N.B. Contact area of rough surfaces Das kontaktgebiet rauher oberflächen *Wear*. 1960. Vol.3. Iss. 3. P. 170-187.
30. Matveevsky R.M., Buyanovsky I.A. Temperature kinetic aspect of friction and wear under boundary lubrication *Proc. JSLE International Tribology* conference, Tokyo, Japan, 1985. P. 339-344.
31. Matveevskii R.M., Sinaisky V.M., Buyanovsky LA. Contributions to the Influence of Retained Austenite Content in Steels on the Temperature Stability of Boundary Lubrication Layers in Friction. *Journal of Lubrication Te*chnology (Trans. ASME). 1975. 2. P 521-525.
32. Kragelsky I.V. Friction and Wear Butterworths, 1982. 346 p.
33. I.V. Kragelsky, M.N. Dobychin, V.S. Kombalov Friction and Wear: Calculation Methods. Elsevier, 2013 . 474 p.
34. S.V. Nikolenko, A.D. Verkhoturov, N.A. Syui, E.N. Kuz'michev Influence of electrospark discharge parameters on roughness and microabrasive wear of steel 45 surface after ESA by TiC-based electrodes. *Surface Engineering and Applied Electrochemistry*. 2016. vol. 52. P. 342–349.

35. Nikolenko S.V., Verkhoturov A.D., Syui, N.A. Generation and study of new electrode materials with self-fluxing additives to improve the efficiency of mechanical electrospark alloying *Surface Engineering and Applied Electrochemistry*. 2015. 51. P. 38–45.

36. Suwas S., Bhowmik A., Biswas S. Ultra-fine grain materials by severe plastic deformation: application to steels *Microstructure and Texture in Steels and Other Materials.* London; New York: Springer, 2009. Ch. 19. P. 325–344.

37. V.V. Tokaruk, O.O. Mikosianchyk, R. G. Mnatsakanov, N.O. Rohozhyna Microgeometrical characteristics of electrospark coatings in the initial state *Problems of Tribologyy*. 2020. №4 (98). C. 33-39.

38. Bershadsky L.I., Iosebidze D.S., Kutelia E.R. Tribosynthesis of graphite-diamond films and its employment for obtaining structurally adaptive coatings *Thin Solid Films*. 1991. Vol. 204, Iss. 2. P. 275-283.

39. Б.І. Костецький, І.Г. Носовський, А.К. Караулов та ін. Поверхнева міцність матеріалів при терті Київ: Техніка, 1976. 296 с.

40. Myshkin N.K., Petrokovets M.I., Kovalev A.V. Tribology of polymers: Adhesion, friction, wear, and mass-transfer Tribology International. 2006. Vol. 38, Iss. 11-12. P. 910-921.

41. I.A. Buyanovskii, Z.V. Ignatyeva, V.A. Levchenko, V.N. Matveenko Orientation ordering of boundary layers and lubricity of oils *Journal of Friction and Wear*. 2008. vol. 29. P. 282–287.

42. Matveevsky R.M. Friction power as a criterion of seizure with sliding lubricated contact Wear. 1992. vol. 155. P. 1-5.

43. Lyashenko I.A. Description of the stationary structural states of a boundary lubricant making use of the relation between the density-modulation and excess-volume order parameters *Ukrainian Journal of Physics.* 2021. 66 (11). P. 993-1008.

44. I.A. Lyashenko, A.E. Filippov, V.L. Popov Effect of stress nonhomogeneity on the shear melting of athin boundary lubrication layer *Physical Review*. 2016. E94. P. 053002.

45. Disckinso J.T. Nanotribology: rubbing on a small scale J. *Chem. Educ*. 2005. Vol. 82, № 5. P. 734-742.

46. Michael P.C., Rabinowicz E., Iwasa Y. Friction and wear of polymeric materials at 293, 77 and 4.2 K *Cryogenics*. 1991. Vol. 31, Iss. 8. P. 695-704.

47. A. Imani, H. Zhang, M. Owais et al. Wear and friction of epoxy based nanocomposites with silica nanoparticles and wax-containing microcapsules *Composites Part A: Applied Science and Manufacturing*. 2018. Vol. 107. P. 607-615.

48. Panin V.E., Panin A.V., Moiseenko D.D. Physical mesomechanics of a deformed solid as a multilevel system. II. Chessboard-like mesoeffect of the interface in heterogeneous media in external fields *Physical Mesomechanics*. 2007. Vol. 10, Iss. 1 – 2. P. 5-14.

49. Bolesta A.V., Fomin V.M. Molecular dynamics simulation of uniaxial deformation of thin Cu film and Al-Cu heterostructure *Physical Mesomechanics*. 2011. Vol. 14, Iss. 3 – 4. P. 107-111.

50. Tarasov S.Y., Kolubaev A.V. Formation of surface layer with nanosize grain-subgrain structure due to friction of a copper – tool steel pair. *Metal Science and Heat Treatment.* 2010. 52. P. 183–188.

51. Jha S.K., John R., Larsen J.M. Nominal vs local shot-peening effects on fatigue lifetime in Ti-6Al-2Sn-4Zn-6Mo at elevated temperature *Metallurgical and materials transactions*. 2009. Vol. 40A. P. 2675-2684.

52. Wang T., Yu J., Dong B. Surface nanocrystallization induced by shot peening and its effect on corrosion resistance of lCrl8Ni9Ti stainless steel. *Surface and Coatings Technology*. 2006. Vol. 200. P. 4777-7781.

53. M.S. Stechyshyn, V.V. Lyukhovets, N.M. Stechyshyn, M. I. Tsepenyuk Wear resistance of structural steels nitroded in cyclic-commuted discharge at limit modes of friction. *Problems of Tribology*. 2022. V. 27, No 3/105. P. 27-33.

54. T.S. Wang, B. Lu, M. Zhang et al. Nanocrystallization and a martensite formation in the surface layer of medium-manganese austenitic wear-resistant steel

caused by shot peening *Materials Science and Engineering* 2007. Vol. 458. P. 249-252.

55. Bezjazychnyj V.F., Sutyagin A.N. Technological providing of surface layer quality parameters during the machining. *Scientific problems of machines operation and maintenan*ce. 2009. 4 (160). P. 7-12.

56. L.A. Hoffmann, L.N. Carenza, J. Eckert, L. Giomi. Theory of defect-mediated morphogenesis. *Science Advances*. 2022. Vol.8 (15). PMC9012457.

57. Umemoto M., Todaka K., Tsuchiya K. Formation of nanocrystalline structured in carbon steels by ball drop and particle impact techniques. *Materials Science and Engineering*. 2004. Vol. 375-377. P. 899-904.

58. Skvortsov A.I., Kondratov V.M. Magnetomechanical damping and physical properties of damping iron alloys. *Metal Science and Heat Treatment*. 1998. 40. P. 179–181.

59. M. Bembenek, J. Krawczyk, K. Pańcikiewicz The wear mechanism of mill beaters for coal grinding made-up from high manganese cast steel. *Engineering Failure Analysis.* 2022. Vol. 142. P. 106843

60. Volosevich P.Yu., Bespalov S.A. Strukturoutvorennya i znosostijkist stali 40H. *Metalofizika i novitni tehnologiyi.* 2004. T.26, №5. S. 691-701.

61. Volosevich P.Yu., Bespalov S.A. Zv'yazok osoblivostej strukturoutvorennya zi znosostijkistyu stali H6VF. *Metalofizika i novitni tehnologiyi.* 2005. T.27, №6. S. 841-850.

62. Aftanaziv I.S., Yurchishin I.I., Klimenko O.D. Vpliv tehnologichnih parametriv procesu VVZK na chistotu zmicnenoyi bokovoyi poverhni zubiv. *Nadijnist instrumentu ta optimizaciya tehnologichnih sistem:* Zb. nauk. pr. Donbaskoyi derzh. mashinobudivnoyi akad. Kramatorsk, 2003. Vip. 14. S. 106–118.

63. Aftanaziv I.S., Strutinska L.R., Klimenko O.D. Efektivnist zmicnennya zubchastih kolis vibracijno-vidcentrovoyu zmicnyuvalnoyu obrobkoyu. *Rozvidka ta rozrobka naftovih i gazovih kopalin:* Vseukr. shokvartalnij nauk.-tehn. zhurn. 2003. № 2 (7). S. 22–28.

64. Quast M., Stock H. R., Mayr P. Plasma-Assisted Nitriding of Aluminum-Alloy Parts. *Metal Science and Heat Treatment.* 2004. 46. P. 299-304.

65. Y.D. Kogan, Z.S. Sazonova, V.D. Aleksandrov et al. Antifriction properties of aluminum alloys after surface laser alloying. *Metal Science and Heat Treatment.* 1991. Vol. 33. P. 772-776.

66. G. Coquerelle, J.L. Fachinetti Coquerelle G., Fachinetti J.L. Friction and wear of laser treated aluminum - silicon alloys. *Laser Treat. Mater. Eur.* Conf., Bad Nauheim, 1986. Oberursel, 1987. P. 171-178.

67. J.A. Picas, A. Form, R. Rilla et al. Mejora de la resistencia al desgaste de aleaciones de aluminio mediante recubri - mientos obtenidos por proyeccing termica HVOF. *Rev. met*. CENIM, 2005. P. 197-201.

68. M. Prieske, H. Hasselbruch, A. Mehner et al. Friction and wear performance of different carbon coatings for use in dry aluminium forming processes. *Surface and Coatings Technology*. 2019. Vol. 357. P. 1048-1059.

69. Lee S. Y., Kim S. H. Metal Nitride Coatings by Physical Vapor Deposition (PVD) for a Wear Resistant Aluminum Extrusion Die. *Journal of Nanoscience and Nanotechnology*. 2014. Vol. 14, № 12. P. 8993-8998(6).

70. S.V. Divinski, N.V. Dubovitskaya, L.N. Larikov et al. Intermetallic coatings with nano- and quasicrystalline structures on Al- based. *Advanced Light Alloys and Composites*. 1998. 59. P. 495-500.

71. Hilpert M., Wendt J., Wagner L. Response of aluminum and magnesium alloys to mechanical Surface treatments. *Journal of the Minerals Metals & Materials Society*. 2000. 52, № 11. P. 63-73.

72. V. Hutsaylyuk, M. Student, Kh. Zadorozhna et al. Improvement of wear resistance of *aluminum alloy by HVOF method. Journal of Materials Research and Technology*. 2020. Vol. 9, Is. 6. P. 16367-16377

73. Zusin V.Ya., Redchic V.V. Pidvishennya shilnosti naplavlenogo metalu pri naplavlenni alyuminiyevih splaviv poroshkovim drotom. *Avtomatichne zvaryuvannya*. 1991. №5. S. 49-50.

74. Eyre T.S., Abdul-Mahdi F. Wear resistance of aluminum and its alloys. *Alum. Technol. 86: Proc.:* Int. Conf., London (11-13 March 1986, London). 1986. P. 485-492.

75. Molina G., Furey L. Ein Werkstoff fur Alle Falle. *Galvanotechnik.* 2000. V. 91. № 2. P. 385-388.

76. Ellermeier J. Plasmaspritzen von keramischen pulver. *HTM: Harter.-techn. Mitt.* 2000. V.55. № 3. P. 177-182.

77. Process for ion nitriding aluminum material. Pat. 4909862 USA. C22F 1/02. Опубл. 20.03.90.

78. Reinhold B., Naumann J., Spies H.-J. et al. Nitrieren von Aluminium werkstoffen im DC-Puls-Plasma. *HTM: Harter.–techn. Mitt.* 1997. 52. №6. S. 350-355.

79. Plasmadiffusionsverfahren – Oberflächen nach Maβ. *Galvanotenik*. 2001. 92, №6. S. 1667-1668.

80. Tkachenko Yu.G., Yurchenko D.Z., Dubovik T.V., Pavlikov V.N., Yulogin V.K., Maj A.V. Visokotemperaturne tertya i okislennya keramiki na osnovi nitridu alyuminiya. *Poroshkova metalurgiya*. 1985. №4. S. 88-90.

81. Podchernyayeva I.O., Panasyuk A.D., Evdokimenko Yu.I., Kisel V.M., Katashinskij V.P., Korol A.A., Frolov G.A., Yuga A.I. Znoso - i okalinostijki pokrittya na osnovi TiCN. *Poroshkova metalurgiya*. 2001. № 5/6. S.57-68.

82. Podchernyayeva I.A., Shepetov V.V., Panasyuk A.D., Gromenko V.Yu., Yurechko D.V., Katashinskij V.P. Struktura i vlastivosti znosostijkih detonacijnih pokrittiv na osnovi karbonitridu titanu. *Poroshkova metalurgiya.* 2003. № 9/10. S. 11-77.

83. Romanenko V.I., Devojno O.G., Kardapolova M.A., Panich G.G. Pidvishennya tribologichnih harakteristik alyuminiyevih splaviv lazernim leguvannyam. *Tertya i znos.* 1995. T. 16. №3. S. 555-562.

84. Ovchinnikov A.A., Vishnevecka I.A. Tribologichni harakteristiki poverhni alyuminiyevogo modifikovanogo splava D16. *Tertya i znos*. 1991. 12. № 6. S. 1129-1132.

85. "Laser-Honen" optimiert Motorenbetrieb. *VDI-Nachr*. 2004. № 37. S. 29.

86. Abeln T., Klink U. Laserstruktureirung - Verbesserung der tribologischen Eigenschaften von Oberflachen. *Tribology and Lubrication Engineering:* 14 Intern. Callog. Tribology, Ostfildern (Jan. 13-15 2004, Ostfildern). 2004. Vol.1. Ostfildern, Techn. Akad. Esslingen. S. 315-319.

87. Dohmen J., Hermsen F.-G., Barbezat G. Untersuchungen an plasmabeschichten Zylinderaufflächen. *MTZ: Motortechn. Z.* 2004. 65. №3. S. 204-208.

88. Borisov Yu.S., Harlamov Yu.O., Sidorenko S.L. ta in. Gazotermichni pokrittya z poroshkovih materialiv. Kiyiv, Nauk. dumka. 1987. 544 s.

89. Picas J.A., Forn A., Rilla R. et al. Mejora de la resistencia al desgaste de aleaciones de aluminio mediante recubri - mientos obtenidos por proyeccing termica HVOF. *Rev. met. CENIM.* 2005. S. 197-201.

90. Znosostijkij material na osnovi alyuminiya i sposib jogo vigotovlennya. Zayavka 297678. Yaponiya. S23S 16/32. Opubl. 10.04.90.

91. Stvorennya tovstogo sharu pidvishenoyi tverdosti na poverhni alyuminiyevogo splavu shlyahom plazmovoyi poroshkovoyi metalizaciyi dugoyu pryamoyi diyi. *Koon gakkaishi = J. High Temp. Soc.* 1993. 19, №4. P. 168-178.

92. Chernenko V.I., Snezhko L.A., Papanova I.I., Litovchenko K.I. Teoriya i tehnologiya anodnih procesiv pri visokih napruzhennyah. Kiyiv, Nauk. dumka. 1995. 197 s.

93. Tyurin Yu.N., Zhadkevich M.L., Golovenko S.I., Chigrinova N.M. Nanesennya oksidnih pokrittiv na poverhni virobiv iz splaviv na osnovi alyuminiya. *Avtomatichne zvaryuvannya.* 2002. №2. S. 44-48.

94. Timoshenko A.V., Magurova Yu.V., Artemova S.Yu. Vpliv dobavok v elektrolit oksiduvannya kompleksnih z'yednan na proces nanesennya mikroplazmovih pokrittiv i yih vlastivosti. *Fizika i himiya obrobki materialiv.* 1996. №2. S. 57-64.

95. Gorchakov A.P., Karpouhov A.P., Oshepkov D.A. Rozrobka elektricheskoyi shemi zhivlennya dlya ustanovki mikrodugovogo oksiduvannya. *Problemi suchasnih materialiv i tehnologij.* 1997. № 1. S. 156-160.

96. Atroshenko E.S, Kazancev I.A., Rozen A.Ye., Golovanova N.V. Galuz vikoristannya pokrittiv, otrimanih mikrodugovim oksiduvannyam. *Fizika i himiya obrobki materialiv.* 1996. №3. S. 8-11.

97. Korkosh S.V. Praktika mikrodugovogo oksiduvannya virobiv iz titanovih i alyuminiyevih splaviv. *Pitannya materialoznavstva.* 1998. №1. S. 40-82.

98. Yerokhin, X. Nie, A. Leyland et al. Plasma electrolysis for surface engineering. *Surface and Coating Technology*. 1999. No. 122. P. 73-93.

99. Sordelet D.I., Besser M.F., Anderson I.E. Particle size effects on chemistry and structure of Al-Cu-Fe quasicrystalline coatings. *J. Therm. Spray Techn.* 1996. 5(2). P. 161-174.

100. Sordelet D.I., Kramer M.1., Unal O. Effect of starting powders on the control of microstructural development of Al-Cu-Fe quasicrystalline plasmo-sprayed coatings. *Ibid*. 1995. 4(3). P. 235-244.

101. Divinski S.V., Dubovitskaya N.V., Larikov L.N., Shmatko O.A. Intermetallic coatings with nano- and quasicrystalline structures on Al-based. *Advanced Light Alloys and Composites.* 1998. 59. P. 495-500.

102. Dubovicka M.V., Larikov L.M. Vpliv rezhimiv iono-plazmovogo nanesennya alyuminidiv na strukturu i tverdist osnovi iz alyuminiya i dyuralya. *Avtomaticheskaya svarka*. 1999. № 2. S. 21-24.

103. Hilpert M., Wendt J., Wagner L. Response of aluminum and magnesium alloys to mechanical Surface treatments. *JOM: J. Miner. Metals and Mater. Soc.* 2000. 52. №11. P. 63-64.

104. Irisawa T., Morishige T., Kawachi H. Kokai Tokkyo Koho. Нанесення керамічних покриттів на металічні основи. Заявка Японії №2-4981. пр. 26.06.88. № 88/155901. Опубл. 9.01.90. МКИ c23c26/10 / Ishikawajima-harima heavy ind. Co. ltd., Japan

105. Guilemany J.M., Llorga-Isern N., Nunez M.D. et al. Study of interface interactions for metal- metal and metal-ceramic coating obtained by plasma and HVOF spraying. *Sci. met et mater*. 1994. V.31. №8. P. 1121-1126.

106. Novikov N.V., Bidnij A.A., Lyashenko B.A. ta in. Metodi zmicnennya poverhon mashinobudivnih detalej. Kiyiv, ISM AN USSR. 1989. 112 s.

107. Schmidt R. Field experience with the Mahle ferrocomp piston. Schiff und Hafen. 2004. 56. №4. S. 17.

108. E.K. Posvyatenko, Ye.K. Solovih, B.A. Lyashenko i in. Tendenciyi pidvishennya znosostijkosti porshniv DVZ. *Visnik Nacionalnogo transportnogo universitetu*: Ch.1. Kiyiv, NTU, 2006. Vip. 13. S. 13–21.

109. Aluminum alloy piston. Pat. 5158052 USA. F02F 3/00. Опубл. 27.10.92.

110. Sposib otrimannya detalej z keramichnim pokrittyam. Zayavka 3260062. Yaponiya. S23S 14/06. Opubl. 20.11.91.

111. Yamaguchi Hiroshi. Tehnologiya tverdogo anoduvannya i viprobuvannya pokrittya.*Intern. Combust. Engine.* 1990. 20, № 12. P. 57–62.

112. Plasma jet sprayed alumina coating on automobile pistons. "SAE Techn. Pap. Ser". 1987. № 870158. P. 179-184.

113. Brigantine installs HVOF technology. Ship repair and Convers. *Technol.* 2003. №4. P. 28.

114. Bransden A.S., Gazzard S.T., Inwood B.C. et al. Laser hardening of ring grooves in medium speed diesel engine pistons. *Surface Eng*. 1986. 2, №2. P. 107-113.

115. Surface hardened aluminum part and method of producing same. Pat. 5352538 USA, B22F 7/04. Опубл. 04.10.94.

116. Krovyanov K.S., Radchenko M.V. Zmicnennya kilcevih kanavok porshnya dizelya elektrono-promenevoyu obrobkoyu. *Tehn. mashinobud*. 2000. №3. S. 23-25.

117. Batirov M.I., Radchenko M.V., Hvorov M.O. i in. Promislove elektrono-promeneve zmicnennya porshniv iz splava AK21M2, 5N2, 5: Tez. dopov. 4-yi Vses. konf. po zvaryuvanni kol. met. (4-7 veresnya 1990, Mariupol). Kiyiv 1990. S. 58-59.

118. Bendovskij Ye.B., Platonov V.M., Shalaj O.M. i in. Stan i perspektivi udoskonalennya kompozicijnih materialiv na osnovi porshnevih siluminiv. *Dvigobuduvannya.* 1991. №10-11. S. 57-60.

119. PM shapes up for the next certury. *MPR: Metal Powder Rept*. 1994. 49. №7-8. P. 19-21.

120. Tonkih L.S., Kabanec A.F., Nosovska O.B. Optimizaciya skladu poroshkovogo drotu dlya naplavlennya zharomicnih alyuminiyevih splaviv. *Avtomatichne zvaryuvannya.* 1991. №9. S. 53-54.

121. Zusin V.Ya., Glozman L.A., Lozovskaya A.V. Osoblivosti strukturi zharomicnogo alyuminiyevogo splavu, naplavlenogo poroshkovim drotom. *Avtomaticheskaya svarka.* 1991. №3. S. 18-20.

122. Voropaj M.M., Lisnih V.V., Mishenkov V.O. Dvodugove naplavlennya alyuminiyevih porshniv kombinovanim neplavyashimsya i plavyashimsya elektrodami. *Avtomatichne zvaryuvannya*. 1996. №6. S. 21-25.

123. Shalaj O.M. Yak pidvishiti dolgovichnist porshnya? *Dvigobuduvannya*. 1996. №2. S. 42, 51.

124. Piston having uncoupled skirt. Pat. 6588320. F16J 1/04. Опубл. 08.07.2003.

125. Ivanov V. I., Verkhoturov A. D., Konevtsov L. A. The development of criteria for evaluating the effectiveness of the surface layer formation and its properties in the process of electrospark alloying (ESA). Part 2. The criteria of the effectiveness of the ESA process and electrospark coatings. *Surface Engineering and Applied Electrochemistry*. 2017. Vol. 53. P. 224–228.

126 Pokritiya i ikh ispolzovanie v tekhnike. Prochnost materialov i konstruktsii. Pod red. V.T. Troshchenko. Kiïv, Akademperiodika. 2006. S. 981-1074.

127 Lyashenko B.A., Solovikh Ye.K., Mirnenko V.I., Rutkovskii A.V., Chernovol M.I. Optimizatsiya tekhnologi naneseniya pokritii po kriteriyam prochnosti i iznosostoikosti. Kiev, IPP imeni G.S.Pisarenko NANU. 2010. 193 s.

128 Yushchenko K.A., Borisov Yu.S., Kuznetsov V.D., Korzh V.N. Inzheneriya poverkhni. Kiïv, Naukova dumka. 2007. 559 s.

129 Pashchenko V.M., Kuznєtsov V.D., Solodkii S.P. Problemi yefektivnosti zakhisnikh pokrittiv u inzhenerії poverkhni mashin i obladnannya. Visnik Natsionalnogo tekhnichnogo universitetu Ukraїni «KPI». 2006. №49. S. 178-187.
130. V.V. Tokaruk, O.O. Mikosyanchik, R.G. Mnatsakanov, O.Yu. Zhosan, D.V. Dolot Analiz mitsnostnikh kharakteristik yelektroiskrovikh pokrittiv. Problemi tertya ta znoshuvannya. 2021. №3 (92). C. 47-53.
131. B.A. Lyashenko, V.V. Yermolaev, V.I. Mirnenko Elektroiskrovoe legirovanie, kak perspektivnii metod vosstanovleniya detalei aviatsionnoi tekhniki Tekhnologiya i instrument iz STM v avtomobilnoi i aviatsionnoi promishlennosti: materiali seminaru. Kiev, ISM NAN Ukraini. 1997. S. 30–31.
132. Soma Raju K., Faisal N.H., Srinivasa Rao D., Joshi S.V., Sundararajan G. Electro-spark coatings for enchanced performance of twist drills. Surface and Coatings Technology. 2008. Vol. 202. №9. P. 1636-1644.
133. Lazarenko N.I. Elektroiskrovoe legirovanie metallicheskikh poverkhnostei. Kiev, Mashinostroenie. 1976. 44 s.
134. Verkhoturov A.D. Obobshchennaya model protsessa elektroiskrovogo legirovaniya. Elektrofizizicheskie i elektrokhimicheskie metodi obrabotki. 1983. №1. S. 3-6.
135. Yurechko D.V. Inzheneriya iznosostoikosti poverkhnosti splavov alyuminiya pri ikh elektroiskrovom legirovanii materialami na osnove sistem AlN-Ti(Zr)B2 i LaB6-ZrB2. Diss. kand. tekhn. nauk, IPM im. I.N. Frantsevicha NANU. Kiev. 2006. 172 s.
136. Yurechko D.V., Podchernyaeva I.A., Panasyuk A.D. Fiziko-khimicheskaya model formirovaniya iznosostoikikh pokritii na alyuminievikh splavakh pri elektroiskrovom massoperenose kompozitsionnoi keramiki. Poroshkovaya metallurgiya. 2006. №1/2. S. 51-58.
137. Podchernyaeva I.A., Panasyuk A.D., Shchepetov V.V., Yurechko D.V., Gromenko V.Yu. Poverkhnostnoe modifitsirovanie splava AL9 pri elektroiskrovom legirovanii materialami sistemi AlN-Ti(Zr)B2-Ti(Zr)Si2. Poroshkovaya metallurgiya. 2004. №3-4. S. 54-62.

138. Podchernyaeva I.A., Panasyuk A.D. Formation of fine-dispersion structures of wear- and corrosion-resistant coatings using AlN-TiB2/ZrB2 composites. Key Engineering Materials. 2002. Vol. 206-213. R. 499-502.
139. Abramchuk A.P. Razrabotka i optimizatsiya protsessa poverkhnostnogo uprochneniya alyuminiya i yego splavov metodom elektroiskrovogo legirovaniya kompaktnimi i poroshkovimi materialami: Diss. na soiskanie uch. stepeni kand. tekhn. nauk. Kishinev. 1988. 255 s.
140. Podchernyaeva I.A., Panasyuk A.D., Lavrenko V.A., Andrievskaya R.A., Teplenko M.A., Kostenko A.D. Struktura i svoistva kompozitsionnikh elektroiskrovikh, lazernikh i magnetronnikh pokritii iz materiala AlN-TiB2. Poroshkovaya metallurgiya. 2001. №9/10. S. 69-77.
141. Podchernyaeva I.A., Panasyuk A.D., Katashinskii V.P., Teplenko M.A. Formirovanie, struktura i svoistva pokritii na osnove TiB2-AlN, poluchennikh elektroiskrovim i lazernim metodami. Poroshkovaya metallurgiya. 2000. №11/12. S. 39-45.
142. Panasyuk A.D., Podchernyaeva I.A., Andrievsky R.A., Teplenko M.A., Katashinsky V.P., Timofeeva I.I. Structure and properties of electric-spark, laser and magnetron coatings using AlN-TiB2/ZrB2 composite materials. Functional materials. 2001. V.8. R. 129-134.
143. Panasyuk A.D., Podchernyaeva I.A., Andrievsky R.A., Teplenko M.A., Kalinnikov G.V., Isaeva L.P. Formation of fine-dispersion structures by electric-spark, laser and magnetron coating with AlN-TiB2/ZrB2 composite materials. Functional Gradient Materials and Surface Layers Prepared by Fine Particles Technology. 2001. R. 111-118.
144. Verkhoturov A.D., Podchernyaeva I.A., Gorbunov Yu.A., Yegorov F.F. Vibor materiala elektroda i massoperenos pri elektroiskrovom legirovanii. Poroshkovaya metallurgiya. 1985. №2. S. 36-39.
145. Verkhoturov A.D., Podchernyaeva I.A., Radchenko V.G., Yegorov F.F. Osobennosti EIL bistrorezhushchei stali tverdimi splavami. Poroshkovaya metallurgiya. 1987. №3. S. 30-36.

146. Abramchuk A.P., Bovkun G.A., Mikhailov V.V., Tkachenko Yu.G. Iznosostoikost pokritii na alyuminii, poluchennikh elektroiskrovim legirovaniem poroshkovimi smesyami. Elektronnaya obrabotka materialov. 1987. № 3. S. 25-29.
147. Tkachenko Yu.G., Parkanskii N.Ya., Yurchenko D.Z. i dr. Elektroiskrovoe formirovanie pokritii iz poroshkovikh smesei i ikh nekotorie ekspluatatsionnie svoistva. Elektronnaya obrabotka materialov. 1986. №2. S. 36-41.
148. Gorchakov A.P., Karpoukhov A.P., Oshepkov D.A. Razrabotka elektricheskoi skhemi pitaniya dlya ustanovki mikrodugovogo oksidirovaniya. Problemi sovremenni materialov i tekhnologii. 1997. № 1. S. 156-160.
149. Atroshchenko E.S, Kazantsev I.A., Rozen A.E., Golovanova N.V. Oblast primeneniya pokritii, poluchaemikh mikrodugovim oksidirovaniem. Fizika i khimiya obrabotki materialov. 1996. №3. S. 8-11.
150. Korkosh S.V. Praktika mikrodugovogo oksidirovaniya izdelii iz titanovikh i alyuminievikh splavov. Vopr. materialovedeniya. 1998. №1. S. 40-82.
151. Kim V.A., Korotaev D.N., Golik A.V. Vliyanie uslovii elektroiskrovoi obrabotki na erozionnii protsess. Fizika i khimiya obrabotki materialov. 2001. №1. S. 78-81.
152. Verkhoturov A.D., Drachinskii A.S., Podchernyaeva I.A. i dr. O fizicheskoi prirode erozii i formirovaniya poverkhnostnogo sloya pri elektroiskrovom legirovanii molibdena poristimi elektrodami zheleza. Poroshkovaya metallurgiya. 1983. №12. S. 51-54.
153. Verkhoturov A.D., Podchernyaeva I.A., Kurilenko L.N., Polovtsev L.P. Kinetika obratnogo massoperenosa pri elektroiskrovom legirovanii i formirovanie vtorichnoi strukturi na anode. Fizika i khimiya obrabotki materialov. 1986. №4. S. 65-68.
154. Teplenko M.A. Strukturoobrazovanie kompozitsionnikh gradientnikh pokritii s povishennoi iznoso- i korrozionnoi stoikostyu pri elektroiskrovom massoperenose keramiki sistemi Al-Ti(Zr)-N-B. Avtoref. dis. kand. tekhn. nauk. Kiev, IPM NANU. 2003. 23 s.
155. Teplenko M.A. Massoperenos pri elektroiskrovom legirovanii

(EIL) konstruktsionnikh splavov kompozitom AlN-ZrB2 Elektricheskie kontakti i elektrodi. Sb. nauch. trudov. Kiev, IPM NANU. 2001. S. 137-143.

156. Mulin Yu.I., Verkhoturov A.D., Vlasenko V.D. Elektroiskrovoe legirovanie poverkhnostei titanovikh splavov. Perspekt. mater. 2006. №1. S.79-85.

157. Teplenko M.A., Podchernyaeva I.A., Panasyuk A.D. i dr. Struktura i iznosostoikost pokritii na titanovom splave i stalyakh, poluchennikh pri elektroiskrovom legirovanii materialom AlN-ZrB2. Poroshkovaya metallurgiya. 2002. №3/4. S. 48-57.

158. Verkhoturov A.D., Mukha I.M. Tekhnologiya elektroiskrovogo legirovaniya. Kiev, Tekhnika. 1982. 182 s.

215. Ляшенко Б.А. и др. Электроискровое легирование алюминиевых сплавов АЛ25 и АК4М. *Электрофизические и электрохимические методы обработки.* 1983. Вып. 8. С. 5-6.

216. V.V. Zaporozhets, V.M. Stadnichenko, V.V. Tokaruk Metodologiya uskorennoi otsenki iznosostoikosti obraztsov s elektroiskrovimi pokritiyami. Problemi tribologiї. 2010. №4. S. 25-31.

217. Poluchenie alyuminievogo splava, soderzhashchego grafit. Zayavka 60-187637. Yaponiya. S22S 1/10. Opubl. 25.09.85.

218. Kharakteristiki iznosa kompozitsionnogo materiala iz Al s dispersnimi vklyucheniyami grafita, poluchennogo ekstruziei poroshkov. J. Jap. Inst. Metals. 1985. 49. №11. P. 981-987.

219. Ovchinnikov A.A., Vishnevetskaya I.A. Tribologicheskie kharakteristiki poverkhnosti alyuminievogo modifitsirovannogo splava D16. Trenie i iznos. 1991. 12. № 6. S. 1129-1132.

220. Tsarev G.L., Chelishev A.P., Volochko A.T. i dr. Svoistva goryachedeformirovannogo alyuminivo-grafitovogo splava. Poroshkovaya metallurgiya. 1986. №1. S. 40-43.

221. Tyo Takao. Protsessi izgotovleniya kompozitsionnikh materialov, naprimer, iz SAP, putem mestnogo reaktsionnogo sinteza. Kinzoku=Metals and Technol. 1996. 66, №3. P. 254-257.

222. З.А. Дурягіна, О.Я. Лизун. Сплави з особливими властивостями. Львів, Львівська політехніка. 2007. 236 с.

223. П.П. Савчук, В.П. Кашицький, М.Д. Мельничук, О.Л. Садова Композитні та порошкові матеріали: навчальний посібник Луцьк, Видавець: ФОП Теліцин О.В. 2017. 368 с. ISBN 978-617-7070-88-6.

224. Romanenko V.I., Devoino O.G., Kardapolova M.A., Panich G.G. Povishenie tribologicheskikh kharakteristik alyuminievikh splavov lazernim legirovaniem. Trenie i iznos. 1995. T.16. № 3. S. 555-562.

225. A.c. №115403 Sposob naneseniya pokritii i ustroistvo dlya yego osushchestvleniya. V.V. Mikhailov, A.E. Gitlevich, V.M. Revutskii, A.P. Abramchuk. Byul. izobr. 1985, № 15.

226. Dispersion-strengthened heat - and wear-resistant aluminum alloy and process for producing same. Pat. 4722751. USA. C22C 29/02. Opubl. 02.02.88.

227. Diaz C., Gonzalez-Carrasco J.L., Caruana G. et al. Ni3Al intermetallic particles as wear-resistent reinforcement for Al-base composites processed by powder metallurgy. *Met. and Mater. Trans. A* [Met. Trans.A]. 1996. 27, № 10. P. 3259-3266.

228. Nukami T., Flemings M.C. In situ synthesis of TiC particulate-reinforced aluminum matrix composites. Met. and Mater. Trans. A. 1995. 26. №7. P. 1877-1884.

229. Astakhov Ye.A. Nauchno-tekhnologicheskie osnovi upravleniya svoistvami detonatsionnikh pokritii. Avt. diss. na soiskanie uchenoi stepeni d.t.n.: Kiev. 2005. IES NANU.

230. Stoikost nemetallicheskikh materialov v rasplavakh: Spravochnik. Kiev, Nauk. Dumka. 1986. 351 s.

231. Samsonov T. V., Markovskii L. Ya., Zhigach A. F., Valyashko M. G. Bor. Yego soedineniya i splavi. Kiev, izd-vo AN USR. 1960. 588 s.

232. Ravikiran A. Effect of interface layers formed during dry sliding of zirconia toughened alumina against steel. Wear. 1994. V. 171. P. 129-134.

233. Mosina T.V., Panasyuk A.D., Grigorev O.N., Yuga A.I. Friktsionnie svoistva kompozitsionnikh materialov sistem TiN-AlN. II. Vliyanie oksidnikh plenok na protsess treniya i iznashivaniya sistemi keramicheskii material-stal. Poroshkovaya metallurgiya. 1996. №5/6. S. 11-15.
234. Allan Matthews and Adrian Zeyland Developments in Vapour Deposited Ceramic Coatings for Tribological Applications. Key Eng. Material., 2001. V. 206-213. R. 459-466.
235. Vilan J., Bomer P. Getting into the Groove. Metalwork Prod. 1998. V. 142. №6. R. 26-32.
236. Baranov N.G., Fedorchenko I.M. Fiziko-khimicheskie protsessi obrazovaniya poverkhnostnikh plenok pri trenii. Poroshkovaya metallurgiya. 1986. №1. S. 78-82.
237. C. Kajdas, M. J. Furey, A.L. Ritter, G.I. Molina. Triboemission as a Basic Part of the Boundary Friction Regime. Tribology 2000 – Plus: 12th Int. Colloquim, (January 11-13, 2000).
238. H. Kloss, M. Woydt, A. Skopp. Wear Prediction in Ultra-High Speed and High Temperature Applications. Tribology 2000 – Plus: 12th Int. Colloquim, (January 11-13, 2000).
239. Lakiza S.M., Redko V.P., Lopato L.M. Triangulyatsiya ta poverkhnya likvidusu diagrami stanu sistemi Al2O3-ZrO2-La2O3. Poroshkovaya metallurgiya. 2002. №11/12. S. 80-90.
240. Tkachenko Yu.G., Varchenko V.T., Britun V.F., Yurchenko D.Z. Vliyanie sostava i strukturi keramiki B4C-Al2O3 na tribotekhnicheskie kharakteristiki pri trenii po stali. Poroshkovaya metallurgiya. 2005. №5/6. S. 49-59.
241. Panteleenko F.I., Snarskii A.S. Osobennosti tribologicheskogo povedeniya pari borosoderzhashchii instrumentalnii material-detal. Trenie i iznos. 1997. T.18. №4. S. 518-522.
242. Lyashenko B.A., Movshovich A.Ya., Dolmatov A.I. Uprochnyayushchie pokritiya diskretnoi strukturi. Tekhnologicheskie sistemi. 2001. № 4 (10). S.17-25.

243. A. s. 677549, S 23 S 9/00, V23R 1/18. Sposob naneseniya pokritii. Lyashenko B.A., Rishin V.V., Umanskii E.S. i dr. Opubl. 30.07.79. Byul. № 28.

244. Tekhnologicheskaya instruktsiya na tipovoi tekhnologicheskii protsess elektroiskrovogo uprochneniya instrumenta diskretnimi pokritiyami povishennoi termomekhanicheskoi stoikosti: TI 170–2–85. Kiev, IPP
NAU. 1985. 14 s.

245. Kalinichenko V.I. Napruzheno-deformovanii stan ta mitsnist znosostiikikh diskretnikh pokrittiv. Avtoref. dis. na zdobuttya naukovogo stupenya kand. tekhn. nauk, IPMits im. G.S.Pisarenka NANU. Kiïv, 2006. S. 21.

246. B.A. Lyashenko, Yu.V. Volkov, Ye.K. Solovikh i dr. Povishenie iznosostoikosti detalei sudovikh mashin i mekhanizmov pokritiyami diskretnoi strukturi elektrokontaktnim pripekaniem. Problemi tertya ta znoshuvannya. 2005. 2(67). S.110-126.

247. B.A. Lyashenko, V.S. Antonyuk, O.B. Soroka, A.V. Rutkovskii Rozrobka novikh znosostiikikh pokrittiv dlya pidvishchennya yekspluatatsiinikh kharakteristik detalei mekhanizmiv. Zb. Dinamika, mitsnist i nadiinist silskogospodarskikh mashin: materiali mizhnar. nauk.-tekhn. konf. Ternopil, TDTU imeni I. Pulyuya . 2004. S. 381-386.

248. B.A. Lyashenko, Yu.A. Kuzema, M.S. Digam, O.V. Tsigulev Uprochnenie poverkhnosti metallov pokritiyami diskretnoi strukturi s povishennoi adgezionnoi i kogezionnoi stoikostyu [Elektronnii resurs]. Kiev, 1984. 57 s. (Prepr. AN IPMits.).

249. Pat. DE 196 26 008 A1 (BRD), C21D1/09. Verfahren zur Härtung von Oberflächen bei Stahl und Guβeisen. Marci G., Lyashenko B.A., Rutkowski A.V. Offenlegungstan 06.02.97.

250. Digam M.S. Prochnost poverkhnosti alyuminievikh splavov s pokritiyami diskretnoi strukturi. Avtoref. kand. diss. Kiev, IPP AN USSR. 1986. 14 s.

251. Antonyuk V.S. Osnovi pidvishchennya pratsezdatnosti rizalnogo instrumentu shlyakhom formuvannya znosostiikikh pokrittiv diskretnogo tipu. Avtoref. dis. na zdobuttya nauk. stupenya d–ra tekhn. nauk. Kiïv, NTUU KPI. 2006. 35 s.

252. Фридляндер И.Н., Белецкий В.М. Алюминиевые сплавы в авиационных конструкциях. *Технологические системы*. 2000. №1. С. 5-17.
253. Харлов А.И., Белецкий В.М. Проблемы и перспективы обеспечения народнохозяйственного комплекса Украины полуфабрикатами из алюминиевых сплавов. *Технологические системы*. 2000. № 1. С. 17-22.
254. Shakhnazarov T.A., Takhtarova Yu.A., Abdurakhmanov Ya.M. Resurs podshipnikov skolzheniya iz splavov Al-Sn i Al-Pb pri realizatsii effekta beziznoskogo treniya. Vestn. mashinostr. 2003. №11. S. 19-20.
255. Pratt G.C. Aluminum alloys for automotive crankshaft bearings: Proc. Jap. Int. Tribol. Conf. (Oct. 29 - Nov.1 1990, Nagoya). Vol.1. Tokyo. 1990. P. 125-130.
256. Ran Guang, Zhou Jing-en, Xi Sheng-qi. Mikrostruktura i kharakteristiki splava vkladisha pidshipnika Al-Pb-Si-Sn-Cu. Jinshu rechuli = Heat Treat. Metals. 2004. 29. № 2. S. 3-6.
257. Pidshipnikovii material na osnovi alyuminiєvogo splavu. Zayavka 2358872, S 22 S 21/00. F 16 S 33/12. Opubl. 08.08.2001.
258. Aluminum alloy for sliding materials. Pat. 5525294 USA. S22S 21/02. Opubl. 11.06.96.
259. Aluminum alloy suitable for use as a material for sliding parts. Pat. 4732820 SShA. V 32 V 15/01. Opubl. 22.03.88.
260. Alyuminievii splav s nizkim KTR, obladayushchii khoroshei iznosostoikostyu. Zayavka 2149629, Yaponiya, S22S 21/00. Opubl. 08.06.90.
261. Alyuminievii splav, obladayushchii khoroshei iznosostoikostyu i visokoi teploprovodnostyu. Zayavka 2149631, Yaponiya, S22S 21/02. Opubl. 08.06.90.
262. Znosostiikii Al-splav dlya shtampovok z visokoyu obroblyuvanistyu rizannyam. Zayavka 63-128145. Yaponiya. S22S 21/02. Opubl. 31.05.88.
263. Chernisheva T.A., Kobeleva L.I., Lemesheva T.V. Dispersno napolnennie kompozitsionnie materiali na baze antifriktsionnogo silumina dlya uzlov treniya skolzheniya. Perspekt. mater. 2004. №3. S. 69-75.
264. Splav dlya detalei, pratsyuyuchikh v umovakh kovzannya. Zayavka 60-63344. Yaponiya. S22S 21/02. Opubl. 11.04.85.

265. Samosmazivayushchiisya kompozitsionnii material na osnove alyuminiya, poluchennii metodom poroshkovoi metallurgii. Zayavka 55-94493. Yaponiya. C25D 11/02. Opubl. 17.07.80.

266. Detali par skolzheniya, izgotovlennie iz Al-splava. Zayavka 62-89833. Yaponiya, S22S 21/00. Opubl. 24.04.87.

267. Volochko A.T. Antifriktsionnie svoistva kompozitsionnikh alyuminievikh materialov v usloviyakh zhidkostnogo i granichnogo treniya. Trenie i iznos. 2005. 26. №6. S. 638-648.

268. Visokoprochnii kompozitsionnii material na osnove Al-splava dlya detalei mashin. Zayavka 63-42343, Yaponiya, S22S 21/02, opubl. 23.02.88.

269. Kompozitsionnii material dlya iznosostoikikh detalei i sposob yego izgotovleniya. Zayavka 58-58243, Yaponiya, S22S 21/00, opubl. 06.04.83.

270. Detali par skolzheniya, izgotovlennie iz Al-splava. Zayavka 62-89833. Yaponiya. S22S 21/00. Opubl. 24.04.87.

271. E.K. Posvyatenko, Ye.K. Solovikh, B.A. Lyashenko i dr. Tendentsii povisheniya iznosostoikosti porshnei DVS. Visnik Natsionalnogo transportnogo universitetu: Ch.1. Kiïv, NTU, 2006. Vip. 13. S. 13–21.

272. Aluminum alloy piston. Pat. 5158052 USA. F02F 3/00. Opubl. 27.10.92.

273. Plasma jet sprayed alumina coating on automobile pistons. "SAE Techn. Pap. Ser". 1987. № 870158. P. 179-184.

274. Krovyanov K.S., Radchenko M.V. Uprochnenie koltsevikh kanavok porshnya dizelya elektronno-luchevoi obrabotkoi. Tekhn. mashinostr. 2000. №3. S.23-25.

275. Batirov N.I., Radchenko M.V., Khvorov M.O. i dr. Promishlennoe elektronno-luchevoe uprochnenie porshnei iz splava AK21M2, 5N2,5: Tez. dokl. 4 Vses. konf. po svarke tsv. met. (4-7 sent. 1990, Mariupol). Kiev 1990. S. 58-59.

276. Bendovskii Ye.B., Platonov V.N., Shalai A.N. i dr. Sostoyanie i perspektivi sovershenstvovaniya kompozitsionnikh materialov na osnove porshnevikh siluminov. Dvigatelestroenie. 1991. №10-11. S. 57-60.

277. Voropai N.M., Lesnikh V.V., Mishenkov V.A. Dvukhdugovaya naplavka alyuminievikh porshnei kombinirovannim neplavyashchimsya i plavyashchimsya elektrodami. Avtomaticheskaya svarka. 1996. №6. S. 21-25.

278. Shalai A.N. Kak povisit dolgovechnost porshnya? Dvigatelestroenie. 1996. №2. S. 42, 51.

279. Aluminum alloy locally having a composite portion. Pat. 5028493 USA. C22C 21/00, P02P 3/00. Opubl. 02.07.91.

280. Porshen. Zayavka 10340291 Germaniya. F02F 3/22. Opubl. 14.04.2005.

281. Alonso A., Ferran G., Chi F. Development of fiber reinforced aluminum alloy for diesel piston applications. SAE Techn. Pap. Ser. 1991. №910632. P. 1-9.

282.. Porshen iz legkogo splava. Zayavka 4019983 FRG. F02F 3/04. Opubl. 01.01.92.

283. Piston for an internal combustion engine. Pat. 6845741 USA. F02F 3/24. Opubl. 25.01.2005.

284. Porshen. Zayavka 10352244 Germaniya, V23R 15/10, 09.06.2005.

285. Internal combustion engine piston assembly and method. Pat. 6164261. USA. F16J 1/04. Opubl. 26.12.2000.

286. Porshen. Zayavka 10149661 Germaniya, F02F 3/28, opubl. 10.04.2003.

287. Porshen s poristoi vstavkoi. Zayavka 10135609. Germaniya. F02F 3/04. Opubl. 06.02.2003.

288. Piston having uncoupled skirt. Pat. 6588320. F16J 1/04. Opubl. 08.07.2003.

289. Method manufacturing a piston. Pat. 5150517 USA. B23P 15/10. Opubl. 29.09.1992.

290. Kolben für Verbrennungsmotoren mit geschmiedeten Bereichen aus Stahk. Pat. 4109628 BRD. P02P 3/00. Opubl. 16.01.92.

291. Vtulka shatuna, izgotovlennaya iz alyuminievogo splava. Zayavka 2217434 Yaponiya. S22S 21/02. Opubl. 30.08.90.

292. Solovikh Ye.K., Lyashenko B.A., Bezrukavii A.N. Tendentsii povisheniya iznosostoikosti porshnei DVS. Visnik natsionalnogo transportnogo universitetu. Ch.1. Vip. 13. 2006. S.13-21.

293. Varvarov V.V. Pidvishchennya resursu tribosistem v agregatobuduvanni perevedennyam ïkh v rezhim anomalno nizkogo tertya ta znoshuvannya. Disertatsiya na zdobuttya naukovogo stupenya kandidata tekhnichnikh nauk (doktora filosofiï) za spetsialnistyu 05.02.04 «Tertya ta znoshuvannya v mashinakh». Kharkivskii natsionalnii tekhnichnii universitet silskogo gospodarstva imeni Petra Vasilenka, Kharkiv, 2021. 192s.

294. Solovikh Ye.K. Tendentsii povisheniya rabotosposobnosti gilz tsilindrov DVS. Probl. tribologiï. 2009. № 2. S. 47–57.

295. Zayavka 63179036, Yaponiya, S22S 21/02. Alyuminievii splav dlya tsilindrov, imeyushchikh visokoe kachestvo poverkhnosti. Opubl. 23.07.88.

296. Zayavka 63179037, Yaponiya, S22S 21/00. Alyuminievii splav dlya tsilindrov. Opubl. 23.07.88.

297. Zayavka 63179038, Yaponiya, S22S 21/00, G03G 5/10. Alyuminievii splav dlya tsilindrov. Opubl. 23.07.88.

298. Zayavka 63179039, Yaponiya, S22S 21/00, G03G 5/10. Alyuminievii splav dlya tsilindrov. Opubl. 23.07.88.

299. Zayavka 63179040, Yaponiya, S22S 21/00, G03G 5/10. Alyuminievii splav dlya tsilindrov. Opubl. 23.07.88.

300. Zayavka 63179041, Yaponiya, S22S 21/02, G03G 5/10. Alyuminievii splav dlya tsilindrov. Opubl. 23.07.88.

301. Ushio Hideaki, Tadayoshi Hayashi, Kazuo Shibata et al. Kharakteristiki iznosa kompozitsionnikh materialov na osnove alyuminievoi matritsi, uprochnennikh voloknami, i ikh primenenie dlya blokov tsilindrov avtomobilnikh dvigatelei. J. Jap. Inst. Ligth Metals. 1990. 40, № 10. P. 787–792.

302. Köhler E. Aluminium in Automobilbau: Stand, Anwendung und Perspektive am Beispiel von Technologien für Zylinderlaufflächen im Motorblock. Galvanotechnik. 1994. 85, №9. S. 2885–2893.

303. Pat. 694664, Shveitsariya, S23S 04/08. Durch Plasmaspritzen eines Spritzpulvers aufgebrachte eisenhaltige Schicht auf einer Zylinderlauffläche. Opubl. 31.05.2005.

304. Goncharov V.G. Pidvishchennya resursu transportnoï tekhniki udoskonalennyam tekhnologiï remontu kolinchastikh valiv: disertatsiya na zdobuttya naukovogo stupenya kandidata tekhnichnikh nauk za spetsialnistyu 05.22.20. Kharkiv. 2008. 24 s.

305. M.A. Podrigalo, V.G. Goncharov, B.V. Savchenkov Povishenie nadezhnosti kolenchatikh valov dizelnikh dvigatelei naneseniem diskretnikh pokritii. Vestnik NTU «KhPI». Kharkov, Izd–vo NTU «KhPI». 2003. №4. S. 115–123.

306. M.A. Podrigalo, V.G. Goncharov, B.V. Savchenkov Metodi uprochneniya diskretnimi pokritiyami sheek kolenchatikh valov avtomobilei dlya povisheniya resursa ikh raboti. Mir tekhniki i tekhnologii. 2004. №10. S. 52–55.

307. Soroka O.B. Metodologiya optimizatsiï znosostiikikh pokrittiv za kriteriyami mitsnosti i robotozdatnosti. Avtoref. dis. na zdobuttya naukovogo stupenya dokt. tekhn. nauk. Kiïv, IPMits im. G.S.Pisarenka NANU. 2011. 36 s.

308. Soroka O.B. Metodologiya optimizatsiï znosostiikikh pokrittiv za kriteriyami mitsnosti i robotozdatnosti. Avtoref. dis. na zdobuttya naukovogo stupenya dokt. tekhn. nauk. Kiïv, IPMits im. G.S.Pisarenka NANU. 2011. 36 s.

309. Tsigulev O.V. Metodi povisheniya dolgovechnosti elementov konstruktsii mnogofunktsionalnimi uprochnyayushchimi pokritiyami: avtoref. dis. na soiskanie uchenoi stepeni d–ra tekhn. nauk. Kiev, IPP AN USSR. 1989. 32 s.

310. Rutkovskii A.V. Konstruktsionnaya prochnost materialov s vakuum-plazmennimi pokritiyami. Avtoref. dis. na zdobuttya naukovogo stupenya kand. tekhn. nauk. Kiev, IPP NANU. 2000. 24 s.

311. S.A. Klimenko, S.V. Milevskii, V.A. Dutka Uprochnenie poverkhnosti detalei diskretnoi termicheskoi obrabotkoi. Uprochnyayushchie tekhnologii i pokritiya, 2006. № 1. S. 9–15.

312. M.V. Kindrachuk, M.S. Yakhya, A.O. Kornienko ta in. Viznachennya parametriv diskretnoï strukturi pokrittiv. Probl. tertya ta znoshuvannya. Kiïv, „NAU–druk", 2008. Vip. 50. S. 5–15.

313. A.s. 1784788 A1 (SSSR). Friktsionnii element. Morgun V.V., Lyashenko B.A., Svergunov A.G., Tsigulev O.V., Rutkovskii A.V. Opubl. 30.12.92. Byul. № 48.

314. Patent PCT/SU 90/00225 (EU). F16D 69/102, B32B 5/16. Friktsionnii element pari treniya. Morgun V.V., Lyashenko B.A., Svergunov A.G. i dr. Opubl. 03.10.91. WO 91/14881.

315. M. Hua, H.Y. Tam, H.Y. Ma et al. Patterned PVD TiN spot coatings on M2 steel: Tribological behaviours under different sliding speed. Wear. 260 (2006). P. 1153–1165.

316. G. Dong, M. Hua, J. Li et al. Tribological behaviours of spot–textured TiN coatings on M2 high–speed steel under boundary lubricated conditions. J. Univ. Sci. and Technol. Beijing. 2007. 14, № 4. S. 350–355.

317. A.S. Sakharov, I. Altenbakh Metod konechnikh elementov v mekhanike tverdikh tel. Kiïv, Vishcha shk. 1982. 480 s.

318. 225SN=1410876–07592353bb492cfce94a.

319. G.S. Pisarenko, A.A. Lebedev Deformirovanie i prochnost materialov pri slozhnom napryazhennom sostoyanii. Kiev, Naukova dumka. 1976. 515 s.

320. I.N. Frantsevich, F.F. Voronov, S.A. Bakuma Uprugie postoyannie i moduli uprugosti metallov i nemetallov. Spravochnik. Kiev, Nauk. dumka. 1982. 287 s.

321. Yamaguchi Hiroshi. Tekhnologiya tverdogo anodirovaniya i ispitaniya pokritiya. Intern. Combust. Engine. 1990. 20, № 12. R. 57–62.

322. V.I Kravchenko, A.L. Kvitka, A.N. Shalai Otsenka nadezhnosti porshnei s kameroi sgoraniya tipa TsNIDI. Dvigatelestroenie. 1991. №5 C. 15–18.

323. Zscherning W. Kolbenschaden an Kraftfahrzeug–Hubkolbenmotoren. Kraftfahrzeug technik. 1976. №4. S. 113–115.

324. Schwaderlapp M., Dohmen Y., Andraos N. Base engine design improves fuel efficiency. Ing. Automob. 2003. № 762. R. 44-46.

325. H. Fuchs, M. Wappelhorst Leichtmetallwerkstoffe MTZ: Motortechn. Z. 2003. 64 № 1. S. 868–875.

326. Sauer H. Höhere Laufbahn. Auto, Met. Und Sport. 1999. № 20. S. 92–93.

327. MMC offers promise of all–aluminium engine. MRP: Metal Powder Rept. 1994. 49. № 10. C. 1.

328. Pat. 6637108 USA, V23R 15/00. Method for manufacturing cylinder block for internal combustion engine Suzuki Motor Corp. Opubl. 28.10.2003.

329. Zayavka 57–60047, Yaponiya, S22S 21/02. Iznosostoikii legkii splav, primenyaemii v tsilindrakh DVS. Opubl. 10.04.82.

330. Pat. 57–9426, Yaponiya, S22F 1/04, S22S 21/02. Alyuminievii splav dlya bloka tsilindrov dvigatelya. Opubl. 22.02.82.

331. Zayavka 61–44149, Yaponiya, S22S 21/02, S22F 1/043. Alyuminievii splav. Opubl. 03.03.86.

332. Zayavka 60–228645, Yaponiya, S22S 21/02, B22D 11/06. Alyuminievii splav s visokoi iznosostoikostyu i nizkim koeffitsientom teplovogo rasshireniya i sposob yego polucheniya. Opubl. 13.11.85.

333. High–strength, wear–resistant aluminium alloys. New Mater. Dev. Jap., 1987. C. 386–388.

334. Zayavka 3199336, Yaponiya, S22S 21/02. Iznosostoikii splav alyuminiya. Opubl. 30.08.91.

335. Poroshkovii alyuminievii splav dlya dvigatelei. Avtomobilnaya Promishlennost SShA. 1997, №1. S. 24.

336. Bähr R. Wege zur Ausschöpfung der Werkstoffpotentiale bei Aluminiumgusslegierungen im Automobilbau. Giesserei Rdsch. 2001. 48, №11–12. S. 6–18.

337. Zayavka 56–116851, Yaponiya, S22S 21/00, S22S 32/00. Material dlya gilz tsilindrov dvigatelei vnutrennego sgoraniya. Opubl. 12.09.81.

338. Zayavka 57–98647, Yaponiya, S22S 21/02. Iznosostoikii alyuminievii material. Opubl. 18.09.81.

339. Zayavka 58–110652, Yaponiya, S22S 21/02, S22S 1/05. Iznosostoikii kompozitsionnii material na osnove alyuminiya. Opubl. 01.07.83.

340. M. Schwaderlapp, W. Bick, M. Duesmann et al. Leichtbaulösungen für zukünftige Dieselmotorblöcke. MTZ: Motortechn. Z. 2004. 65, №2. S. 84–88.

341. I.Kh. Chepovetskii, A.V. Barabolya, V.M. Pavliskii i dr. Tribotekhnicheskie svoistva gilz tsilindrov DVS, obrabotannikh metodom antifriktsionnogo ploskovershinnogo khoningovaniya. Trenie i iznos. 1987. 8, №1. S. 173–177.

342. I.Kh. Chepovetskii, S.A. Yushchenko, V.M. Pavliskii Antifriktsionno–deformatsionnii metod formirovaniya poverkhnostei treniya–skolzheniya. Rev. Roum. Sci. Techn. Ser. Mec. appl. 1989. 34, №1. C. 79–83.

343. N. Ilin, L. Novikov, W. Nikolajev i dr. Anwendung der Oberflächentechnologie und herstellung regulärer Mikroreliefs bei der Reibpaarung Kolbenring. Zylinder zur Minderung des Ölaustritts bei kompressoren. Schmierungstechnik. 1990. 21, №12. S. 367–371.

344. "Laser-Honen" optimiert Motorenbetrieb. VDI-Nachr. 2004. № 37. S. 29.

345. Mayer H.W. Weniger Reibunsverluste dank Laserstrahl. AMZ: Auto,

346. B. P. Krichnan, K. N. Swamy AlSiCr – a dream alloy for IC engine cylinders? SAE Techn. Pap. Ser. 1986. № 860063. 15 p.

347. Pat. 4959276 USA, C22C 21/02. Heat–resistant, Wear–resistant and high–strength Al–Si alloy, and cylinder liner employing same. Opubl. 25.09.90.

348. Leichte Motorkomponenten aus Dispal. ATZ: Automobiltechn. Z. 2005. Pril. Werkst. Automobilbau. P. 8.

349. Seyfert. Akuminiumzylinder im Motorradbau. KFZ. 1995. 38, №3. S. 182–187.

350. B. Szcygiel, I. Drela, J. Kubicki Wirtschaftliche Verchromung von Zylinderlaufbuchsen. Metalloberfläche. 1991. 45, №2. S. 56–62.

351. Funatani Kiyosi. Sposobi obrabotki poverkhnostei tsilindrov iz alyuminievikh splavov. Kinzoku = Metals and Technol. 1995. 65, №4. R. 295–305.

352. Köhler E. Aluminium in Automobilbau: Stand, Anwendung und Perspektive am Beispiel von Technologien für Zylinderlaufflächen im Motorblock. Galvanotechnik. 1994. 85, №9. S. 2885–2893.

353. Neue Motorentechnik von BMW wird zukünftig weltweit eingesetz. Galvanotechnik. 1993. 84, №9. S. 3000.

354. Pat. 6902768, SShA, B05D 1/08, C23C 4/06.Method of producing thermally sprayed metallic coating with additives. Opubl. 07.06.2005.
355. Pat. 694664, Shveitsariya, S23S 04/08. Durch Plasmaspritzen eines Spritzpulvers aufgebrachte eisenhaltige Schicht auf einer Zylinderlauffläche. Opubl. 31.05.2005.
356. Guyenot, K. Müller, J.–P. Bergmann Eigenspannungen in laserlegierten AlSi–Schihten. HTM: Härter.–techn. Mitt. 2003. 58, №3. S. 133–140.
357. Zayavka 10347145, Germaniya, S25D 5/48, C25D 3/20. Verfahren zur Herstellung einer Verscheißschutzschicht. Opubl. 12.05.2005.
358. Lyashenko B.A., Tsigulev O.V., Kuznetsov P.B. Neobkhodimo li vsegda povishat adgezionnuyu prochnost zashchitnikh pokritii. Probl. prochnosti 1987. №5. S. 70–74.
359. Pat. 3890069 USA, F04C 1/08. Coating for rotary engine rotor housing and method of making. Opubl. 17.06.75.
360. Pat. 3860367 USA, F01C 21/10. Controlled porous coating for rotary engine side housing. Opubl. 14.01.75.
361. О.В. Сушко, Е.К. Посвятенко, С.В. Кюрчев, С.І. Лодяков Прикладне матеріалознавство: підручник. Мелітополь, ТОВ «Forward press». 2019. 352 с.
362. Матеріалознавство: Підручник. За ред. проф. С.С. Дяченко. Харків, ХНАДУ. 2007. 440 с.
363. B.I. Kostetskii, I.G. Nosovskii, A.K. Karaulov i dr. Poverkhnostnaya prochnost materialov pri trenii. Kiev, Tekhnika. 1976. 296 s.
364. Radchenko S.G. Matematicheskoe modelirovanie tekhnologicheskikh protsessov v mashinostroenii. Kiev, ZAO «Ukrspetsmontazhproekt». 1998. 274 s.
365. Radchenko S.G. Matematichne modelyuvannya ta optimizatsiya tekhnologichnikh sistem. Navchalnii posibnik. Kiev, IVTs “Politekhnika”. 2001. 88 s.
366. S.N. Lapach, S.G. Radchenko, N.I. Litvinchuk Paket prikladnikh programm PRIAM. Informatsionnii listok o nauchno–tekhnicheskom dostizhenii № 88–007. Kiev, UkrNIINTI. 1988. 4 s.

367. Katalog. Programmnie produkti Ukraini. Planirovanie, regressiya i analiz modeli PRIAM. NTU KPI: Pod red. S.N. Lapach, S.G. Radchenko, P.N. Babich. Kiev, SP «Tekpor». 1993. S. 24–27.

368. Lapach S.N., Pasechnik M.F., Chubenko A.V. Statisticheskie metodi v farmakologii i marketinge farmatsevticheskogo rinka. Kiev, ZAT «Ukrspetsmontazhproekt». 1999. 312 s.

369. Tarelnik V.B. Kombinirovannie tekhnologii elektroerozionnogo legirovaniya. Kiïv, Tekhnika. 1997. 126 s.

370. Kolomitsev, A.T. Lisenko, N.I. Siskov i dr. Aviatsionnie materiali i tekhnologiya. Kiev, KVVIAU. 1976. 374 s.